

---

**Pacific Northwest  
National Laboratory**

Operated by Battelle for the  
U.S. Department of Energy

**Natural Recharge to the Unconfined  
Aquifer System on the Hanford Site  
from the Greater Cold Creek  
Watershed: Progress Report 2004**

S.R. Waichler  
M.S. Wigmosta  
A. Coleman

September 2004



Prepared for the U.S. Department of Energy  
under Contract DE-AC06-76RL01830

---

## DISCLAIMER

United States Government. Neither the United States Government nor any agency thereof, nor Battelle Memorial Institute, nor any of their employees, makes **any warranty, express or implied, or assumes any legal liability or responsibility for the accuracy, completeness, or usefulness of any information, apparatus, product, or process disclosed, or represents that its use would not infringe privately owned rights.** Reference herein to any specific commercial product, process, or service by trade name, trademark, manufacturer, or otherwise does not necessarily constitute or imply its endorsement, recommendation, or favoring by the United States Government or any agency thereof, or Battelle Memorial Institute. The views and opinions of authors expressed herein do not necessarily state or reflect those of the United States Government or any agency thereof.

PACIFIC NORTHWEST NATIONAL LABORATORY  
*operated by*  
BATTELLE  
*for the*  
UNITED STATES DEPARTMENT OF ENERGY  
*under Contract DE-AC06-76RLO1830*

Printed in the United States of America

Available to DOE and DOE contractors from the  
Office of Scientific and Technical Information,  
P.O. Box 62, Oak Ridge, TN 37831-0062;  
ph: (865) 576-8401  
fax: (865) 576-5728  
email: reports@adonis.osti.gov

Available to the public from the National Technical Information Service,  
U.S. Department of Commerce, 5285 Port Royal Rd., Springfield, VA 22161  
ph: (800) 553-6847  
fax: (703) 605-6900  
email: orders@ntis.fedworld.gov  
online ordering: <http://www.ntis.gov/ordering.htm>



This document was printed on recycled paper.  
(9/2003)

**Natural Recharge to the Unconfined Aquifer  
System on the Hanford Site from the Greater  
Cold Creek Watershed: Progress Report 2004**

S.R. Waichler  
M.S. Wigmosta  
A. Coleman

September 2004

Prepared for the U.S. Department of Energy  
under Contract DE-AC06-76RL01830

Pacific Northwest National Laboratory  
Richland, Washington 99352

## Executive Summary

Movement of contaminants in groundwater at the Hanford Site is heavily dependent on recharge to the unconfined aquifer. As the effects of past artificial discharges dissipate, the water table is expected to return to more natural conditions, and natural recharge will become the driving force when evaluating future groundwater flow conditions and related contaminant transport. Previous work on the relationship of natural recharge to groundwater movement at the Hanford Site has focused on direct recharge from infiltrating rainfall and snowmelt within the area represented by the Sitewide Groundwater Model (SGM) domain. However, part of the groundwater recharge at Hanford is provided by flow from Greater Cold Creek watershed (GCC), a large drainage area on the western boundary of the Hanford Site that includes Cold Creek Valley, Dry Creek Valley, and the Hanford side of Rattlesnake Mountain.

This study was undertaken to estimate the recharge from GCC, which is believed to enter the unconfined aquifer as both infiltrating streamflow and shallow subsurface flow. To estimate recharge, the Distributed Hydrology-Soil-Vegetation Model (DHSVM) was used to simulate a detailed water balance of GCC from 1956 to 2001 at a spatial resolution of 200 m and a temporal resolution of one hour.

For estimating natural recharge to Hanford from watersheds along its western and southwestern boundaries, the most important aspects that need to be considered are 1) distribution and relative magnitude of precipitation and evapotranspiration over the watershed, 2) streamflow generation at upper elevations and infiltration at lower elevations during rare runoff events, and 3) permeability of the basalt bedrock surface underlying the soil mantle. Some data were available to characterize surface conditions in GCC and to guide modeling of the surface and rootzone water balance, but none were available to guide simulation of shallow groundwater interacting with the underlying basalt bedrock in the upper elevation areas.

The upper bound on recharge was estimated as  $13.33 \text{ Mm}^3\text{y}^{-1}$  based on modeling with DHSVM. This estimate assumes that all precipitated water in GCC that is not lost to evapotranspiration becomes recharge to the unconfined aquifer. The key assumptions for the upper-bound estimate were that the basalt bedrock surface is impermeable and that water moving below the rootzone flows downgradient over the bedrock and eventually reaches the western boundary of the SGM. The lower bound on recharge from GCC was estimated from available streamflow data as  $0.471 \text{ Mm}^3\text{y}^{-1}$ . This estimate assumes that streamflow is the only mode of recharge from GCC to the SGM domain and is the sum of the observed perennial flow at Rattlesnake Springs and the mean annual flow from Upper Cold Creek as derived from a statistical model (Appendix D).

Ephemeral streamflow occurs in channels such as Cold Creek and Dry Creek during rare and poorly understood conditions of meteorology, soil moisture, and snow cover. Data from January 1995 were used to characterize such events and calibrate DHSVM; unfortunately, the resulting model predicted relatively frequent runoff events when applied to other time periods, and the results appear to be inconsistent with limited field observation. At present, the main benefit of DHSVM for estimating natural recharge at Hanford is to provide an analysis framework for estimating recharge, particularly estimates of distributed precipitation and evapotranspiration. This study sets a foundation for further work by directly addressing mode and spatial extent of recharge that

originates outside the SGM domain. The model developed for GCC can be used to explore specific scenarios of site conditions and can provide spatially and temporally explicit estimates of the local water balance, including recharge to the SGM.

A recently completed analysis of streamflow frequency in a larger region around Hanford could provide a different and probably sounder basis for estimating long-term recharge from runoff as simulated by DHSVM. Also, if additional field data become available in the future, it may be possible to better characterize the conditions that generate runoff and to more successfully apply the relevant processes in DHSVM.

This is a progress report for an ongoing study. In future work we will examine the sensitivity of the SGM to a range of recharge estimates, improve the distribution of meteorology, improve land cover and hydrogeology information, and update the recharge estimates based on these findings and model input improvements.

[This report was produced in Portable Document Format (PDF). When viewed onscreen, this file (PNNL-14717.pdf) contains hyperlinks to facilitate navigation. Hyperlinks are provided for all cross-referenced material, including section headings, figures, tables, and references. Hyperlinks are not colored but will become obvious when you move your mouse over them.]

## **Acknowledgments**

Financial support was provided by the U.S. Department of Energy under Contract AC06-76RL01830. We thank Richard Dinicola and Greg Ruppert of the U.S. Geological Survey for providing unpublished data.

## Abbreviations and Acronyms

|                 |  |
|-----------------|--|
| ALE             | Arid Lands Ecology Reserve                           |
| CFEST           | Coupled Fluid, Energy, and Solute Transport model    |
| DEM             | Digital Elevation Model                              |
| DHSVM           | Distributed Hydrology-Soil-Vegetation Model          |
| EOC             | Emergency Operations Center meteorology station      |
| ET              | evapotranspiration                                   |
| G               | recharge to basalt aquifer in GCC                    |
| GCC             | Greater Cold Creek watershed                         |
| HMS             | Hanford Meteorological Station                       |
| HSPF            | Hydrological Simulation Program-Fortran              |
| LAI             | leaf area index                                      |
| LC              | Lower Cold Creek gauge                               |
| LD              | Lower Dry Creek gauge                                |
| Mm <sup>3</sup> | millions of cubic meters                             |
| MOX             | Moxie City 10 E meteorological station               |
| NWS             | National Weather Service                             |
| P               | precipitation  |
| PNNL            | Pacific Northwest National Laboratory                |
| PRD             | Priest Rapids Dam meteorological station             |
| R               | recharge to SGM unconfined aquifer from GCC          |
| RMTN            | Rattlesnake Mountain meteorology station             |
| RR              | recharge ratio (recharge/precipitation)              |
| RSPG            | Rattlesnake Springs meteorology station              |
| SCS             | Soil Conservation Service                            |
| SGM             | Sitewide Groundwater Model                           |
| SHAW            | Simultaneous Heat And Water model                    |
| SUN             | Sunnyside meteorological station                     |
| UC              | Upper Cold Creek gauge                               |
| UD              | Upper Dry Creek gauge                                |
| UNSAT-H         | Unsaturated Soil Water and Heat Flow model           |
| USGS            | United States Geological Survey                      |
| WY              | water year: the year ending September 30 (10/1–9/30) |
| YTC             | Yakima Training Center                               |

## Notation

|            |  |
|------------|--|
| $D$        | flow duration  |
| $f$        | factor limiting maximum infiltration                                 |
| $H$        | heat flux from upper soil layer                                      |
| $f_{hf}$   | heat flux factor   |
| $H_L$      | lower bound on heat flux   |
| $H_U$      | upper bound on heat flux   |
| $\theta$   | soil moisture content from upper soil layer                          |
| $f_{mc}$   | soil moisture content factor   |
| $\theta_L$ | lower bound on soil moisture content                                 |
| $\theta_U$ | upper bound on soil moisture content                                 |
| $i$        | infiltration rate  |
| $i_{max}$  | maximum infiltration rate  |
| $P$        | precipitation  |
| $Q$        | flow rate  |
| $Q_p$      | peak flow rate   |
| $s$        | snow water equivalent  |
| $s_T$      | snow water equivalent threshold above which there is no infiltration |
| $T$        | temperature  |
| $V$        | flow volume  |

# Contents

|  |      |
|--|------|
| Executive Summary . . . . .  | iii  |
| Acknowledgments . . . . .  | v    |
| Abbreviations and Acronyms . . . . .   | vii  |
| Notation . . . . .   | viii |
| 1.0 Introduction . . . . .   | 1    |
| 1.1 Background . . . . .   | 1    |
| 1.2 Purpose and Scope of Report . . . . .  | 2    |
| 2.0 Previous Estimates of Natural Recharge . . . . .                                 | 5    |
| 3.0 Watershed Characteristics . . . . .  | 9    |
| 3.1 Physical Description . . . . .   | 9    |
| 3.2 Climate, Soil, and Channel Characteristics . . . . .                             | 9    |
| 3.3 Observed Streamflow . . . . .  | 10   |
| 3.4 Extreme Event Modeling Based on Observed Streamflow . . . . .                    | 13   |
| 4.0 Description of the Distributed Hydrology-Soil-Vegetation Model (DHSVM) . . . . . | 17   |
| 4.1 Basic Structure and Processes . . . . .  | 17   |
| 4.2 Model Modifications and Improvements . . . . .                                   | 18   |
| 5.0 DHSVM Application . . . . .  | 23   |
| 5.1 Model Inputs . . . . .   | 23   |
| 5.1.1 Topography, Soil, and Vegetation . . . . .                                     | 23   |
| 5.1.2 Meteorology . . . . .  | 23   |
| 5.2 Model Calibration . . . . .  | 24   |
| 5.2.1 Calibration of Streamflow to Observed Runoff in Cold Creek . . . . .           | 25   |

|   |  |     |
|---|--|-----|
| 5.2.2   | Calibration of Evapotranspiration . . . . .            | 30  |
| 5.3   | Other Models Evaluated . . . . .                       | 35  |
| 6.0   | Results . . . . .                                      | 41  |
| 7.0   | Discussion . . . . .                                   | 47  |
| 7.1   | Recharge in Sitewide Groundwater Model ACM-2 . . . . . | 47  |
| 7.2   | Future Improvements . . . . .                          | 48  |
| 8.0   | Conclusions . . . . .                                  | 51  |
| 9.0   | References . . . . .                                   | 53  |
| Appendix A – New DHSVM Features . . . . .                     |  | A.1 |
| Appendix B – Statistics for Evaluating Model Skill . . . . .  |  | B.1 |
| Appendix C – Greater Cold Creek Meteorology Data . . . . .    |  | C.1 |
| Appendix D – Regional Streamflow Frequency Analysis . . . . . |  | D.1 |

# Figures

|      |  |     |
|------|--|-----|
| 1.1  | The Greater Cold Creek Watershed and the Western Hanford Site. . . . .         | 3   |
| 3.1  | Cold Creek streamflow and meteorology during January 1995. . . . .             | 12  |
| 3.2  | Flow volume versus peak flow rate at UC . . . . .                              | 14  |
| 4.1  | DHSVM schematic . . . . .  | 17  |
| 4.2  | Surface and subsurface water pathways used in revised DHSVM . . . . .          | 19  |
| 5.1  | Lower boundary specification for watershed modeling . . . . .                  | 24  |
| 5.2  | DHSVM simulation of UC, January 1995 . . . . .                                 | 28  |
| 5.3  | DHSVM simulation of LC, January 1995 . . . . .                                 | 29  |
| 5.4  | ET components at a grid cell near HMS, WY1963 . . . . .                        | 31  |
| 5.5  | Soil moisture at a grid cell near HMS, WY1963 . . . . .                        | 32  |
| 5.6  | Daily simulated streamflow at UC, WY56-01 . . . . .                            | 33  |
| 5.7  | Annual simulated streamflow at UC, WY56-01 . . . . .                           | 34  |
| 5.8  | Time windows used in regression modeling of streamflow at UC . . . . .         | 35  |
| 5.9  | 1:1 plot for best-fitting regression model of daily streamflow at UC . . . . . | 37  |
| 5.10 | Daily regression model streamflow, WY56-01 . . . . .                           | 38  |
| 5.11 | Annual regression model streamflow, WY56-01 . . . . .                          | 39  |
| 6.1  | Reference areas for recharge estimates . . . . .                               | 41  |
| 6.2  | Map of mean annual precipitation . . . . .                                     | 44  |
| 6.3  | Map of mean annual precipitation minus ET . . . . .                            | 44  |
| 6.4  | Map of mean annual shallow recharge . . . . .                                  | 45  |
| C.1  | Annual precipitation at four stations near the Hanford Site . . . . .          | C.2 |
| C.2  | Precipitation adjustment factors for Cold and Dry Creeks . . . . .             | C.5 |

|     |  |      |
|-----|--|------|
| C.3 | January to June precipitation at non-ridgetop ALE sites . . . . .  | C.6  |
| C.4 | July to December precipitation at non-ridgetop ALE sites . . . . . | C.7  |
| C.5 | January to June precipitation at non-ridgetop ALE sites . . . . .  | C.9  |
| C.6 | July to December precipitation at non-ridgetop ALE sites . . . . . | C.10 |
| C.7 | Regression models for ALE precipitation . . . . .                  | C.12 |
| D.1 | Crest height gauges near Hanford . . . . .                         | D.1  |
| D.2 | Annual peak flows at regional crest height gauges . . . . .        | D.2  |
| D.3 | Monthly distribution of instantaneous peak annual flows . . . . .  | D.2  |
| D.4 | Cumulative probability of annual peak flows . . . . .              | D.4  |

## Tables

|     |  |      |
|-----|--|------|
| 2.1 | Hanford natural recharge estimates . . . . .                                 | 6    |
| 3.1 | Greater Cold Creek basins and mean climate . . . . .                         | 10   |
| 3.2 | Runoff events, Cold Creek, January 1995 . . . . .                            | 13   |
| 3.3 | Measured streamflow volumes as annualized recharge rates . . . . .           | 14   |
| 5.1 | Climate stations used to generate input for DHSVM. . . . .                   | 25   |
| 5.2 | Final DHSVM parameter values . . . . .                                       | 30   |
| 5.3 | Options used in January 1995 regression models of streamflow at UC . . . . . | 36   |
| 6.1 | Simulated fluxes for regions in GCC . . . . .                                | 42   |
| 7.1 | Recharge rates from all sources in ACM-2 of the SGM . . . . .                | 48   |
| C.1 | Summary of missing climate data, Hanford Meteorology Station . . . . .       | C.1  |
| C.2 | Summary of missing precipitation data, NWS stations . . . . .                | C.3  |
| C.3 | Factors for distributing precipitation . . . . .                             | C.4  |
| C.4 | Regression models for predicting ALE precipitation . . . . .                 | C.11 |

## 1.0 Introduction

Over the history of Hanford operations, the large volumes of wastewater discharged to a variety of waste facilities resulted in large water table changes over most of the Hanford Site and created significant groundwater mounds (in excess of 20 m) under waste management facilities in the central part of the Site. Since 1988, the mission of the Hanford Site has changed from producing weapons to restoring the environment, and wastewater discharges have declined significantly, which has caused significant water table declines.

As the effects of past artificial discharges dissipate, the water table is expected to return to more natural conditions, and natural recharge will become the driving force when evaluating future groundwater flow conditions and related contaminant transport.

### 1.1 Background

Development of the Site-wide Groundwater Model (SGM) described in Cole et al. (2001) and Vermeul et al. (2001) considered several categories of natural recharge to the unconfined aquifer system that included:

- Infiltration of rainfall and snowmelt within the modeled domain, which is implemented as a specified flux at the uppermost boundary in SGM implementations by Cole et al. (2001) and Vermeul et al. (2001)
- Lateral subsurface flow in sediments from upgradient areas at the entry of Cold Creek and Dry Creek Valleys and along the base of the north-facing slope of Rattlesnake Mountain. These sources of recharge are also introduced into the modeled domain as a specified flux along the west and southwest boundary of the model in both SGM implementations (Cole et al. 2001; Vermeul et al. 2001).
- Leakage from the underlying uppermost confined basalt to the unconfined aquifer system as a head-dependent leakage boundary at the base of the modeled domain. This component is included only in the Vermeul et al. (2001) model.

Leakage (e.g., spring discharge) from basalt aquifers in the areas outside the SGM domain were assumed to be integrated into the estimate for lateral subsurface flow from those areas. Implementation of basalt leakage in the model by Vermeul et al. (2001) was accomplished by adding the following intercommunication mechanisms to the baseline inverse model (i.e., the model developed in Cole et al. 2001) in steps to investigate each feature's sensitivity and relationship with other estimated parameters:

- Head-dependent, areally distributed leakage through the basalt confining layer
- Increased leakage at an erosional window near Gable Mountain/Gable Butte
- Increased leakage at a smaller erosional feature near B-Pond

- Increased leakage along two fault zones: the Cold Creek Fault zone west of 200 West area and May Junction Fault located east of 200 East Area.

In recent modeling efforts described in Vermeul et al. (2003), the SGM domain was expanded to the head of the Dry Creek and Cold Creek valleys where the water table intersects the basalt surface. This was done to reduce the uncertainty associated with these boundary conditions and to better approximate the implementation of recharge from upland areas along the western boundary of the modeled region. This enhancement has required the use of a process-based, distributed-parameter hydrologic model to estimate recharge components not previously considered along the western boundary of the SGM. These natural recharge components include:

- Infiltration of streamflow from Cold Creek and Dry Creek to the unconfined aquifer
- Infiltration of surface runoff from upland areas on the north face of Rattlesnake Mountain as it collects into localized ephemeral drainages and recharges the unconfined aquifer sediments at the base of the mountain.

## **1.2 Purpose and Scope of Report**

The purpose of this report is to describe the development and initial implementation of the process-based, distributed-parameter Distributed Hydrology Soil Vegetation Model (DHSVM) (Wigmosta et al. 1994, 2002) to estimate the natural recharge to the SGM domain that occurs as streamflow and subsurface flow within sediments from the areas to the west of the SGM. This area, here named the Greater Cold Creek watershed (GCC), is in the same topographic watershed as the SGM domain and includes Cold Creek Valley, Dry Creek Valley, and the northeast face of Rattlesnake Mountain (Figure 1.1). GCC includes nearly all of the land mass beyond the Hanford Site border that contributes recharge to the unconfined aquifer at Hanford. Previous Pacific Northwest National Laboratory (PNNL) studies of natural recharge at Hanford have focused on direct recharge within the Hanford Site boundary. Most previous estimates of recharge originating from the offsite areas of GCC were based on simple assumptions and minimal supporting information. A United States Geological Survey (USGS) study did estimate runoff from Cold and Dry Creeks using field and modeling methods but was hampered by a lack of observed streamflow during the period of study (Dinicola 1997). This analysis used streamflow and meteorological data collected subsequently to characterize the watershed conditions that produce runoff. This information was combined with long-term meteorology data and the DHSVM to improve estimates of recharge from streamflow runoff and shallow subsurface flow.

A brief literature review of previous efforts to estimate natural recharge at Hanford is given in Section 2. GCC is described in Section 3, including the runoff-producing conditions and ephemeral flows that occurred in January 1995. The conceptual model for GCC, an overview of DHSVM, and a detailed description of DHSVM structural improvements made for this project are described in Section 4. The specific DHSVM implementation for GCC is described in Section 5, including the terrain inputs, meteorology input, and model calibration. Results of the watershed modeling are presented in Section 6. The primary outcome was an estimate of annual average recharge from streamflow and subsurface flow into the SGM domain, which Vermeul et al. (2003) used as a starting point to calibrate the SGM. A discussion of these results and how offsite recharge

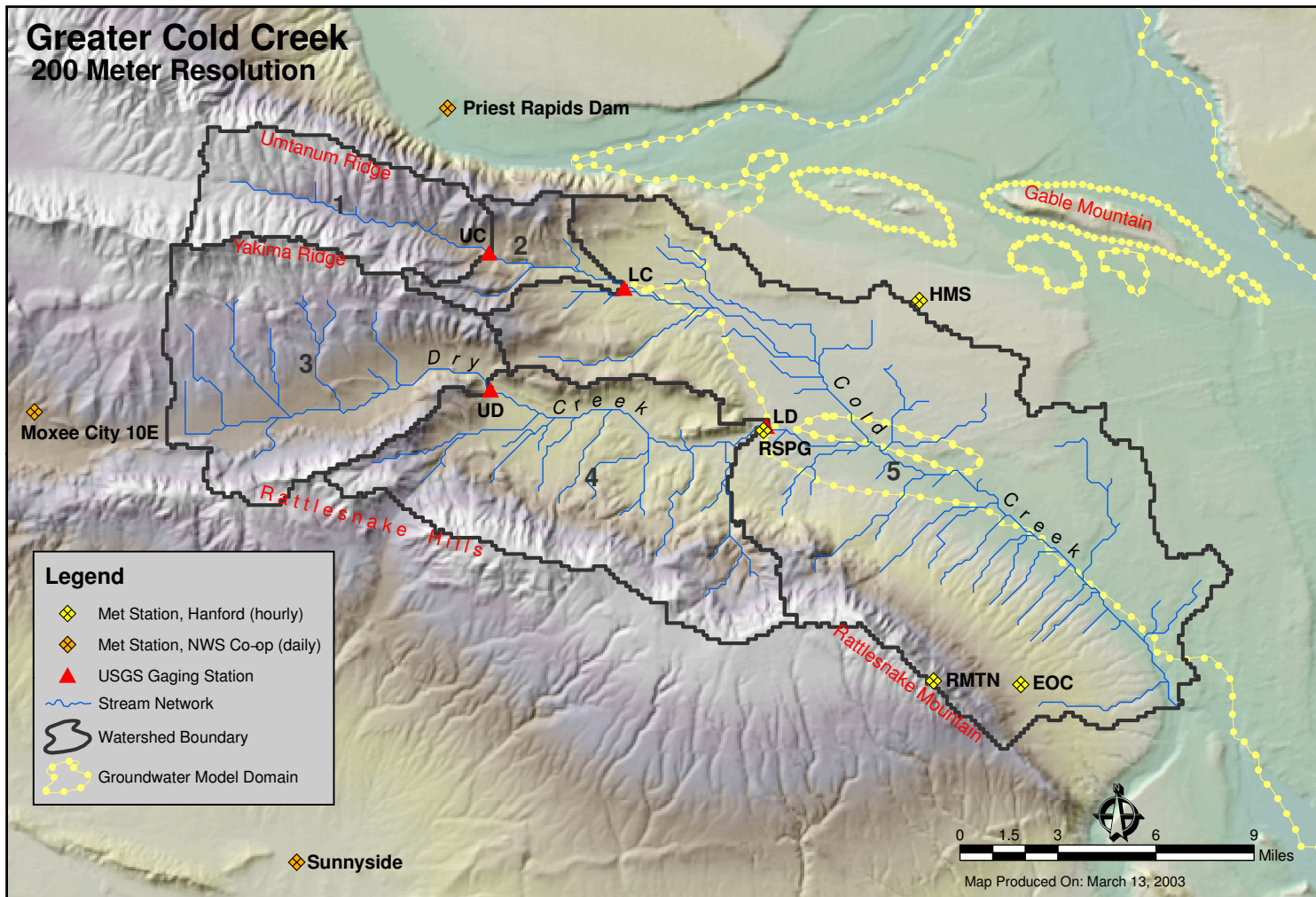


**Figure 1.1.** The Greater Cold Creek Watershed and the Western Hanford Site. Topography at 200 m resolution. Basin 1 is above Upper Cold gauge (UC); Basin 2 is above Lower Cold gauge (LC); Basin 3 is above Upper Dry gauge (UD); Basin 4 is above Lower Dry gauge (LD); Basin 5 is remaining area within the topographic watershed of GCC; Basin 6 is the entire watershed. HMS = Hanford Meteorology Station, RSPG = Rattlesnake Springs, RMTN = Rattlesnake Mountain, EOC = Emergency Operations Center.

might be addressed in the future is found in Section 7, followed by conclusions in Section 8. Appendix A describes the code and input changes made to DSHVM for this study; Appendix B defines the goodness-of-fit statistics used in this report; Appendix C describes meteorology data gleaned from older PNNL reports and an assessment of that information for distributed modeling; and Appendix D contains an analysis of regional streamflow records and a statistical estimate of mean annual recharge from Cold Creek streamflow.

## 2.0 Previous Estimates of Natural Recharge

Several previous studies have estimated natural recharge in the Hanford region from direct infiltration, surface runoff, and lateral groundwater flow. In the discussion that follows, the original published recharge rates given in units of water depth over areas of various extents have been normalized to the same land area to facilitate comparison and are presented in consistent units (Table 2.1). Some authors have conceptualized recharge as only a vertical process and did not consider lateral movement away from the source area. Others have included lateral movement in their conceptual model for recharge but did not distinguish between streamflow and lateral subsurface flow, and tended to call both of these “runoff.” Infiltration of streamflow away from the source area is rapid in the arid setting of Hanford; therefore, characterizing the surface or subsurface nature of runoff depends on location and one’s particular objectives.

Newcomb et al. (1972) examined water level records from wells and gathered anecdotal information about runoff events in Cold Creek as part of the first comprehensive study of Hanford Site hydrogeology. They estimated surface runoff from Cold Creek as 0.376 millions of cubic meters per year ( $\text{Mm}^3\text{y}^{-1}$ ) ( $=300 \text{ ac-ft y}^{-1}$ ), and from Dry Creek and Rattlesnake Spring as  $0.185 \text{ Mm}^3\text{y}^{-1}$  ( $150 \text{ ac-ft y}^{-1}$ ). They focused on streamflow as the primary mechanism of recharge but recognized that infiltration of streamflow can happen outside the Hanford Site and would therefore recharge the Hanford Site as groundwater flow. They did not estimate direct recharge on the Hanford Site itself.

Jacobson and Freshley (1990) estimated natural recharge by inversing (calibrating) an early version of the Coupled Fluid, Energy, and Solute Transport (CFEST) site-wide groundwater model. They estimated total recharge from Cold Creek Valley as  $3.218 \text{ Mm}^3\text{y}^{-1}$  of groundwater inflow and  $17.31 \text{ Mm}^3\text{y}^{-1}$  as direct recharge within the SGM area.

Bauer and Vaccaro (1990) conducted the first detailed modeling of the upper vadose zone in a study of recharge over the entire mid-Columbia basin. They applied the one-dimensional Deep Percolation Model to  $1\text{-km}^2$  cells in the Hanford region and explicitly accounted for soil type, land use/land cover, and local climate effects. They did not explicitly account for streamflow generation or lateral subsurface flow between grid cells. Recharge in Cold Creek Valley was estimated as  $3.298 \text{ Mm}^3\text{y}^{-1}$ , Dry Creek Valley as  $3.360 \text{ Mm}^3\text{y}^{-1}$ , and recharge within the SGM area as  $6.794 \text{ Mm}^3\text{y}^{-1}$ .

Fayer and Walters (1995) used a combination of lysimeter, tracer, and neutron probe soil moisture data from Hanford Site locations together with the one-dimensional Unsaturated Soil Water and Heat Flow (UNSAT-H) model to estimate direct recharge over a range of combined soil and vegetation conditions. Their study area included the entire area owned by the Department of Energy south and west of the Columbia River, including lower Cold Creek and Dry Creek Valleys and Rattlesnake Mountain. Estimated rates ranged from zero in areas with loamy soils and significant vegetation to more than  $100 \text{ mm y}^{-1}$  in areas with rocky soils and no vegetation. Although Fayer and Walters (1995) addressed the important effects of soil texture and vegetation cover, they did not account for increasing precipitation and lower evapotranspiration at higher elevations, or for the potential lateral movement of water from higher to lower elevation areas. Their recharge estimates for the entire DOE area and the SGM part of it were  $10.01 \text{ Mm}^3\text{y}^{-1}$

**Table 2.1.** Hanford natural recharge estimates. Recharge includes both direct infiltration within and runoff from the recharge source area unless otherwise noted.

| Recharge Source Area                     | Recharge           |                                 | Study                          |
|--|--------------------|---------------------------------|--------------------------------|
|  | mm y <sup>-1</sup> | Mm <sup>3</sup> y <sup>-1</sup> |                                |
| Cold Creek, runoff only (Basins 1 and 2) |                    | 0.376 <sup>(a)</sup>            | Newcomb et al. (1972)          |
| Cold Creek (Basins 1 and 2)              | 33 <sup>(b)</sup>  | 3.298 <sup>(c)</sup>            | Bauer and Vaccaro (1990)       |
| Cold Creek (Basins 1 and 2)              | 32 <sup>(d)</sup>  | 3.218 <sup>(c)</sup>            | Jacobson and Freshley (1990)   |
| Cold Creek, runoff only (Basins 1 and 2) |                    | 0.530 <sup>(e)</sup>            | Dinicola (1997)                |
| Dry Creek, runoff only (Basins 3 and 4)  |                    | 0.185 <sup>(a)</sup>            | Newcomb et al. (1972)          |
| Upper Dry Creek (Basin 3)                | 10 <sup>(b)</sup>  |                                 | Bauer and Vaccaro (1990)       |
| Lower Dry Creek (Basin 4)                | 11 <sup>(b)</sup>  |                                 | Bauer and Vaccaro (1990)       |
| Dry Creek (Basins 3 and 4)               | 11                 | 3.360 <sup>(c)</sup>            | after Bauer and Vaccaro (1990) |
| Dry Creek, runoff only (Basins 3 and 4)  |                    | 1.023 <sup>(e)</sup>            | Dinicola (1997)                |
| Entire Hanford Site                      | 8 <sup>(b)</sup>   | 9.277 <sup>(f)</sup>            | Bauer and Vaccaro (1990)       |
| Entire Hanford Site                      | 9 <sup>(g)</sup>   | 10.01 <sup>(f)</sup>            | Fayer and Walters (1995)       |
| SGM portion of Hanford Site              | 8 <sup>(b)</sup>   | 6.794 <sup>(h)</sup>            | Bauer and Vaccaro (1990)       |
| SGM portion of Hanford Site              | 23 <sup>(d)</sup>  | 17.31 <sup>(h)</sup>            | Jacobson and Freshley (1990)   |
| SGM portion of Hanford Site              | 11 <sup>(f)</sup>  | 8.474 <sup>(h)</sup>            | Fayer and Walters (1995)       |

- (a) From runoff estimate reported in ac-ft y<sup>-1</sup>.
- (b) From recharge simulation of WY1956-77 using the Deep Percolation Model.
- (c) Computed from recharge in mm y<sup>-1</sup> and watershed areas in Table 3.1.
- (d) From calibration of early CFEST groundwater flow model.
- (e) From runoff simulation of WY1958-93 using HSPF.
- (f) Computed from recharge in mm y<sup>-1</sup> and area of 1105.6 km<sup>2</sup> (see Fayer and Walters (1995) for extent of area).
- (g) From field measurements and simulation with UNSAT-H.
- (h) Computed from recharge in mm y<sup>-1</sup> and area of 810 km<sup>2</sup> (see Vermeul et al. (2003) for extent of area).

(9 mm y<sup>-1</sup>) and 8.474 Mm<sup>3</sup>y<sup>-1</sup> (11 mm y<sup>-1</sup>), respectively. The estimate for just the SGM area was higher when normalized to land area (mm y<sup>-1</sup>) because the SGM has a greater proportion of area with coarse-grained soil and sparse or absent vegetation, both of which tend to decrease evapotranspiration (ET) and increase recharge.

In the early 1990s, Dinicola (1997) conducted a study of recharge originating from high-elevation areas. Field data and the semi-distributed Hydrological Simulation Program-Fortran (HSPF) watershed model were used to estimate long-term recharge from Cold and Dry Creek runoff. This study noted that most runoff events in the region occur during winter, typically under conditions involving a combination of rainfall, snowmelt, and frozen soil. Unfortunately, only data through 1993 were considered in that report, and very little runoff occurred during that time, lim-

iting the effectiveness of the modeling. Dinicola measured the perennial flow at Lower Dry Creek gauge (LD) from nearby Rattlesnake Springs as  $0.391 \text{ Mm}^3\text{y}^{-1}$  and estimated recharge from ephemeral runoff in Cold Creek as  $0.530 \text{ Mm}^3\text{y}^{-1}$  and Dry Creek as  $1.023 \text{ Mm}^3\text{y}^{-1}$ .

Taken together, these previous studies of natural recharge at Hanford suggest that recharge normalized to land area is greatest in Cold Creek Valley, at around  $33 \text{ mm y}^{-1}$  ( $3.287 \text{ Mm}^3\text{y}^{-1}$ ), and close to  $10 \text{ mm y}^{-1}$  in Dry Creek Valley and the Hanford Site (Table 2.1). The larger size of Dry Creek Valley compared to Cold Creek Valley leads to similar estimated volumes of recharge from the two valleys. Based on the estimates of runoff by Newcomb et al. (1972) and Dinicola (1997) and total recharge by Bauer and Vaccaro (1990), only 5 to 30% of total recharge from these basins is in the form of runoff (streamflow). Total recharge from Cold and Dry Creek Valleys of around  $6.575 \text{ Mm}^3\text{y}^{-1}$  is equivalent to 78% of the direct recharge estimated for the SGM area by Fayer and Walters (1995).

## 3.0 Watershed Characteristics

In this section, the physical characteristics of GCC are described, including major topographic features, elevation ranges, and nomenclature for subwatersheds (Section 3.1). Next, the climate, soil, and channel characteristics pertinent to natural recharge are described (Section 3.2). Streamflow observed in Cold and Dry Creeks during January 1995 is described in Section 3.3.

### 3.1 Physical Description

The extents of GCC and its interior drainage are defined by the Umtanum and Yakima Ridges and Rattlesnake Mountain (Figure 1.1). Umtanum Ridge divides the Cold Creek basin from the Columbia River basin. Yakima Ridge divides the Cold Creek and Dry Creek Valleys. Rattlesnake Mountain and its westerly extension form the southern boundary of GCC, separating Dry Creek and lower Cold Creek from the Yakima basin. Elevations range from 200 m (650 ft) in lower Cold Creek to 1090 m (3650 ft) at the Rattlesnake summit. Most of upper Cold Creek Valley is part of the U.S. Department of Defense Yakima Training Center (YTC) and is used for limited training but is otherwise mostly in a natural state. Lower Cold Creek between the YTC and the Hanford Site is privately owned, and land uses include grazing and grape and alfalfa production. Most of upper Dry Creek Valley is privately owned and is used for grazing, dryland farming, and some irrigated farming. The eastern parts of the Valleys and Rattlesnake Mountain are mostly part of the Department of Energy Arid Lands Ecology Reserve (ALE), now managed by the U.S. Fish and Wildlife Service.

For this study, GCC was divided into five basins (Figure 1.1): Basin 1 above Upper Cold Creek gauge (UC), Basin 2 above Lower Cold Creek gauge (LC), Basin 3 above upper Dry Creek gauge (UD), Basin 4 above lower Dry Creek gauge (LD), and Basin 5, the remainder of GCC. The extents of Basins 1–4 correspond to the stream gauge locations (UC, LC, UD, LD) established by the USGS in the early 1990s. Basin 5 includes the Hanford side of Rattlesnake Mountain and the low-gradient valley west of the Hanford Central Plateau. The topographic watershed extends to the eastern side of Highway 240 and includes an area within the SGM domain. That area inside the SGM domain was excluded from the final estimate of recharge in this study to avoid double-counting direct recharge there [the SGM already uses direct recharge estimates based on Fayer and Walters (1995) in this area].

### 3.2 Climate, Soil, and Channel Characteristics

Mean annual precipitation and air temperature in GCC are approximately 181 mm and 11.4°C, respectively (Table 3.1). Vegetation in GCC consists mostly of sagebrush-steppe types. Soils are thin, especially in Basin 1 (upper Cold Creek), where depth to bedrock is less than 0.75 m for several of the soil types present (Lenfesty and Reedy 1985; Rasmussen 1971). Basin 1 is also v-shaped, with most of the valley bottom less than 60 m wide, and surrounded by steep (30–65%) side slopes. Soil at UC is classified as Kiona very stony silt loam, having 25–55% angular basalt gravel and cobbles in the upper 0.5 m and 70% gravel and cobbles from 0.5 to 1.5 m (Lenfesty and Reedy 1985). Permeability of the upper and lower layers is rated at 0.5–20 mm h<sup>-1</sup> and 20–65 mm h<sup>-1</sup>, respectively. In contrast, Basin 2 has a wider valley bottom (at least 120 m) surrounded by gentler (0–30%) slopes. Soil at the location of LC is classified as Finley stony fine

**Table 3.1.** Greater Cold Creek basins and mean climate. Areas and elevations are based on 200 m digital elevation model (DEM). Hanford Meteorological Station (HMS) climate is based on WY1956-2001 hourly data. Basin climate is based on DHSVM distribution of HMS and National Weather Service (NWS) data for WY1956-2001.

| Location   | Min. Elev. (m) | Mean Elev. (m) | Max. Elev. (m) | Mean Annual Temperature (°C) | Mean Annual Precipitation (mm) | Area (km <sup>2</sup> ) | Number of Grid Cells in DEM |
|------------|----------------|----------------|----------------|------------------------------|--------------------------------|-------------------------|-----------------------------|
| Basin 1    | 442            | 773            | 1217           | 10.5                         | 214                            | 73.5                    | 1837                        |
| Basin 2    | 289            | 508            | 850            | 11.3                         | 192                            | 27.0                    | 676                         |
| Basin 3    | 347            | 649            | 1255           | 10.8                         | 190                            | 150                     | 3740                        |
| Basin 4    | 208            | 510            | 1080           | 11.3                         | 188                            | 167                     | 4185                        |
| Basin 5    | 131            | 282            | 1082           | 11.9                         | 168                            | 431                     | 10765                       |
| Basins 1–4 | 208            | 606            | 1255           | 11.0                         | 194                            | 417                     | 10438                       |
| Basins 1–5 | 131            | 442            | 1255           | 11.4                         | 181                            | 848                     | 21203                       |
| HMS        |                | 220            |                | 12.1                         | 167                            |                         |                             |

sandy loam, which has gravelly fine sandy loam in the upper 0.7 m and sandy gravel and cobbles from 0.7 to 1.5 m (Rasmussen 1971). The permeability of the Finley soil upper and lower layers is rated higher than that of the Kiona soil, at 65–125 mm h<sup>-1</sup> and greater than 25 mm h<sup>-1</sup>, respectively. The gentler slopes and greater permeability of the Basin 2 and Basin 5 valley bottoms provide more opportunity for runoff to infiltrate before reaching the main channel. Streambeds in Basins 1 and 2 are typically sand, gravel, and cobbles. The Cold Creek Valley widens, and the alluvium thickness appears to increase significantly downstream from a point approximately 4 km above LC. Below LC, the channel is braided and eventually dissipates in a broad alluvial valley. Channel gradients in Cold Creek range from approximately 0.02 above UC to 0.005 in the broad valley next to Highway 240.

Dry Creek and lower Cold Creek have deeper soils and offer more opportunity for tributary flow to infiltrate before reaching the main channel. In Dry Creek, alluvium and infiltration potential appear to greatly increase downstream from UD, where the channel enters a much wider valley. The Dry Creek channel is deeply incised for about a mile above LD, with walls 10 m high and about 40 m wide. LD is immediately downstream of Rattlesnake Spring, which produces a perennial flow of approximately 0.014 m<sup>3</sup>s<sup>-1</sup> (0.5 cfs) (Dinicola 1997). The perennial flow supports a vibrant riparian plant community along the channel. The perennial flow is completely infiltrated into the Dry Creek bed at a point about 1.5 miles downstream of LD. The upper water table is approximately 70 m below ground surface near the western Hanford Site boundary (Hartman et al. 2002).

### 3.3 Observed Streamflow

Although no significant runoff events occurred during the initial field campaign described in Dinicola (1997), the local USGS field office continued the stream gauging through March 1995.

Significant streamflow was finally measured by the USGS during January 1995. The rather large runoff events of 1995 were recorded at 15-minute intervals using shaft-float encoders, a broad-crested v-notch weir (Brakensiek et al. 1979) at the Upper Cold Creek gauge (UC), and a supercritical flow flume (Kilpatrick and Schneider 1983) at the Lower Cold Creek gauge (LC). During that month, mean flow rates of  $16,040 \text{ m}^3\text{d}^{-1}$  and  $13,170 \text{ m}^3\text{d}^{-1}$  were recorded at UC and LD, respectively. This data set of ephemeral streamflow in Cold and Dry Creeks was influential in framing subsequent PNNL work and provided a basis for adapting a distributed watershed model to the arid hydrology of Hanford, particularly in the prediction of ephemeral streamflow and channel infiltration. Unfortunately for subsequent modeling efforts, measurement of meteorology near the streamflow source areas within GCC had already been discontinued by January 1995.

Cold Creek streamflow, precipitation, and air temperature during this month are shown in Figure 3.1. Air temperatures were below freezing during part of the month, and the combination of rainfall, frozen ground, and melting snow appeared to produce the runoff during these events (Dinicola, personal communication, 2001). Flow volumes for the Cold Creek runoff events ranged from  $1,635$  to  $126,100 \text{ m}^3$  (Table 3.2). Most of the flows had durations of less than a day, and the hydrographs indicated powerful streamflows surging down channel, with rapid cresting (Figure 3.1). For example, event LC6 rose from  $0$  to  $3 \text{ m}^3\text{s}^{-1}$  in 15 minutes and reached its peak of  $5.5 \text{ m}^3\text{s}^{-1}$  in only one hour. Cold Creek flows had a regular pattern of larger volumes at the upper gauge and smaller volumes at the lower gauge. Hydrographs at LC began sharply a short time after the rise at UC, suggesting that most if not all flow recorded at LC originated as runoff from the upper basin.

A linear relationship was derived for flow volume as a function of peak flow rate at UC and is shown in Figure 3.2. The relationship,  $\text{Volume} (\text{m}^3) = 432,162 \times \text{peak flow rate} (\text{mm h}^{-1})$ , is used in Appendix D to estimate a lower bound for recharge originating in Cold Creek Valley.

Flows were also observed in Dry Creek during January 1995. Unlike Cold Creek, lateral inflow to Dry Creek between the upper and lower gauges (UD, LD) appeared to be a significant but unknown component in flow at LD because Dry Creek flows were minimal at UD but substantial at LD. No flows were recorded at UD in the data set supplied by the USGS for January 1995; however, flows up to  $0.085 \text{ m}^3\text{s}^{-1}$  (exceeding the  $0.014 \text{ m}^3\text{s}^{-1}$  perennial flow from Rattlesnake Springs) were observed at UD, so data recording may have been inadequate (Dinicola, personal communication, 2001). Also, the channel bed at UD is relatively wide and free of vegetation, suggesting that significant flows do occur there with some regularity. Five distinct flow events were recorded at LD, and all were smaller than corresponding flows at LC, even though the total area in Dry Creek is 68% larger than Cold Creek. Additional information about the January 1995 runoff events can be found in Waichler and Wigmosta (2004).

The observed streamflows provide additional reference points for estimating mean annual natural recharge from GCC. The total January 1995 volume from Cold Creek was  $0.497 \text{ Mm}^3$ , but the WY1991-92 data suggest a mean annual volume of less than  $0.004 \text{ Mm}^3$  (Table 3.3). In Dry Creek the January 1995 volume was  $0.408 \text{ Mm}^3$ , but the perennial flow of  $0.391 \text{ Mm}^3\text{y}^{-1}$  from Rattlesnake Spring provides a recharge volume every year that is nearly as great as that single month's ephemeral flow.

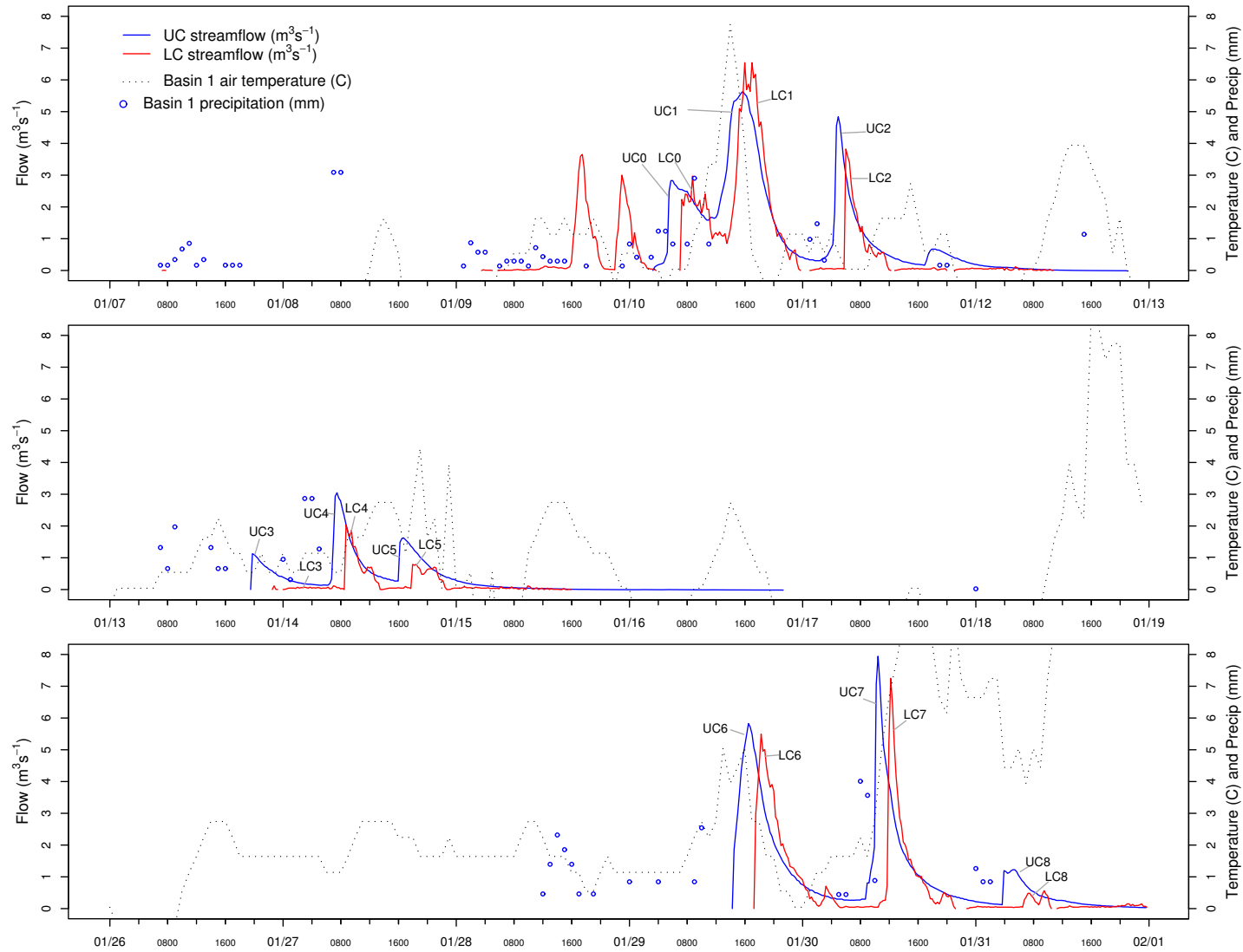


**Figure 3.1.** Cold Creek streamflow events and hourly meteorological conditions during January 1995. Streamflow labels correspond to events summarized in Table 3.2. Air temperature and precipating are Basin 1 means, computed using distributed meteorology in DHSVM. Only precipitation  $\geq 0.254$  mm (0.01 inch) is shown. Zero-valued streamflow is omitted.

**Table 3.2.** Runoff events, Cold Creek, January 1995.  $V$ =volume,  $D$ =duration,  $Q_p$ =peak flow rate. Storm events and corresponding flow events are numbered chronologically. Volume expressed as mm corresponds to Upper Cold Creek area (Basin 1 for UC, Basins 1 and 2 for LC). Precipitation values are for Upper Cold Creek (Basin 1) and were estimated from data collected at HMS and three NWS cooperative stations using the inverse-distance weighting algorithm in DHSVM. No observed precipitation corresponded with flow event 5.

| Storm Event | Precipitation |          | Flow Event | Streamflow    |          |          |                       |
|-------------|---------------|----------|------------|---------------|----------|----------|-----------------------|
|             | $V$ (mm)      | $D$ (hr) |            | $V$ ( $m^3$ ) | $V$ (mm) | $D$ (hr) | $Q_p$ ( $m^3s^{-1}$ ) |
| 1           | 24.6          | 77       | UC1        | 126,100       | 1.71     | 15       | 5.64                  |
|             |               |          | LC1        | 103,800       |          |          | 10                    |
| 2           | 2.8           | 3        | UC2        | 57,990        | 0.79     | 15       | 4.84                  |
|             |               |          | LC2        | 28,410        |          |          | 7                     |
| 3           | 6.6           | 10       | UC3        | 16,070        | 0.22     | 11       | 1.13                  |
|             |               |          | LC3        | 1,635         |          |          | 10                    |
| 4           | 8.3           | 6        | UC4        | 36,540        | 0.50     | 10       | 3.05                  |
|             |               |          | LC4        | 16,100        |          |          | 5                     |
| 5           | 0             |          | UC5        | 31,760        | 0.43     | 32       | 1.64                  |
|             |               |          | LC5        | 11,890        |          |          | 22                    |
| 6           | 13.4          | 23       | UC6        | 110,100       | 1.49     | 19       | 5.83                  |
|             |               |          | LC6        | 73,660        |          |          | 19                    |
| 7           | 9.3           | 6        | UC7        | 93,240        | 1.26     | 20       | 7.95                  |
|             |               |          | LC7        | 54,670        |          |          | 10                    |
| 8           | 3             | 3        | UC8        | 25,500        | 0.35     | 21       | 1.24                  |
|             |               |          | LC8        | 7,785         |          |          | 18                    |

### 3.4 Extreme Event Modeling Based on Observed Streamflow

Initial efforts of this study used the USGS streamflow data set to derive runoff curve numbers (SCS 1972), and estimate potential extreme-storm runoff from the Cold and Dry Creek basins under two hypothetical precipitation events.<sup>(a)</sup> Wigmosta and Guensch derived curve numbers ranging from 78 to 92 for several storm events during January 1995. Precipitation of 68.9 mm (2.71 inches), estimated for the 100-year recurrence interval and seven-day duration, yielded 22.2 to 45.6  $Mm^3$  of runoff and recharge, depending on curve number used. Precipitation of 117 mm (4.6 inches), the estimate of probable maximum precipitation over 6 hours (Skaggs and Walters 1981), yielded runoff of 56.7 to 88.8  $Mm^3$ . The main advantages of the Soil Conservation Service (SCS) curve number method are its simplicity and applicability to situations with minimal data. The primary disadvantages for application to GCC are the assumption that curve numbers derived for Upper Cold Creek are valid for the other basins, and the omission of recharge by

(a) MS Wigmosta and GR Guensch, 2000, *Progress Report: Potential Groundwater Recharge from the Infiltration of Surface Runoff in Cold and Dry Creeks*, Pacific Northwest National Laboratory, Richland, WA.

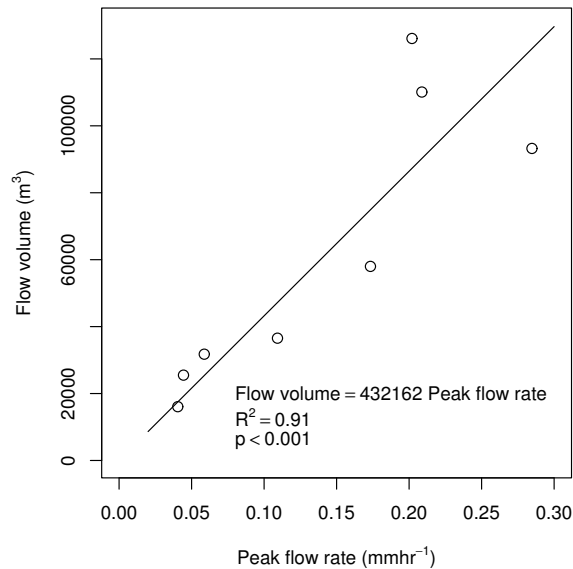


**Figure 3.2.** Flow volume versus peak flow rate at UC, January 1995. This relationship is used with a flow frequency analysis to estimate recharge volume frequency in Appendix D.

**Table 3.3.** Measured streamflow volumes as annualized recharge rates.

| Recharge Source Area                      | Recharge<br>Mm <sup>3</sup> y <sup>-1</sup> | Study           |
|---|---|-----------------|
| Streamflow at UC, WY1995 <sup>(a)</sup>   | 0.497                                       |                 |
| Streamflow at LD, WY1995 <sup>(a,b)</sup> | 0.408                                       |                 |
| Streamflow at LC, WY1991-92               | 0.0037                                      | Dinicola (1997) |
| Streamflow at LD, WY1991-92               | 0.402                                       | Dinicola (1997) |
| Perennial streamflow at LD <sup>(c)</sup> | 0.391                                       | Dinicola (1997) |

- (a) All ephemeral streamflow during water year 1995 occurred in January.
- (b) Based on streamflow during January 1995 only; excludes perennial flow during rest of year.
- (c) Source of perennial flow is Rattlesnake Spring, just upstream from LD.

subsurface flow paths. The SCS method also assumes that probabilities of precipitation and recharge events are equivalent, whereas in reality only some precipitation events have the necessary antecedent soil moisture, soil temperature, and snow pack conditions to result in streamflow.

In subsequent efforts the SCS runoff approach was extended to estimate location of the recharge from runoff by accounting for infiltration in the streambed.<sup>(a)</sup> Weather and the runoff data from the January 1995 storm events were analyzed in greater detail to support a simple runoff/recharge model constructed from SCS methods and an exponential-decay channel infiltration equation proposed by Lane et al. (1985). The model was used to estimate the magnitude and downstream distance of recharge from several design storm events. Most of the predicted recharge occurred more than 15 km downstream from the lower stream gauges, within the broad valley to the west of Highway 240.

In contrast to this event-based modeling, the current study focused on estimating historical recharge using the actual meteorologic record and a physically based model. The fully distributed watershed model DHSVM was used to estimate recharge from both direct infiltration and runoff in the GCC watershed. The time period of interest was the same as in the Hanford modeling activities, 1943 to present, but available meteorology data limited watershed modeling to water years (WY) 1956–2001.

---

(a) SR Waichler, 2002, *Progress Report: Potential Groundwater Recharge from the Infiltration of Surface Runoff in Cold and Dry Creeks*, Pacific Northwest National Laboratory, Richland, WA.

## 4.0 Description of the Distributed Hydrology-Soil-Vegetation Model (DHSVM)

Preliminary estimates of recharge from GCC were computed with DHSVM, a process-based, distributed parameter hydrologic model that allows the simulation of runoff processes in environments with highly variable terrain (Wigmosta et al. 1994, 2002). A particular strength of DHSVM is its grid-based representation of the watershed, allowing specification of terrain, vegetation, and soil at the resolution of an available digital elevation model (DEM). Topographic controls on precipitation, air temperature, and downslope water movement in DHSVM are key to the simulated water balance and streamflow generation.

### 4.1 Basic Structure and Processes

Major processes simulated with DHSVM are canopy interception, evaporation, transpiration, snow accumulation and melt in the canopy and on the ground, vertical unsaturated water flow, and lateral saturated groundwater flow (Figure 4.1).

The major inputs are grid files of surface elevation, soil type, soil thickness, and vegetation type; tables of soil and vegetation biophysical parameter values; and time-series files of the meteorologic

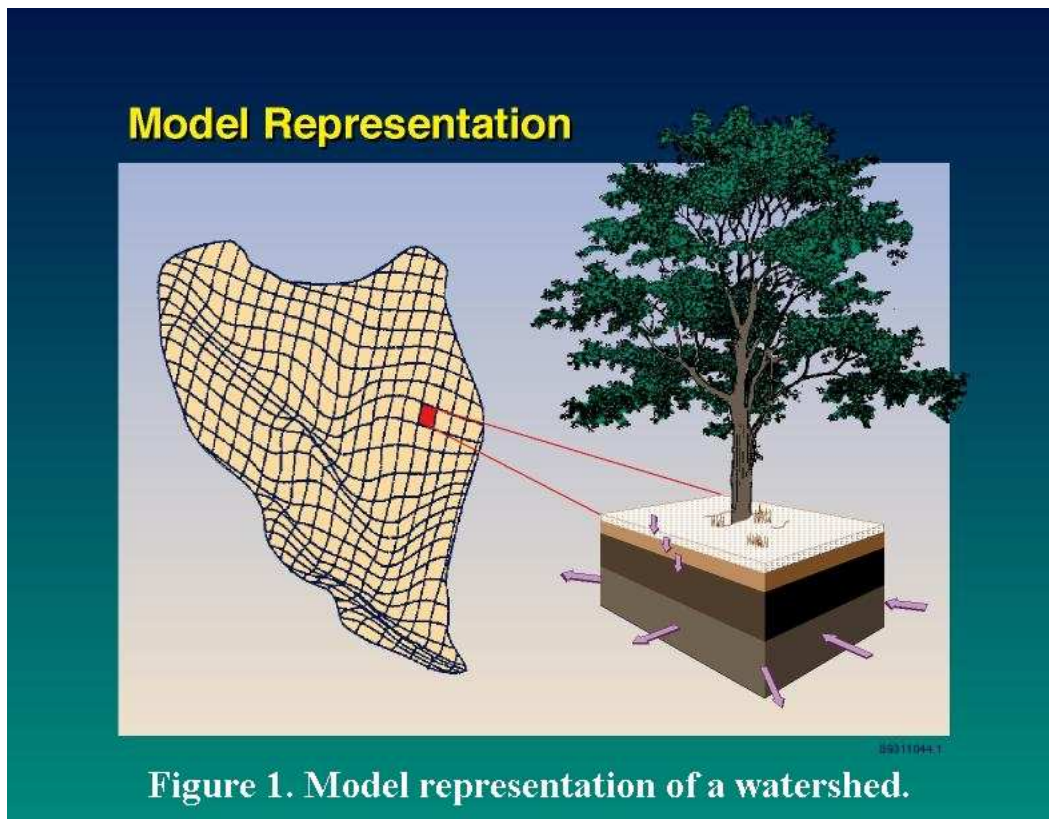


Figure 4.1. DHSVM schematic.

variables air temperature, precipitation, wind speed, relative humidity, solar radiation, and long-wave radiation from one or more stations. In the version used in this analysis, local meteorologic data are mapped to each cell during the model run using lapse rates for vertical distribution of temperature and precipitation and inverse distance weighting for lateral distribution of all variables. Incoming solar radiation is adjusted according to topographic slope and aspect. Canopy evapotranspiration is simulated for each cell with the Penman-Monteith equation and local aerodynamic and canopy resistances. An explicit energy balance approach is used for snow accumulation and ablation, both in the canopy and on the ground. Unsaturated soil water movement is downward only and driven by a unit gradient with hydraulic conductivity as a function of soil moisture content using the Brooks and Corey (1966) equation. Lateral saturated soil water movement is simulated with Darcy's Law, where hydraulic gradient is based on either land surface or water table elevations (the land surface option was used here).

Surface overland flow is generated where the water table rises above the land surface or where infiltration into the soil profile is limited. In humid environments, macropore flow is an important mechanism for streamflow generation and is represented by limiting infiltration into the soil matrix using the Holtan (1961) equation and directing more water into surface runoff than would otherwise be indicated by soils with high infiltration capacity. The surface runoff is then routed using a simple kinematic approach or a hydraulic approach like that of Szilagyi and Parlange (1999). Streamflow is generated by channel interception of surface and subsurface runoff. Vegetation may be represented with up to two layers. An overstory, if present, may cover all or some fraction of the cell. An understory, if present, is assumed to cover the entire cell. Vegetation types ranging from bare soil to low-lying vegetation to closed-canopy forests with understory may be specified in DHSVM. Climate variables are specified at a height above the top of the vegetation. Wind speed and solar radiation are attenuated down through the vegetation layers based on fractional area covered, vegetation height, and leaf area index (LAI). Stomatal resistance is computed separately for each root zone-vegetation layer combination, using soil moisture (Feddes et al. 1978), air temperature, vapor pressure deficit, and solar radiation (Dickinson et al. 1991).

## **4.2 Model Modifications and Improvements**

Water flow processes and pathways in the surface and subsurface that were included for this analysis are shown in Figure 4.2. Several important features depicted in Figure 4.2 were added to DHSVM for this study to make the model more suitable for the arid setting of Hanford. These included:

1. A second groundwater layer to store water that percolates below the perched water table and stream channel bed (shallow recharge)
2. Percolation loss from the second groundwater layer
3. Infiltration through the channel bed for losing streams
4. Soil infiltration limited by freezing temperatures and high moisture content in the upper soil layer

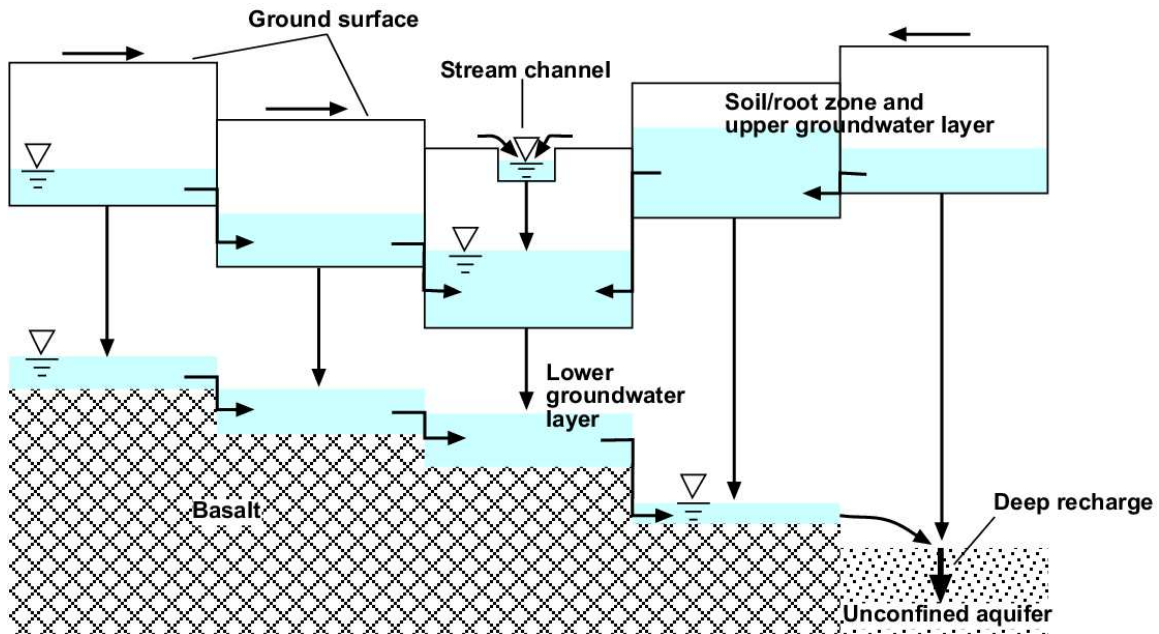


**Figure 4.2.** Surface and subsurface water pathways used in revised DHSVM.

5. Modified cell-to-cell routing of water on the ground surface to better represent overland flow.

The rationale and method for each of these code modifications are described below.

Improvements 1 and 2 allowed us to better account for the fate of groundwater after infiltrating beyond the root zone. A second unconfined groundwater layer was added to facilitate movement below the root zone and represent deeper and slower lateral groundwater movement in the upper part of the unconfined aquifer. This layer in DHSVM is hereafter referred to as the “deep” layer and uses the same cell-to-cell routing method as the upper groundwater layer.

Improvement 3 allowed us to recharge shallow groundwater from the stream channel in those channel reaches where alluvium is thick and the stream is thought to be losing water when flowing. Flow routing in stream channels was modified to include infiltration into the channel bed and the simulation of “losing” streams.

Improvement 5 allowed us to represent a key process in the generation of runoff at Hanford. Infiltration capacity of the soil was limited by freezing temperatures and high soil moisture to simulate the ephemeral runoff-generating conditions at Hanford. A frozen soil condition was defined as the interaction of cumulative heat flux (Cary et al. 1978) and the moisture content of the soil such that colder, more saturated conditions decreased the local maximum infiltration. The method is described in more detail in Section 5.2.1.

Improvement 6 allowed us to maintain and hasten overland flow to the stream channels during runoff events. Overland flow routing was modified to allow faster movement of runoff down the hillslope to simulate the ephemeral “flash floods” of Cold and Dry Creeks.

Along with these changes to model functions, new variables were added to DHSVM to permit mapping of channel infiltration, recharge from the upper to lower groundwater layer, and deep recharge from the lower groundwater layer into a bedrock aquifer.

A more detailed description of the subsurface flow processes and pathways simulated in the revised DHSVM follows. Overland flow, if any, is subject to infiltration in lower grid cells and interception by stream channels (Figure 4.2). Subsurface flow moves in an upper (shallow) layer and a lower (deep) layer. If the shallow water table is below the streambed, the stream may lose water to the shallow water table. Travel time from the streambed to the water table is neglected and the infiltrated water added immediately to the shallow water table in the respective model grid cell. Similarly, water percolates through the upper groundwater layer as Darcian flow, but vertical travel time within the lower layer is neglected, and recharge from the upper layer is added immediately to the lower layer in the respective model grid cell. As implemented here, once water enters the lower groundwater layer, it may not return to the surface as a baseflow contribution to streams. For the current recharge estimates, the underlying basalt is assumed to be impermeable and all deep groundwater follows a lateral flowpath until a cell defined as “unconfined aquifer” is encountered. A very large hydraulic conductivity is defined for the unconfined aquifer, resulting in recharge of all lower groundwater entering such a cell. In the GCC application, the flowpath map for the deep groundwater was set equal to the surface and shallow flowpath map, but the model allows different flow directions.

The other major area of model improvement was in modification of overland flow (surface) routing. Formerly, DHSVM was limited in moving water in overland flow to a rate of one cell per time step. This type of algorithm permits the grid cells to be processed in any order and is relatively inconsequential in areas where little overland flow takes place or where flow paths to stream channels are short. Neither condition prevails in the upper basins at Hanford, however, and the possibility of a different approach was spurred by some limited success in generating sharper hydrographs with DHSVM’s elevation band mode. Therefore, three new options were created for surface flow routing: a linear cascade, limited linear cascade, and a power-law cascade option. Under all three options, grid cells are processed in order of decreasing elevation so that flow from upslope cells are available to downslope cells within the same time step.

In the linear cascade option, surface flow moves from ridgetop to valley bottom within one time step. Infiltration can still occur along the way, but any excess present in a grid cell containing a stream channel is intercepted by the stream in the same timestep. This method represents an upper bound on surface flow rate and assumes that the time of concentration is essentially zero.

A modification of this method, limited linear cascade, is the same as linear cascade except that water moves to the next grid cell only if the current cell had surface water at the start of the time step. In other words, limited linear cascade specifies that surface flow into a cell is halted on that cell if there was no pre-existing ponded water. New water on a cell has a chance to infiltrate during the next time step; if some remains, it is then routed to the next cell.

The power-law cascade is similar to the linear cascade except that only some of the flow is made available to the next downslope cell, leaving some water on the originating cell. In the power-law cascade, even if the hillslope is saturated, not all of the ponded water reaches the channel

in the same time step. In this method, outflow from a cell is based on the power-law equation  $Q = \alpha S^\beta$ , where  $Q$  = outflow,  $S$  = water ponded on the cell (storage), and  $\alpha$  and  $\beta$  are constants. For this report, the limited linear cascade method was used.

## 5.0 DHSVM Application

The application of DHSVM to GCC is based on a conceptual model of adjoining basins containing a soil mantle underlain by either a basalt bedrock surface or the regional water table. Relevant soil and vegetation properties for modeling the entire study area, particularly land outside the Hanford Site, were not readily available in digital format, so the implementation of DHSVM for GCC assumes a uniform, generic arid vegetation rooted in a sandy loam soil with uniform thickness and hydraulic properties. Below the root zone, the model includes an additional unconsolidated layer of unspecified thickness, which is bounded underneath by the bedrock surface or the water table, whichever is higher. Hydraulic gradient and stream channel locations in the model are defined by the land surface topography. The model implementation for GCC assumed that any water entering the lower unconsolidated layer, either by percolation below the root zone in the uplands or by infiltration of streamflow in channels, remained below the surface and was simulated as subsurface flow for the remainder of the simulation. This deep groundwater was assumed to follow the same flow directions as surface water, resulting in subsurface outflow from basins at the same locations as streamflow.

### 5.1 Model Inputs

#### 5.1.1 Topography, Soil, and Vegetation

DHSVM input grid files were prepared at 200-m resolution for all basins. Input grids needed for each watershed include the DEM, mask (for defining basin boundary), soil type map, vegetation type map, and flow direction map. Two soil types were specified: one with an impermeable lower boundary to represent areas where basalt lies above the water table and one with essentially unlimited permeability to represent areas where the water table is the lower boundary (Figure 5.1). All other properties of the two soil types were identical. Vegetation consisted of one generic type, sagebrush-steppe, covering 50% of the ground surface.

Flow direction grids were defined using the standard ArcInfo 8-neighbor method (ESRI 1999) and were based on surface topography for both layers. In the basalt area west of the groundwater model domain (Figure 5.1), surface topography is probably a good approximation of the real flow directions of groundwater. In basalt areas within the central Hanford Site, the real flow directions are probably different because the bedrock surface map diverges from surface topography to a greater degree. However, the resulting error in recharge patterns is probably small and insignificant compared with other sources of error in the simulation, especially the representation of the soil-basalt interface. The thickness of the deep layer in DHSVM is not defined, but a DEM is still specified for this layer to permit calculation of hydraulic gradient used in subsurface flow. The ground surface DEM was used for this purpose.

#### 5.1.2 Meteorology

DHSVM requires the following meteorologic variables for each time step: air temperature, wind speed, relative humidity, solar radiation, longwave radiation, soil temperature, and precipitation. Meteorologic input to the model was developed from hourly data from the HMS and daily precipitation data from three NWS cooperative stations: Moxie City 10 E, Priest Rapids Dam, and

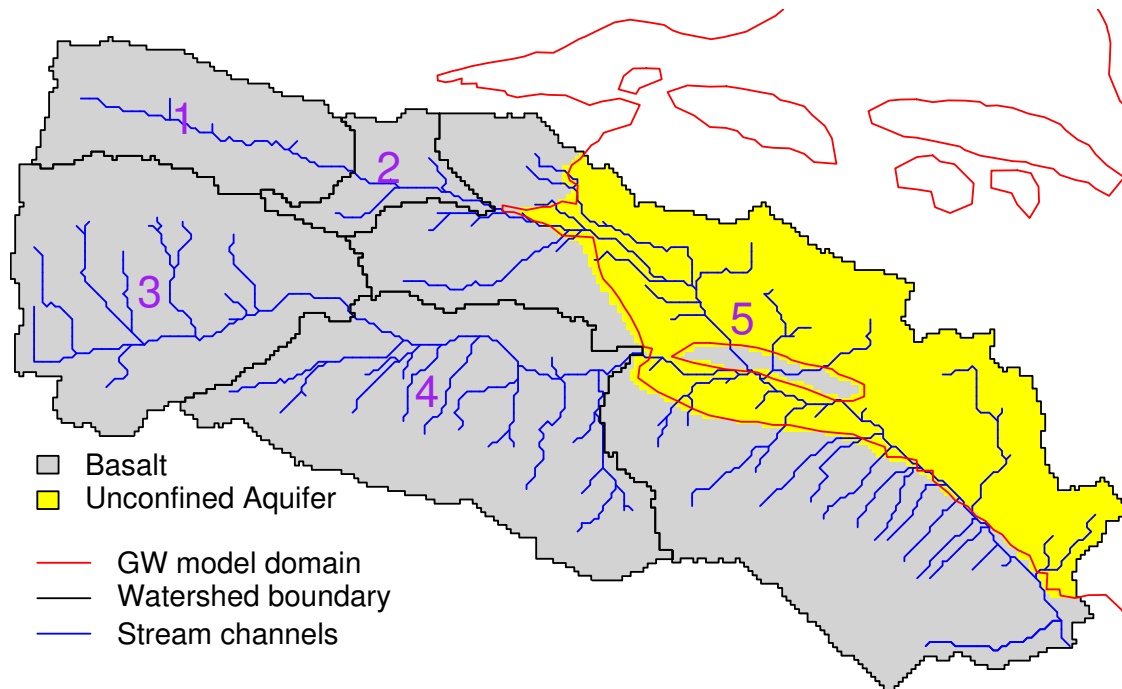


**Figure 5.1.** Lower boundary specification for watershed modeling.

Sunnyside (Table 5.1). HMS hourly data are available beginning January 1, 1955. To initialize DHSVM, it is preferable to begin simulations at a relatively dry time of year; for Hanford’s climate the beginning of the water year, October 1, is ideal. Therefore, a meteorological input for water years 1956–2001 (WY56-01) was created. Inverse-distance weighting of the four met stations and lapse rates from Dinicola (1997) were used to calculate precipitation values at each grid cell. A potential problem with this approach was “smearing”—predicting small amounts of precipitation on more days than actually occurred because some stations are dry while others may have some rainfall on a given day. Complete details of meteorology input derivation for DHSVM are described in Appendix C.

## 5.2 Model Calibration

DHSVM was calibrated by adjusting model parameters to obtain the optimal simulation of two critical facets of the water balance: ephemeral streamflow in Cold Creek during January 1995 and the average annual root zone water balance for a typical undisturbed location on the Hanford Site. The first objective was important because of the project hypothesis that streamflow run-on from GCC is a significant source of natural recharge to the Hanford unconfined aquifer. The second objective was important because we relied on distributed estimates of precipitation and ET to also estimate *total* natural recharge from GCC, which included subsurface as well as surface flow.

**Table 5.1.** Climate stations used to generate input for DHSVM.

| Station                            | Coordinates<br>(lat, long) | Elev.<br>(m) | NWS #  | Start<br>date | Available parameters   |
|------------------------------------|----------------------------|--------------|--------|---------------|--|
| Hanford Met Station <sup>(a)</sup> | 46.563 119.599             | 220          | 453448 | 01/01/55      | Hourly air temperature, precipitation, relative humidity, wind speed, solar radiation, sky cover, atmospheric pressure, etc. |
| Moxie City 10 E <sup>(b)</sup>     | 46 31 120 10               | 472          | 455688 | 06/01/48      | Daily total precipitation, total snowfall, snowdepth, Tmax, Tmin   |
| Priest Rapids Dam <sup>(b)</sup>   | 46 39 119 54               | 140          | 456747 | 12/06/56      | (same as Moxie City)   |
| Sunnyside <sup>(b)</sup>           | 46 19 120 00               | 229          | 458207 | 06/01/48      | (same as Moxie City)   |

(a) Source of HMS data: <http://etd.pnl.gov:2080/HMS/>.

(b) Source of NWS data: <http://wrcc.dri.edu>.

### 5.2.1 Calibration of Streamflow to Observed Runoff in Cold Creek

Calibration of the GCC model focused on runoff measured in Cold Creek during January 1995. Reproducing the observed hydrographs with the model was challenging for at least two reasons:

- Meteorological conditions in Upper Cold Creek had to be inferred from distant stations and therefore were probably significantly different from true local conditions.
- Only a small fraction (13%) of inferred January 1995 precipitation became streamflow, indicating that runoff was generated only under special conditions of meteorology, soil moisture, and snowpack. These conditions are not yet well understood.

The calibration process for the DHSVM model to observed flows in Cold Creek focused on evaluation of model processes that could effect the generation of runoff. Areas initially examined included:

- the water-holding capacity of soil profiles used in the model
- infiltration capacity and snowmelt
- channel infiltration

Discussion of these calibration areas is provided in the following paragraphs.

One way runoff is generated in the model is to exceed the water holding capacity of the soil profile. Because Basin 1, in particular, has thin soils locally, this model process represented a plausible mechanism that was evaluated in the calibration process. Water holding capacity for the simulated soil profile was estimated at 240 mm, so one possible way to generate runoff in the model was to decrease the soil thickness, thereby reducing potential storage in soil. However, we found these adjustments reduced evapotranspiration too much at longer timescales. Another problem with relying on limited water-holding capacity to generate runoff is that the capacity of even a droughty soil profile with an estimated field capacity of 0.1 and thickness of 20 cm is about 20 mm, which is still greater than the amount of precipitation estimated for most events (Table 3.2).

The other way to generate runoff in DHSVM is to limit infiltration of rainfall and snowmelt into the soil. The available meteorology data and field observations (Dinicola, personal communication, 2001) suggest that limited infiltration capacity and snowmelt were indeed important drivers of January 1995 runoff. Three ways of limiting infiltration were investigated: 1) the cumulative heat flux method of Cary et al. (1978), 2) a linear function of snow water content, 3) a combined heat flux and soil moisture content method. In the heat flux method, a threshold of  $-25 \text{ W m}^{-2}$  was used to determine frozen/unfrozen status and to turn infiltration on and off, following the practice of Cary et al. (1978). This method produced a large spurious pulse of runoff during the middle of January 1995 and none at all during the large runoff episode at the end of that month, which was inconsistent with observations. A range of air temperature lapse rates were also evaluated to see whether a different rain/snow partitioning of precipitation would improve the runoff simulation. None did.

The snow water content method was developed as a way to implicitly link the formation of snow and its insulating effect with frozen soil. In this method, infiltration  $i$  was a function of snow water content:

$$i = f i_{\max} \quad (5.1)$$

$$f = \begin{cases} 0 & \text{if } s \geq s_T \\ 1 - s/s_T & \text{if } s < s_T \end{cases} \quad (5.2)$$

where  $f$  is the limiting factor,  $i_{\max}$  is maximum infiltration rate,  $s$  is snow water equivalent, and  $s_T$  is a threshold value of snow water equivalent above which there is no infiltration. Using an optimized value of  $s_T = 17 \text{ mm}$ , the error in total streamflow volume for January 1995 was an acceptable  $-3.7\%$ , but it was determined that the method was too sensitive to  $s_T$  for reliable application over long time-scales, and this method was therefore abandoned.

A combined heat flux-soil moisture content method was developed and used to generate the final results. In this method, factors ranging from 0 to 1.0 that represented soil coldness (cumulative heat flux from it) and soil moisture content were multiplied together to yield the final factor  $f$  that was applied to maximum infiltration. If the cumulative heat flux  $H$  from the soil was greater than or equal to  $-20 \text{ W m}^{-2}$ , maximum infiltration was not reduced; otherwise, the combined method was invoked and Equations 5.1, 5.3–5.5 were used to define  $f$  and reduce maximum infiltration:

$$f = f_{\text{hf}} f_{\text{mc}} \quad (5.3)$$

where  $f_{hf}$  is the heat flux factor and  $f_{mc}$  is the moisture content factor.

$$f_{hf} = \begin{cases} 0 & \text{if } H \leq H_L \\ 1 & \text{if } H \geq H_U \\ \frac{H-H_L}{H_U-H_L} & \text{otherwise} \end{cases} \quad (5.4)$$

where  $H_L$  is a lower bound on heat flux, and  $H_U$  is an upper bound on heat flux. For this application the calibrated values were  $H_L = -33.6 \text{ W m}^{-2}$  and  $H_U = -20 \text{ W m}^{-2}$ . The soil moisture factor was

$$f_{mc} = \begin{cases} 1 & \text{if } \theta \leq \theta_L \\ 0 & \text{if } \theta \geq \theta_U \\ 1 - \frac{\theta - \theta_L}{\theta_U - \theta_L} & \text{otherwise} \end{cases} \quad (5.5)$$

where  $\theta_L$  is a lower bound on soil moisture content, and  $\theta_U$  is an upper bound on moisture content. For this application  $\theta_L$  was set to 0.325, the mean of field capacity and porosity of the upper soil layer, and  $\theta_U$  was set equal to porosity, 0.45.

Limiting infiltration affected the total volume of runoff, but the overland flow routing between grid cells also had to be improved to reproduce the sharp peaks of the observed ephemeral flows. The linear cascade method yielded much sharper peaks than the original DHSVM one-cell-at-a-time routing. The linear cascade method also yielded a simulated hydrograph for the last storm event, whereas the original routing method did not, but it also created a large, unobserved flow event in the middle of the month. The limited linear cascade method was found to yield the best compromise between attempting to match the peak flow timing and rates and the overall flow volumes and was selected for the final simulation.

The last major consideration for simulating streamflow was channel infiltration, or loss of water from the flowing stream. The degree of channel infiltration was calibrated to reproduce the observed reduction in streamflow between UC and LC. All stream segments in rocky, thin-soiled Basin 1, except the last one before UC, were assumed to have non-infiltrating, impermeable stream beds, consistent with observations and inferences of Dinicola (1997). All other stream segments in GCC were assumed to be infiltrating, and the same calibrated rate was applied to each.

Ultimately, however, no combination of methods led to simulated hydrographs that matched the observations well (Figures 5.2 and 5.3). In calibrating DHSVM, we found a tradeoff between streamflow timing and total runoff volume, and it was not possible to do both well for the runoff events observed in January 1995. Given the overall aim of the recharge task and the long time steps of the SGM, we thought it was more important to reproduce the total volume well. Therefore, the final result had a volume error of less than 5 percent, but hourly flow efficiency was negative, indicating that the mean of the observations was a better predictor than the model for these short-term flow rates.

A summary of the calibrated parameters and their final values is given in Table 5.2.

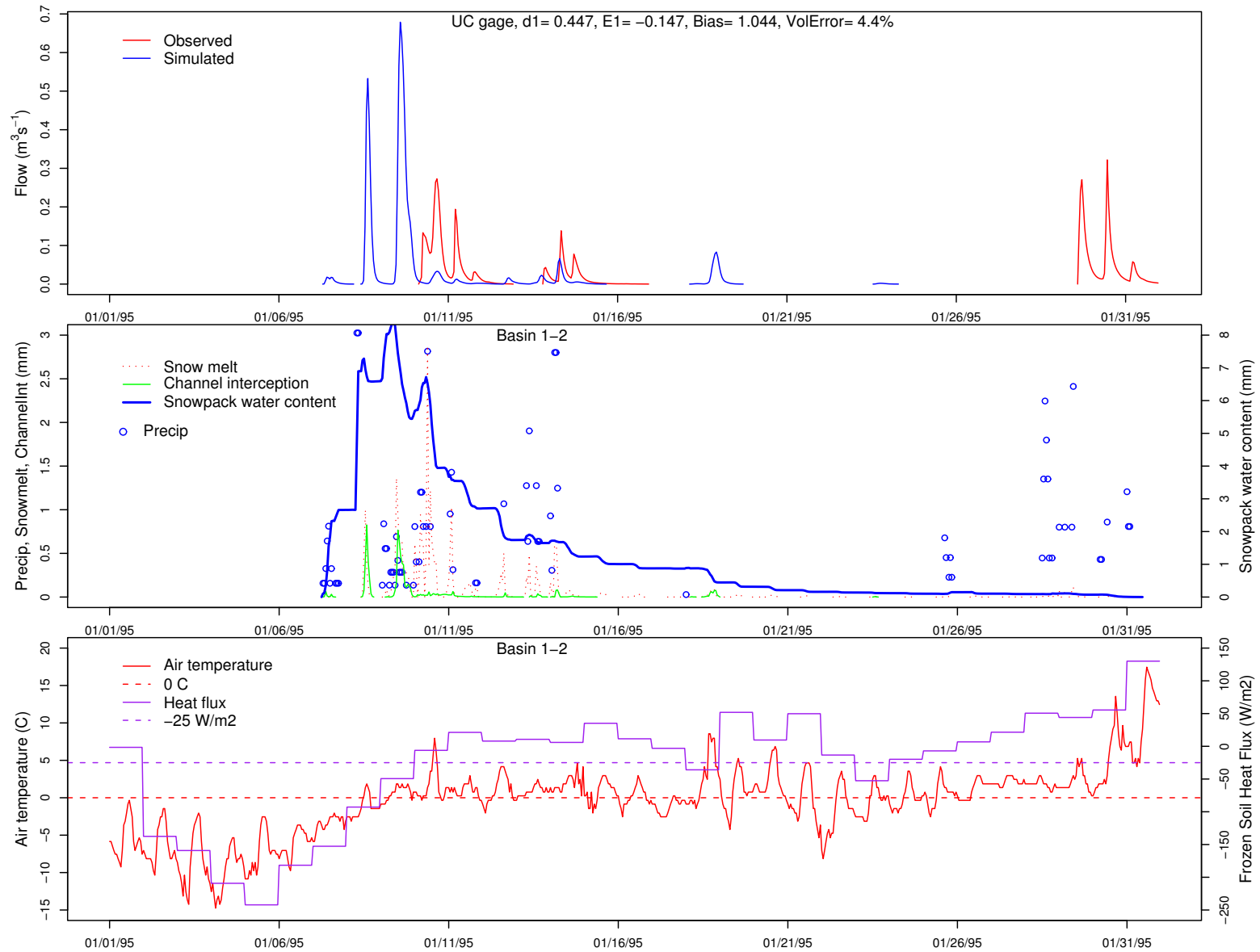


**Figure 5.2.** DHSVM simulation of streamflow at UC gauge and other mean fluxes and state variables over Basins 1 and 2, January 1995. For definition of streamflow goodness-of-fit statistics in top panel, see Appendix B.

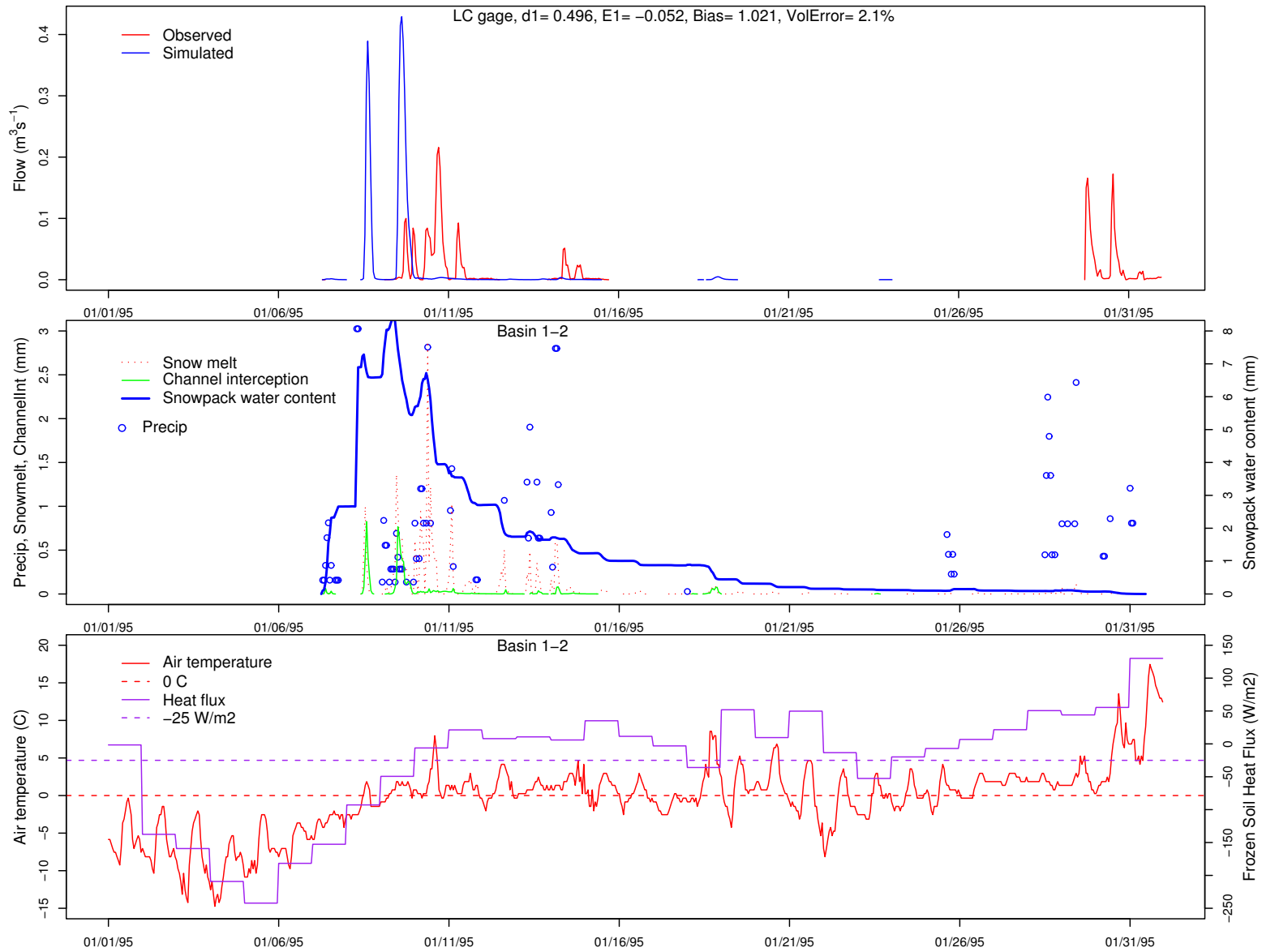


**Figure 5.3.** DHSVM simulation of streamflow at LC gauge and other mean fluxes and state variables over Basins 1 and 2, January 1995

**Table 5.2.** Final values for DHSVM parameters that were subject to calibration<sup>(a)</sup>.

| Parameter                              | Value   |
|--|---|
| Stream channel infiltration rate       | 0.00085 <sup>(b)</sup> m s <sup>-1</sup>                      |
| Soil thickness                         | 1.2 m   |
| Thickness of root zone soil layers     | 0.60, 0.25, 0.15 m  |
| Soil moisture threshold <sup>(c)</sup> | 0.08 <sup>(d)</sup>   |
| Porosity of root zone soil layers      | 0.45, 0.40, 0.30  |
| Field capacity                         | 0.20 <sup>(d)</sup>   |
| Wilting point                          | 0.03 <sup>(d)</sup>   |
| Lateral hydraulic conductivity         | $3.63 \times 10^{-3}$ m s <sup>-1</sup>                       |
| Vertical hydraulic conductivity        | $3.63 \times 10^{-4}$ m s <sup>-1</sup>                       |
| Quick flow coefficient                 | 1.0   |
| Quick flow exponent                    | 5/3   |
| Monthly leaf area index (Jan–Dec)      | 0.8, 0.8, 1.2, 1.5, 2.0, 2.0,<br>1.5, 1.2, 0.8, 0.8, 0.8, 0.8 |
| Lower bound on heat flux, $H_L$        | -33.6 W m <sup>-2</sup>                                       |
| Upper bound on heat flux, $H_U$        | -20.0 W m <sup>-2</sup>                                       |

- (a) The complete input specifications for the final DHSVM model run are in the file /projects/cold\_creek/input/input\_pnnlreport\_04-04.dat.
- (b) Channel bed infiltration was zero for stream reaches in upper Cold Creek.
- (c) Soil moisture threshold is volumetric water content below which stomatal resistance increases.
- (d) As volumetric water content, m<sup>3</sup>m<sup>-3</sup>.

### 5.2.2 Calibration of Evapotranspiration

Besides runoff production, the other major aspect of DHSVM calibration was simulation of ET and vertical water balance. The simulated water balance over whole water years was compared with estimates made in previous studies and adjusted to bring it closer to these previous findings. ET consumes 95 to 99% of precipitation over much of the lower elevation area of Hanford and probably more than 50% of precipitation at higher elevations, so the vertical, one-dimensional water balance of the soil horizon that defines direct recharge is critical to total natural recharge. On silt loam sites, recharge is perhaps only 1 mm/yr, as reported in a study based on chloride isotope analysis (Prych 1994). To calibrate ET in DHSVM, water year 1963 was selected for having HMS precipitation and air temperature closest to the WY1956-2001 averages. We applied DHSVM to a single grid cell near HMS and adjusted soil and vegetation parameters to obtain 100% ET for WY63 (Figures 5.4 and 5.5). To do this, the upper root zone was increased in thickness, the wilting point was decreased, and LAI was increased (Table 5.2). When DHSVM was applied over the entire period of WY56–01 at this location, ET was equal to P and there was no simulated recharge.

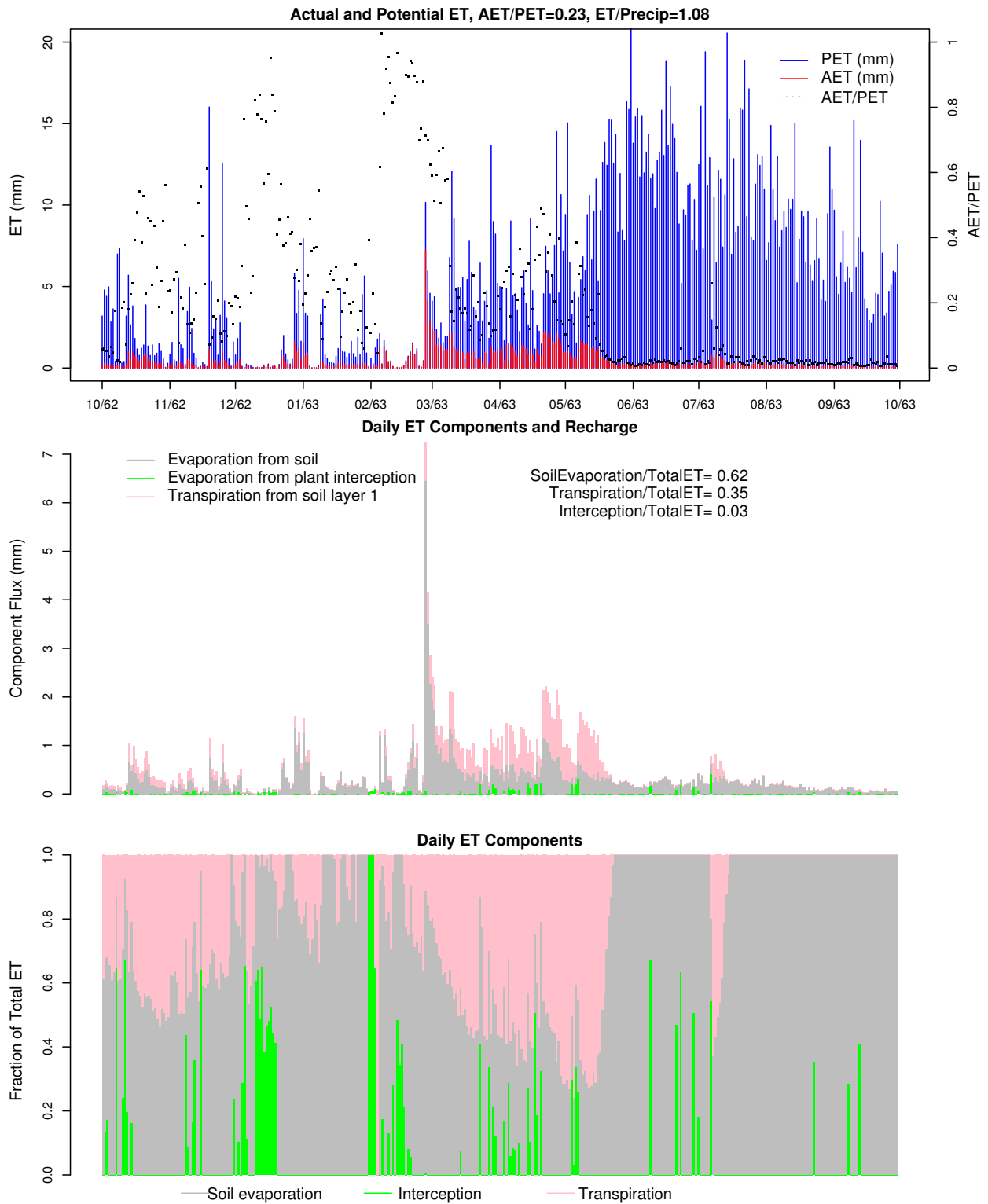


**Figure 5.4.** ET components at a grid cell near HMS, water year 1963. ET exceeded precipitation because of extra soil moisture at start of water year. All transpiration at this location is from the upper soil layer.

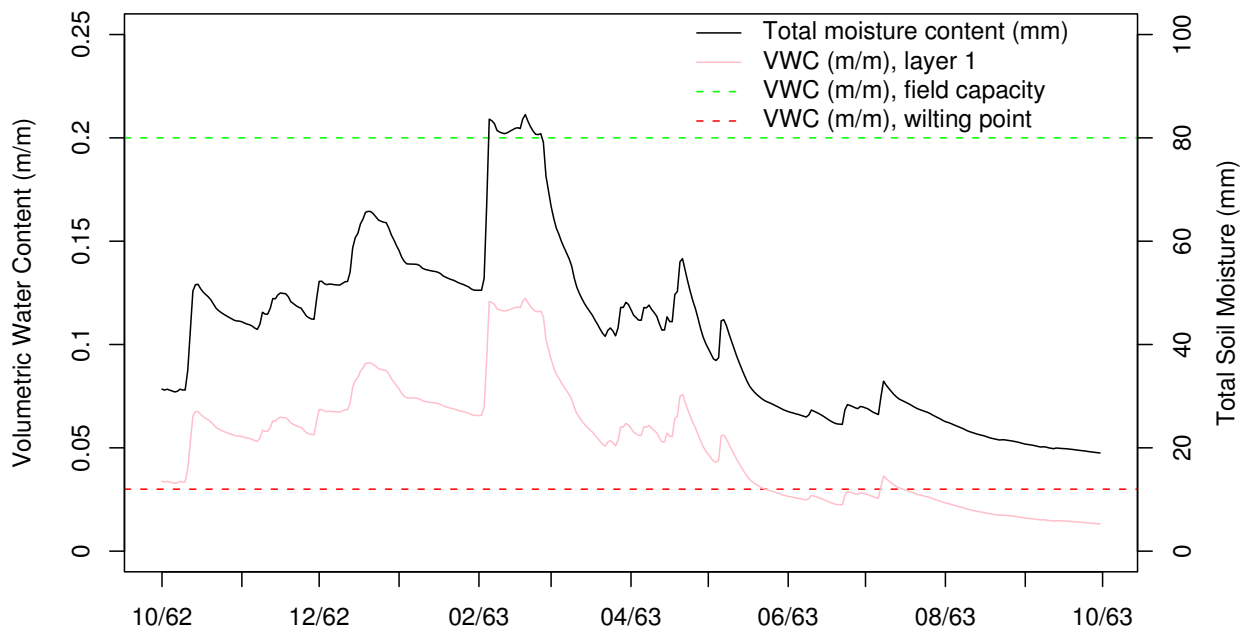


**Figure 5.5.** Soil moisture at a grid cell near HMS, water year 1963. VWC = volumetric water content. Soil evaporation causes volumetric water content of layer 1 to go below wilting point.

After obtaining parameter estimates in the initial calibration of the GCC model, the model was used to simulate the entire time period of WY56-01 to check predicted frequency and magnitude of streamflow events at UC. This initial simulation predicted many more runoff events than are likely to have occurred (Figures 5.6 and 5.7). Every year had at least one daily runoff event greater than 0.5 mm, and there were many daily runoff events greater than 5 mm. In comparison, the largest flow observed in January 1995 was just 1.7 mm. The annual streamflow predictions were also high, with a mean runoff of 28 mm. This was considerably higher than the measured total runoff of just 6.8 mm during January 1995, which we believe was unusual.

The very low runoff ratios of the observed events may indicate that a significant portion of the watershed probably did not contribute any runoff. Many of the overland flow paths (distance to the nearest stream channel) are fairly long, up to 2.5 km in Basin 1. In these kinds of situations, it is less likely that simulated runoff reaches a stream, and greater opportunity exists for the runoff to infiltrate a downgradient cell before reaching the channel. To test this possibility, we also ran DHSVM in elevation band mode, wherein regions of elevation range rather than discrete grid cells are used to provide the spatial model input. In this scheme, each elevation band mode contributed directly to a stream channel, eliminating the possibility of infiltration occurring between runoff generation and interception by the stream channel. Elevation band mode did reduce infiltration and produced sharper hydrographs; however, this general approach could not easily be made compatible with the grid-based system for channel infiltration and recharge and was therefore not considered further.

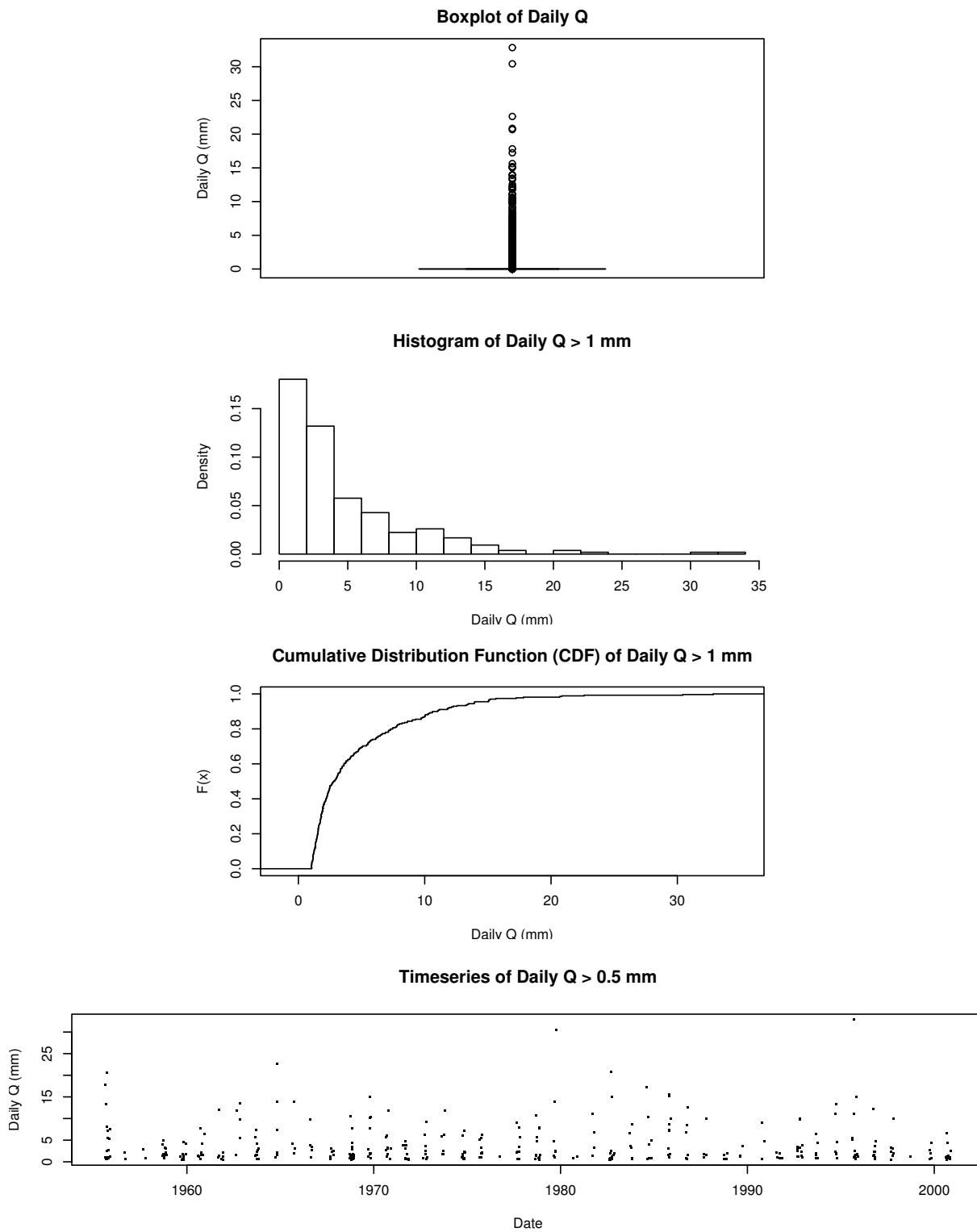


**Figure 5.6.** Daily simulated streamflow at UC, WY56-01

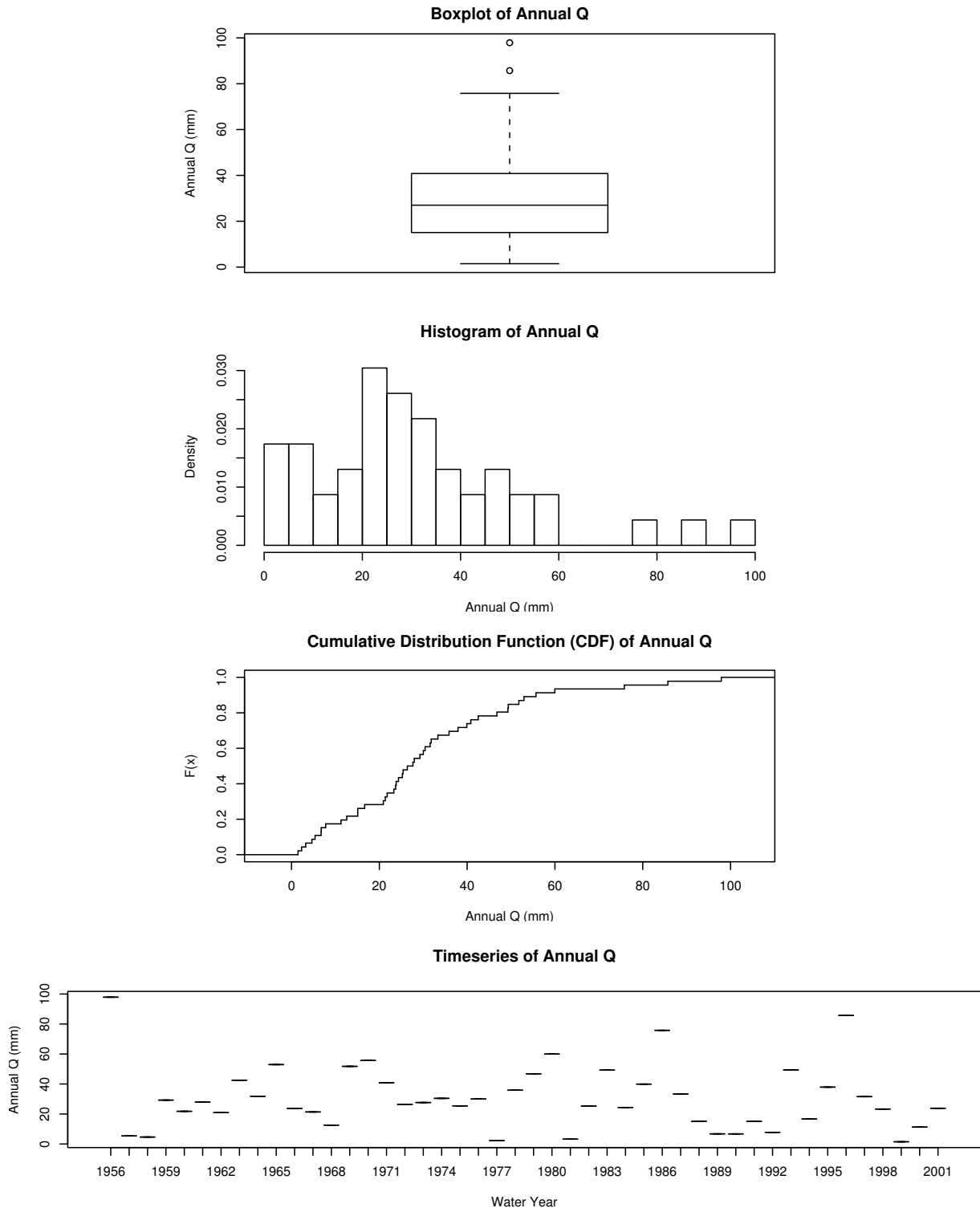


**Figure 5.7.** Annual simulated streamflow at UC, WY56-01

### 5.3 Other Models Evaluated

Lack of initial success in matching observed runoff with DHSVM led us to experiment briefly with the Simultaneous Heat and Water (SHAW) model, which was developed specifically for calculating surface and subsurface water and energy budgets in cold, arid environments [e.g., Flerchinger and Saxton (1989a,b); Flerchinger et al. (1996, 1998)]. SHAW is a one-dimensional model with a high level of process detail about the movement, freezing, and melting of water near the surface, so it is probably the model that adheres most closely to the actual physical processes occurring at a plot scale. Meteorology input for SHAW was generated for eight representative locations in GCC, using the same techniques as before. Unfortunately, SHAW did no better than DHSVM in predicting runoff; like DHSVM, it predicted a persistent snowpack during January 1995 and failed to predict the timing of runoff well.

Difficulty in simulating the ephemeral flows during January 1995 with the process-based models led us to analyze the available data further to see whether any strong empirical relationships could be found between meteorological conditions and streamflows. Such relationships might lead to improvement of certain aspects of DHSVM or even replace this physically based modeling approach. Regression models were used to relate January 1995 streamflow to mean basin air temperature and precipitation. Runoff production in the real system depends on antecedent conditions, particularly soil moisture and freezing conditions, as well as rainfall and snowmelt over the short period of the hydrograph. Antecedent conditions were accounted for by using windows of prior total precipitation and mean air temperature as the regressor variables (Figure 5.8). A fairly exhaustive search was conducted involving hundreds of different models, using various combinations of regressor terms and timescales for aggregating them (Table 5.3). Interaction terms were included to account for the important condition of combined precipitation and cold temperatures to create a frozen soil surface. Models having the highest R-squared used a moving window for streamflow and the longest aggregation period (48 hours). However, this resulted in

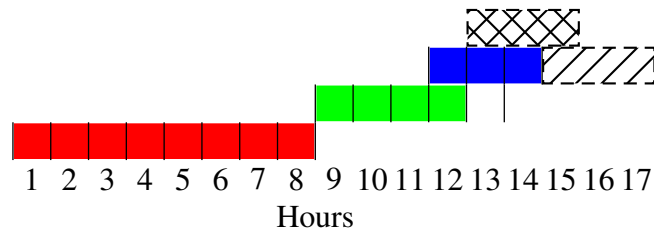


**Figure 5.8.** Schematic diagram of time windows used in regression modeling of streamflow at UC. Blue window, for streamflow  $Q$ , is 3 hours long, and centered on hour 13. Green window, 5 hours long, is first backward-looking window from hour 13, used for antecedent precipitation  $P$  and air temperature  $T$ . Red window, 8 hours long, is second backward-looking window, also for  $P$  and  $T$ . The next streamflow window is shown for discrete windowing (diagonal lines), and moving windowing (cross-hatched). Optimal window sizes for Cold Creek were much longer; see text.

**Table 5.3.** Options used in regression models relating streamflow at UC to precipitation and air temperature, January 1995.

| Model parameter                                    | Parameter values   |
|--|--|
| Response variable                                  | $Q$ , streamflow (mm over Basin 1)   |
| Independent (regressor) variables                  | Precipitation, $P$ (basin mean, mm); air temperature, $T$ (basin mean °C).   |
| Type of window for aggregation                     | Discrete and moving. Discrete used adjacent, non over-lapping windows on the hourly input. Moving used consecutive windows overlapping by (WindowSize - 1) hours.                |
| Window “view” for aggregation                      | Centered and Backward. Centered used an equal number of hours on either side of the time step (WindowSize/2, rounded down). Backward used WindowSize hours before the time step. |
| Window size (hours) for response variable $Q$      | 1, 4, 6, 12, 24, 48  |
| Window size (hours) for regressor variables $P, T$ | 4, 6, 12, 24, 48   |
| Aggregation function                               | Total for $Q, P$ ; mean for $T$  |

only 14 data points for the month-long period of interest. For this reason and to facilitate direct comparisons with DHSVM output, the highest-ranking model with a discrete, 24-hour window for streamflow  $Q$  was selected:

$$Q = 0.0404276 P_1 + 0.0160439 P_1 T_1 - 0.0048434 P_1 P_2 T_2 \quad (5.6)$$

In this model, precipitation  $P_1$  and air temperature  $T_1$  were summed and averaged, respectively, over 48 hours ending at the center of the streamflow window;  $P_2$  and  $T_2$  were summed and averaged over the 24 hours before  $P_1$  and  $T_1$ . For this model,  $R^2 = 0.91$ ; overall p-value < 0.0001; and each model term was significant with individual p-value < 0.0001 (Figure 5.9). However, when this regression model was applied to whole water years, it too predicted too-frequent runoff events, with an average annual streamflow of 52 mm from Basin 1, or more than seven times the January 1995 flow. Overall, the regression model predicted a higher mean and less variable runoff than DSHVM (Figures 5.10 and 5.11).

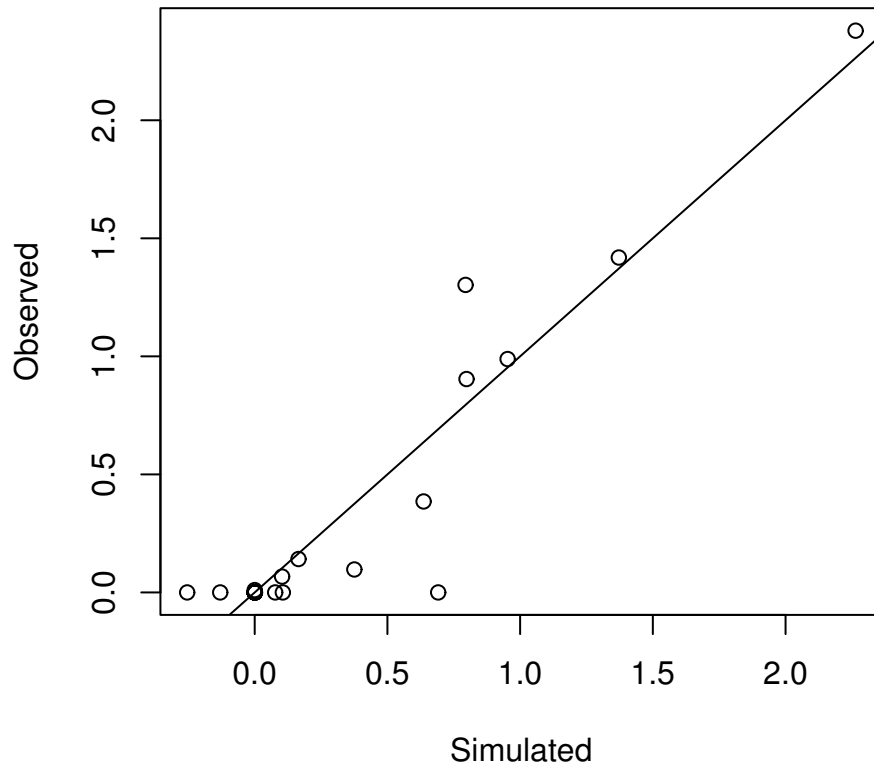


**Figure 5.9.** 1:1 plot for best-fitting regression model of daily streamflow at UC, in mm over Basin 1.

Streamflow (mm), Basin 1, 200m, WY56-01, Regression

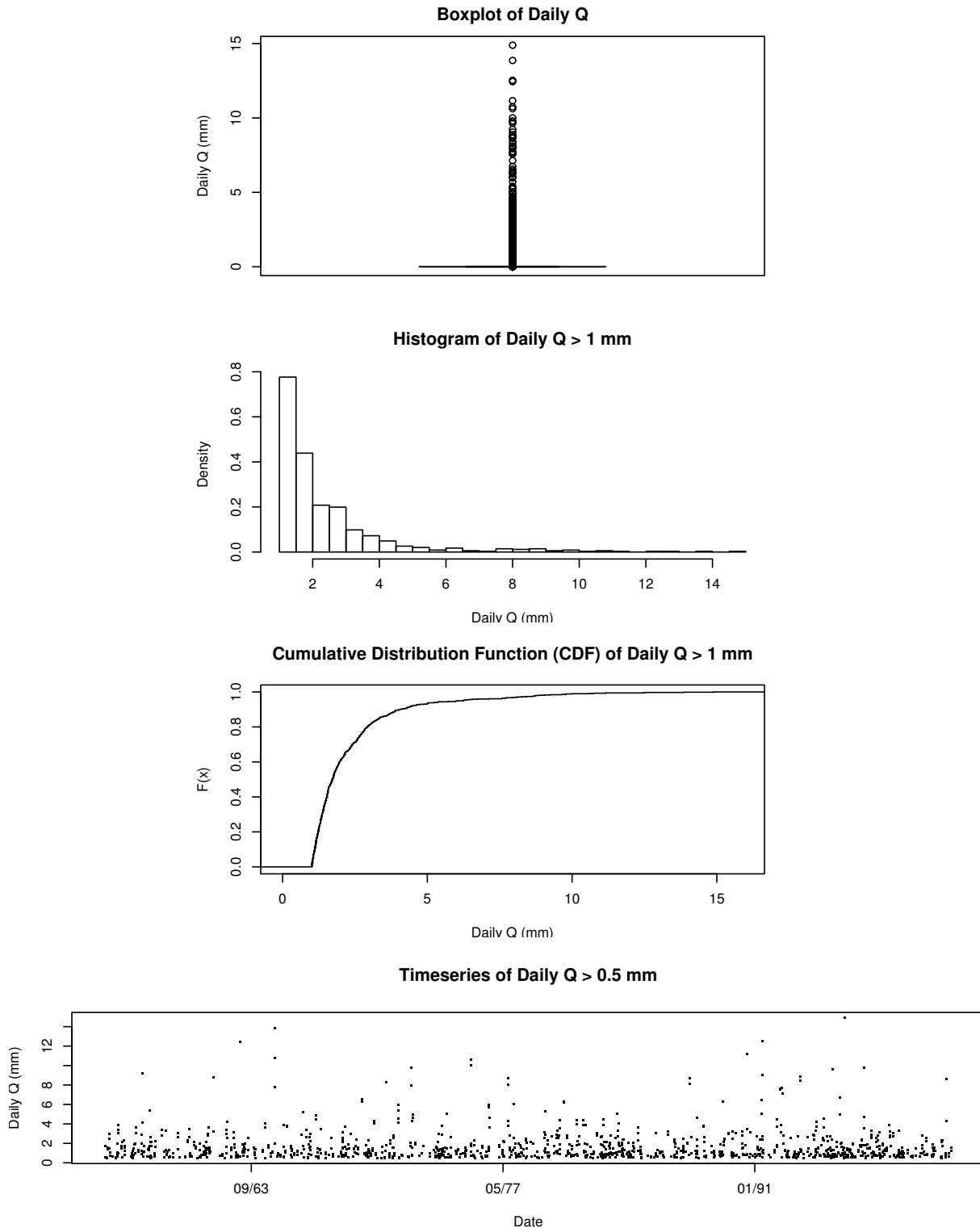


Figure 5.10. Daily regression model streamflow, WY56-01

Streamflow (mm), Basin 1, 200m, WY56-01, Regression

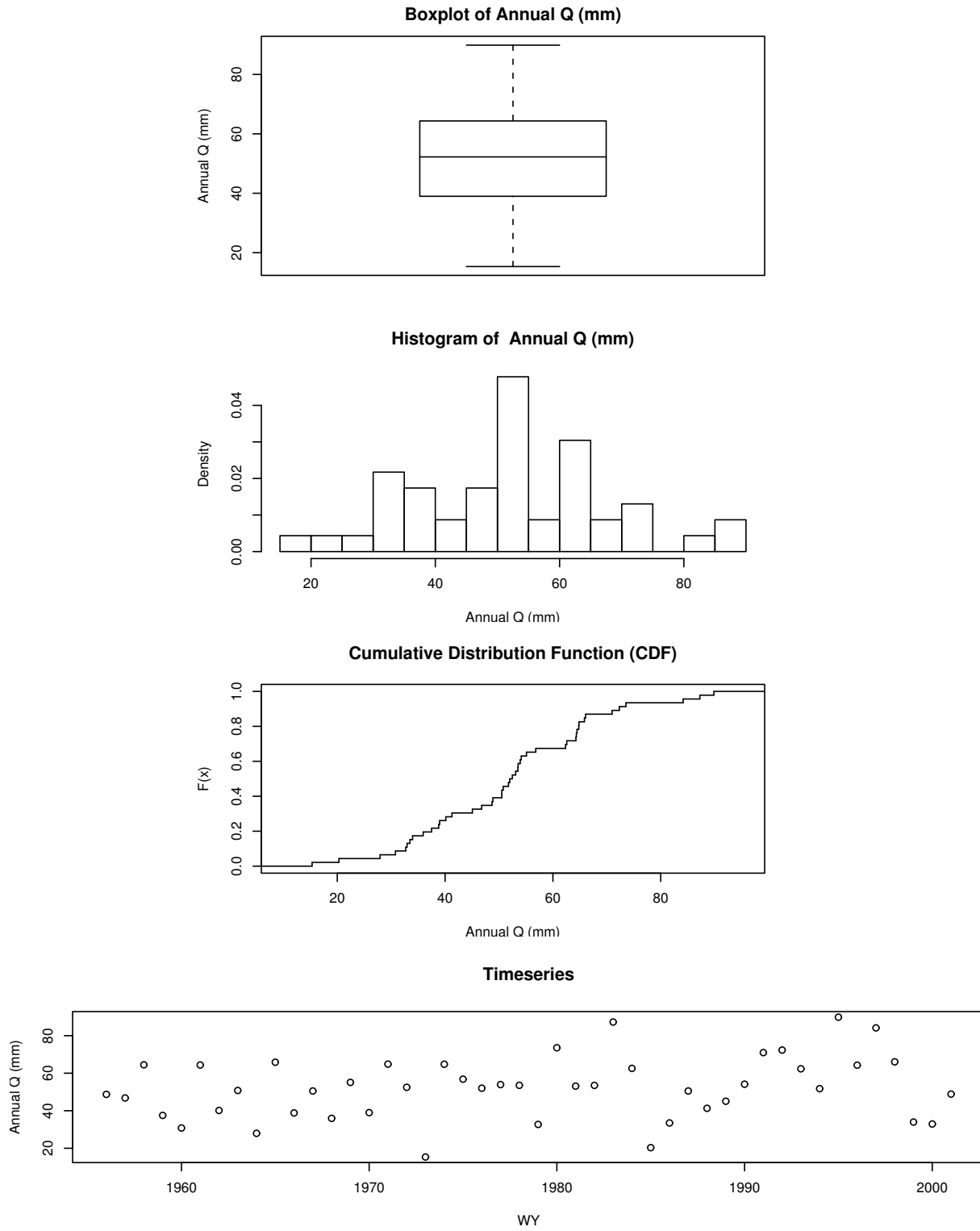


Figure 5.11. Annual regression model streamflow, WY56-01

## 6.0 Results

Estimates of recharge to the Hanford unconfined aquifer from GCC were generated by running DHSVM over WY56-01. We focused on the difference between precipitation and ET (P–ET) over the entire area of GCC as the basis for estimating recharge rather than the actual spatial and temporal distribution of water flow to the water table for the following reasons:

- Initial simulation of GCC streamflow with DHSVM did not have sufficient skill to justify general implementation of the results,
- Simulations with the SGM use a six-month time step during the historical period of interest (1943–present), so a fine temporal resolution of recharge is not appropriate or needed,
- Consideration of P–ET is simpler and more directly comparable to previous recharge studies such as Fayer and Walters (1995) and Bauer and Vaccaro (1990).

Using P–ET within the GCC model as the estimate of water flux from GCC into the SGM domain provides a reasonable upper bound on the recharge estimate because the conceptual model assumes that the basalt bedrock surface in GCC is impermeable and that all precipitation within GCC not consumed by ET reaches the Hanford Site as surface or subsurface flow. In reality, some portion of the water moving below the root zone percolates into the basalt and recharges that aquifer instead of flowing over the basalt surface. The magnitude of this flux is unknown. The upper-bound mean annual recharge rates that correspond to the various regions within GCC are given in Table 6.1. The regions are shown in Figure 6.1

Normalized to land area, Basins 1 and 2 had the highest annual precipitation, 207 mm, and yielded the highest recharge rate, 29 mm, which corresponds to a recharge rate of  $2.915 \text{ Mm}^3\text{y}^{-1}$ . The

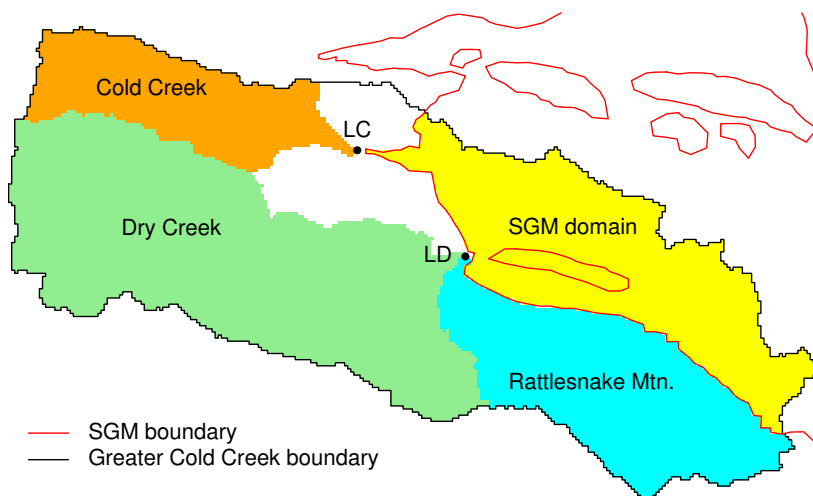


**Figure 6.1.** Reference areas for recharge estimates listed in Table 6.1. Non-SGM area is all of GCC west of the SGM domain.

**Table 6.1.** Simulated fluxes for regions in GCC.<sup>(a)</sup> For extent of regions, see Figure 6.1.

| Region                    | Area<br>(km <sup>2</sup> ) | P<br>(mm y <sup>-1</sup> ) | P<br>(Mm <sup>3</sup> y <sup>-1</sup> ) | ET<br>(mm y <sup>-1</sup> ) | P-ET<br>(mm y <sup>-1</sup> ) | P-ET<br>(Mm <sup>3</sup> y <sup>-1</sup> ) | Streamflow<br>(Mm <sup>3</sup> y <sup>-1</sup> ) | RR   | ACM-2<br>(Mm <sup>3</sup> y <sup>-1</sup> ) |
|---------------------------|----------------------------|----------------------------|---|-----------------------------|-------------------------------|--|--|------|---|
| Basins 1 and 2 (Cold Cr.) | 101                        | 207                        | 20.81                                   | 178                         | 29                            | 2.915                                      | 2.118  | 0.14 | 11.72                                       |
| Basins 3 and 4 (Dry Cr.)  | 317                        | 188                        | 59.61                                   | 168                         | 20                            | 6.235                                      | 0.829  | 0.10 | 7.122                                       |
| Rattlesnake Mountain      | 164                        | 177                        | 28.96                                   | 160                         | 17                            | 2.780                                      |  | 0.09 | 1.023                                       |
| SGM portion of GCC        | 182                        | 157                        | 28.53                                   | 147                         | 10                            | 1.874                                      |  | 0.06 |   |
| non-SGM portion of GCC    | 666                        | 187                        | 124.6                                   | 166                         | 20                            | 13.33                                      |  | 0.10 |   |
| SGM Domain <sup>(b)</sup> | 810                        | 167                        | 135.3                                   | 156                         | 11                            | 8.470                                      |  | 0.07 | 8.583                                       |

(a) P = precipitation, ET = evapotranspiration, RR = recharge ratio, (P-ET)/P

(b) Recharge estimate for “future Hanford Site” from Fayer and Walters (1995); ET calculated as difference between HMS P and recharge

recharge rate from Rattlesnake Mountain was similar at  $2.780 \text{ Mm}^3\text{y}^{-1}$ . The largest volume of recharge was generated by the largest area, Dry Creek, at  $6.235 \text{ Mm}^3\text{y}^{-1}$ . For the entire GCC area that is not part of the SGM, the recharge rate was  $13.33 \text{ Mm}^3\text{y}^{-1}$ , equivalent to 10% of precipitation in the watershed.

Overall, the recharge estimates from modeling GCC with DHSVM are similar to values from previous studies. The recharge rates for Cold Creek Valley in this study are similar to estimates made by Bauer and Vaccaro (1990), and Jacobson and Freshley (1990). Recharge rates for Dry Creek Valley and the portion of GCC that overlaps with the SGM domain were estimated at approximately  $10 \text{ mm y}^{-1}$  in this study and studies by Bauer and Vaccaro (1990), and Fayer and Walters (1995). However, the average recharge rate over the non-SGM portion of GCC was  $20 \text{ mm y}^{-1}$ , or almost double the mean rate of  $11 \text{ mm y}^{-1}$  for the SGM as estimated by Fayer and Walters (1995).

Streamflow was explicitly tracked at the four former gauging stations at the bottom of Basins 1 through 4, allowing a breakdown by type of recharge flux from those basins. For Rattlesnake Mountain and the SGM area, streamflow had short flowpaths when present at all and was not a significant component of recharge. Perennial flow in lower Dry Creek from Rattlesnake Springs was not specifically simulated with DHSVM but was assumed to be adequately accounted for in the total recharge from Basins 3 and 4. In this initial simulation study, streamflow made up 13% of total recharge from Dry Creek Valley, but 73% of the recharge from Cold Creek Valley. The estimate for Cold Creek Valley is probably excessive given the available field data and anecdotal information about that area.

Some of the maps of distributed fluxes that were used to compute the mean recharge fluxes are shown in Figures 6.2–6.4. The maps show the distribution of precipitation, shallow recharge, channel infiltration, and deep recharge to the unconfined aquifer. If opportunities for distributed model verification improve in the future, or if spatial distribution of recharge becomes more important to future groundwater modeling predictions, such maps will be available for further analysis.

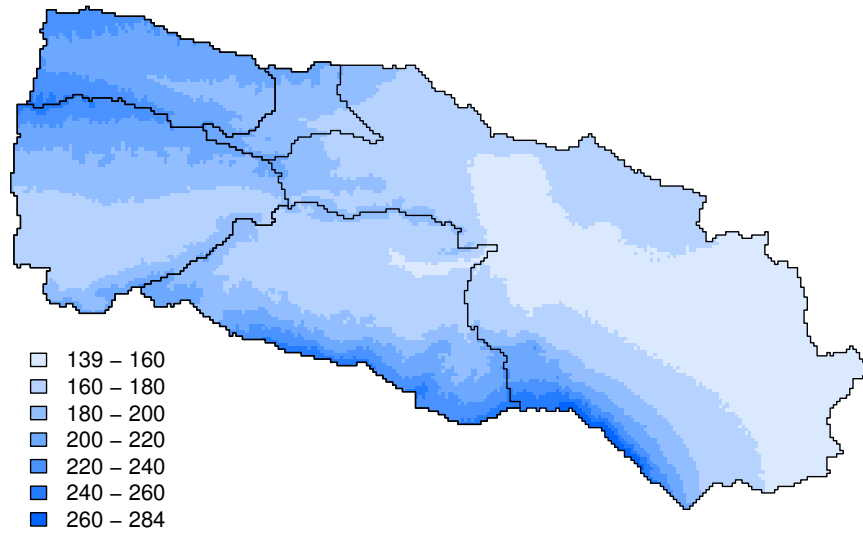


**Figure 6.2.** Map of mean annual precipitation ( $\text{mm y}^{-1}$ )

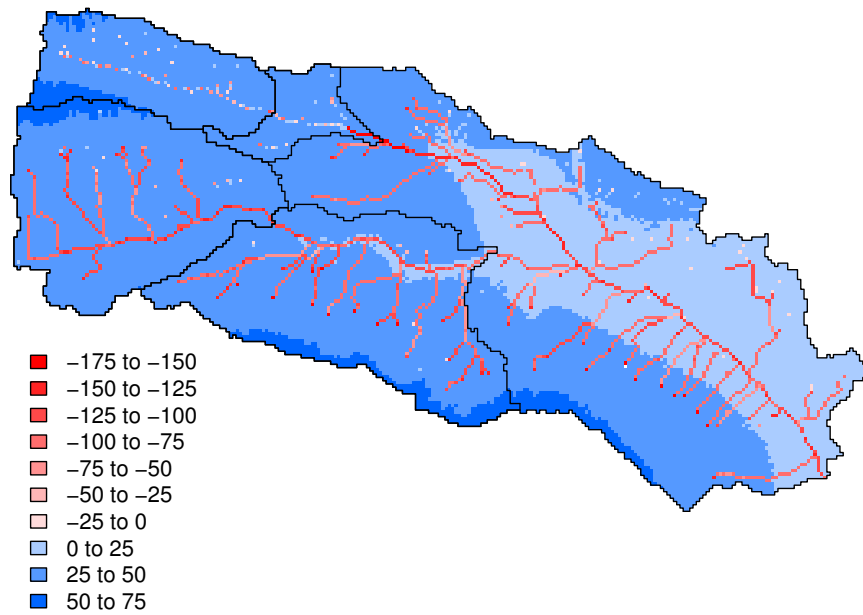


**Figure 6.3.** Map of mean annual precipitation minus ET ( $\text{mm y}^{-1}$ ). Red areas are stream channels where water collected from uplands drives high ET.

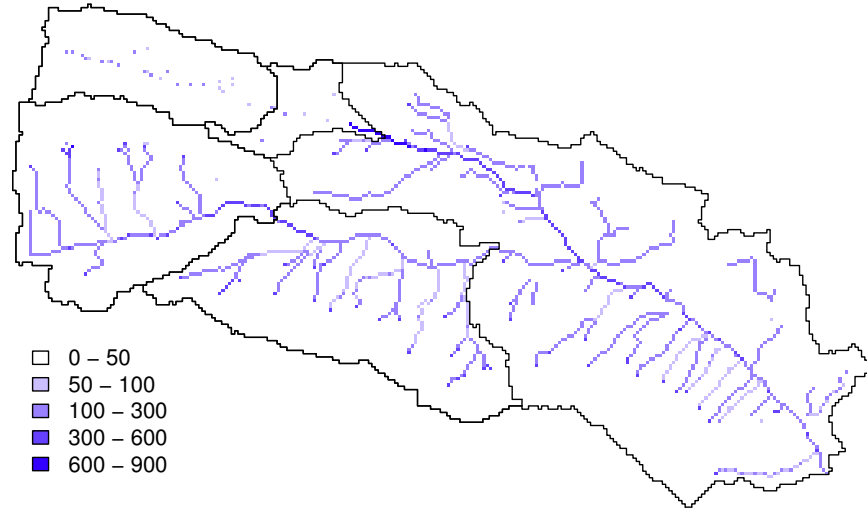


**Figure 6.4.** Map of mean annual shallow recharge ( $\text{mm y}^{-1}$ ). Most recharge is simulated in high elevation areas and stream channels.



## 7.0 Discussion

The hydrology of GCC was simulated over most of the HMS period of record, providing an initial, comprehensive framework for evaluating the water balance for this large watershed draining into the Hanford Site. Methods were developed to distribute meteorology and simulate the key characteristics of this arid environment, including runoff during frozen soil episodes, channel infiltration (losing streams), deep vadose zones, and the duality of basalt versus water table for lower boundary. The framework is now established to estimate recharge to the SGM along its western boundary with high spatial and temporal resolution.

The amount of recharge contributed by GCC to the area of the SGM is still uncertain, however. Conceptually, recharge to the SGM domain from GCC can be stated as

$$R = P - ET - G \quad (7.1)$$

where R is SGM unconfined aquifer recharge from GCC, P is precipitation in GCC, ET is evapotranspiration in GCC, and G is basalt aquifer recharge in GCC. Change in storage and recharge to the SGM unconfined aquifer from the basalt aquifer are neglected in Equation 7.1. Therefore, P, ET, and G are the fundamental quantities for long-term recharge estimates and contain all of the significant uncertainty. If appropriate bounds are identified for these terms, the likely range for R can be estimated.

### 7.1 Recharge in Sitewide Groundwater Model ACM-2

The simulated recharge rates (P–ET) for Cold Creek, Dry Creek, and Rattlesnake Mountain were used as initial values in the calibration of the SGM for the second alternative conceptual model (ACM-2), as reported by Vermeul et al. (2003). That study presented the second Alternative Conceptual Model (ACM-2) for the SGM and included, in addition to artificial recharge, five sources of natural recharge: recharge from GCC, direct recharge from precipitation and snowmelt within the SGM domain, areally distributed leakage from the underlying basalt aquifer, leakage from faults in the basalt aquifer, and leakage from an area of the basalt aquifer where the upper part has been removed by erosion (Table 7.1). The natural recharge rates used in ACM-2 were a combination of *a priori* estimates and calibrated values computed by inverting the SGM. The direct recharge rate in ACM-2 was the Fayer and Walters (1995) estimate of  $8.583 \text{ Mm}^3\text{y}^{-1}$ . The recharge rates for areally distributed leakage from the basalt aquifer and leakage from the basalt erosional window were also based on *a priori* estimates. In contrast, the final ACM-2 rates for recharge from GCC and the basalt aquifer faults were calibrated; the calibration process used *a priori* estimates as the initial values. For the GCC recharge estimates the initial values were those found for this report. Recharge from GCC was simulated in ACM-2 as a constant-flux boundary condition for selected nodes near LC, LD, and along the SGM boundary adjacent to Rattlesnake Mountain. The actual calibration was performed on factors that scaled the base recharge rate at the select cells, where the base rate was equal to the direct recharge rate.

In the final recharge estimates for ACM-2 by Vermeul et al. (2003), GCC was the largest source of total natural recharge (68%), followed by direct recharge 29%. The inverting process for ACM-2 led to recharge values that were four times higher than the DHSVM estimate for Cold Creek, 14% more for Dry Creek, and 63% less for Rattlesnake Mountain (Table 6.1). Although

**Table 7.1.** Recharge rates from all sources in ACM-2 of the SGM (Vermeul et al. 2003). Rates were either fixed or subject to calibration.

| Recharge Source                      | Flux (Mm <sup>3</sup> y <sup>-1</sup> ) | Calibrated |
|--------------------------------------|---|------------|
| Recharge from GCC                    |   |            |
| Cold Creek Valley                    | 11.72                                   | •          |
| Dry Creek Valley                     | 7.122                                   | •          |
| Rattlesnake Mountain                 | 1.023                                   | •          |
| Total from GCC                       | 19.87                                   |            |
| Direct recharge                      | 8.583                                   |            |
| Leakage from basalt faults           | 0.354                                   | •          |
| Areally distributed basalt leakage   | 0.325                                   |            |
| Leakage from basalt erosional window | 0.080                                   |            |

much larger than estimates made here, the estimates by Vermeul et al. (2003) for GCC are less than precipitation in the corresponding watersheds and therefore fall below a realistic upper limit. However, the ACM-2 recharge rate from Cold Creek Valley is equal to 56% of precipitation in that basin and is probably excessive considering that evapotranspiration consumes over 95% of precipitation on the Hanford Site.

## 7.2 Future Improvements

The initial efforts to model GCC had several limitations. Currently, precipitation in GCC can be estimated only with data from meteorology stations located outside the watershed and at low elevations. A proposal has been made to measure meteorology and streamflow at four locations within Cold and Dry Creek Valleys. Such data would allow for characterization of local meteorology with much greater accuracy and lead to new insights about how runoff is generated.

Estimation of ET would also benefit from more accurate local meteorology, but the main improvement for modeling ET in GCC will come from more use of previous studies to constrain DHSVM simulations and from distributed soil and vegetation data. In this study, only a rough correspondence to previous field and modeling work was attempted, and uniform soil and vegetation properties were assumed in modeling GCC. The next logical step would be to systematically review previous findings regarding ET and its relationship to soil and vegetation types at Hanford, and incorporate these refinements into DHSVM.

The recharge to the basalt aquifer, G, is the most difficult part of the water balance to evaluate. No data exist to allow direct characterization of the basalt bedrock surface and the connectedness of the basalt aquifer to the overlying vadose zone in high elevation areas, although maps of basalt groundwater potential suggest that upper elevations do represent areas of recharge to that aquifer (Vermeul et al. 2001, 2003). Previous studies typically assumed that all water moving below the root zone in areas with shallow bedrock enters the basalt aquifer and is lost from the unconfined flow system. However, it is also plausible and likely that some of the water that recharges the

basalt aquifer may leak into the unconfined aquifer at a downgradient location. An upper bound on estimates of recharge from GCC to the SGM area follows from assuming that the bedrock surface is impermeable, forcing water percolating below the root zone to eventually enter the unconfined sedimentary aquifer at some downgradient location. A lower bound on SGM recharge follows from assuming the opposite—that all water reaching the bedrock surface is lost from the watershed flow system. Previous studies have not addressed both possibilities and have typically made one of two assumptions regarding recharge from GCC to the Hanford unconfined aquifer: 1) streamflow runoff is the only significant contribution or 2) only precipitation falling on alluvial areas near the SGM is available for recharge. The first view neglects all subsurface flow from GCC, and the second view neglects subsurface flow from upper elevations and areas underlain by basalt. This study established a modeling approach to explicitly evaluate the significance of these and similar assumptions.

Further sensitivity analysis to the results of this study will be conducted with the SGM to evaluate whether the range of recharge rates indicated here and modes of recharge are significant for key groundwater modeling predictions. Modes of recharge could include streamflow runoff versus subsurface flow, and concentration of subsurface flow near stream channels versus more distributed recharge along a greater length of the SGM boundary. Significant sensitivity of the SGM to either total recharge or its mode would help guide further modeling analysis of GCC.

Another potential improvement to the watershed model is using a regional flow frequency analysis (see Appendix D) to improve the calibration of DHSVM with respect to streamflow predictions. That analysis provides a much longer perspective than the January 1995 flow data and would provide a basis for eliminating many of the spurious runoff events currently predicted by DHSVM. The flow frequency analysis also indicated that Cold Creek runoff events are at the low end of what is typical in the region, suggesting that either the Cold Creek watersheds are inherently less prone to generating flows or that the available data set is insufficient. This is another reason to undertake a field measurement program that includes reactivating stream gauges at Basins 1–4.

If the SGM is also sensitive to the spatial distribution of channel infiltration, the modeling approach would need to incorporate channel and floodplain widths in a more informed and systematic way. Channel morphologies of Cold and Dry Creeks change significantly below the lower gauges, and active channel widths probably vary considerably along channel and through time during flow events. Anecdotal descriptions of past runoff events describe small lakes forming below the lower gauges on the low-gradient valley floor (Dinicola, personal communication, 2001), so improved modeling of the spatial distribution of channel infiltration would require more data on channel and floodplain widths.

The temporal distribution of recharge over long time periods was not evaluated in this study. DHSVM simulations provide the capability to look at the effects of extreme weather and ephemeral flows from timescales of hours to years. In contrast, SGM runs on a semi-annual time step, and the recharge estimates have been aggregated to mean annual values. If it is found that SGM predictions are sensitive to short-term recharge fluctuations, the temporal resolution of the DHSVM simulations could be used to greater effect.

Other as yet unexplored factors that could affect the water balance in GCC are altered land use, water storage, and long-term climate change. Land use in Cold and Dry Creek Valleys has been changing, most notably with the increase of irrigated agriculture, which pumps water from the basalt aquifer and probably recharges the unconfined aquifer to a degree.

Efforts are underway to evaluate the feasibility of constructing a major water storage reservoir in the Black Rock Valley (Basin 3). Water for the reservoir would be imported from the Columbia River, and the storage capacity of the proposed Black Rock Reservoir would exceed the combined storage of all the other storage basins in the Yakima Valley. Leakage from the reservoir could potentially exceed all of the natural recharge flux from Dry Creek or even the entire GCC.

## 8.0 Conclusions

The purpose of this study was to improve estimates of natural recharge from the GCC watershed to the unconfined aquifer along the edge of the SGM domain. Recharge along the western boundary includes both surface (streamflow) and subsurface (shallow lateral groundwater flow) components. Therefore, two modes of recharge were explicitly evaluated in the watershed modeling: streamflow runoff and subsurface flow above a basalt bedrock surface. The new estimates of recharge take advantage of distributed meteorology, the state-of-science watershed model DHSVM, and ephemeral streamflow data not available to previous studies.

DHSVM was used to simulate the surface and subsurface water balance in GCC and the movement of water into the SGM domain. DHSVM processes were improved substantially for application in this arid setting. However, a lack of data limited our initial calibration and verification of the developed model. The model calibrated to January 1995 data produced excessive estimates of streamflow when applied to the entire period of water years 1956–2001. Nevertheless, this study provided some recharge estimates that should be useful for further sensitivity analysis of GCC recharge in the SGM. The lower bound on annual average recharge from GCC to the SGM is estimated as  $0.471 \text{ Mm}^3\text{y}^{-1}$ . This estimate is based on available streamflow data and a flow frequency analysis and assumes that recharge consists only of the perennial spring flow in lower Dry Creek and infrequent runoff from Upper Cold Creek. The upper bound on annual average recharge from GCC is  $13.33 \text{ Mm}^3\text{y}^{-1}$ . This estimate is based on modeling with DHSVM and assumes that all rain and snowfall in the GCC watershed that is not lost to evapotranspiration becomes recharge to the unconfined aquifer.

Although most of the recharge along the western boundary is thought to be from shallow groundwater flow, the contribution from ephemeral streamflow (flash floods) is potentially significant in certain years. For example, a few weeks of runoff during January 1995 recharged the unconfined aquifer with more than  $497,300 \text{ m}^3$  of water from an estimated 68 mm of precipitation over Cold Creek Valley alone.

Future efforts to improve recharge estimates will need to address key aspects of this hydrologic setting: consumption of most precipitation by evapotranspiration, lateral subsurface flow of percolated water, degree of hydraulic connection to the basalt aquifer, infrequent runoff production at higher elevations, mostly during winter, and streamflow that reaches the valley floor during such events. A field program to gather basic meteorology and streamflow data in GCC is recommended and would probably much improve our understanding of natural recharge to the Hanford Site.

## 9.0 References

- Bauer DG and JJ Vaccaro. 1990. *Estimates of Ground-Water Recharge to the Columbia Plateau Regional Aquifer System, Washington, Oregon, and Idaho, for Predevelopment and Current Land-Use Conditions*. Water Resources Investigative Report 88-4108, U.S. Geological Survey, Washington, DC.
- Brakensiek DL, HB Osborn, and WJ Rawls. 1979. *Field manual for research in agricultural hydrology*. Agricultural Handbook No. 224. U.S. Department of Agriculture, Washington, DC.
- Brooks RH and AT Corey. 1966. "Properties of porous media affecting fluid flow." *ASCE Journal of the Irrigation and Drainage Division* 92:61–88.
- Cary JW, GS Campbell, and RI Papendick. 1978. "Is the Soil Frozen or Not? An Algorithm Using Weather Records." *Water Resources Research* 14(6):1117–2244.
- Cole CR, MP Bergeron, SK Wurstner, PD Thorne, S Orr, and MI McKinley. 2001. *Transient Inverse Calibration of Site-Wide Groundwater Model to Hanford Operational Impacts—1943 to 1996*. PNNL-13447, Pacific Northwest National Laboratory, Richland, Washington.
- Dickinson RE, A Henderson-Sellers, C Rosenzweig, and PJ Sellers. 1991. "Evapotranspiration models with canopy resistance for use in climate models, a review." *Agricultural and Forest Meteorology* 54:373–388.
- Dinicola RS. 1997. *Estimates of Recharge from Runoff at the Hanford Site, Washington*. Water-Resources Investigations Report 97-4038, U.S. Geological Survey, Washington, DC.
- ESRI. 1999. *ArcInfo version 8.0.1 and ArcDoc 8.0.1 on-line documentation*. Environmental Systems Research Institute, Redlands, California.
- Fayer MJ and TB Walters. 1995. *Estimated Recharge Rates at the Hanford Site*. PNL-10285, Pacific Northwest National Laboratory, Richland, Washington.
- Feddes RA, PJ Kowalik, and H Zaradny. 1978. *Simulation of field water use and crop yield*. Wiley and Sons, New York.
- Flerchinger GN, CL Hanson, and JR Wight. 1996. "Modeling evapotranspiration and surface energy budgets across a watershed." *Water Resources Research* 32(8):2539–2548.
- Flerchinger GN, WP Kustas, and MA Weltz. 1998. "Simulating Surface Energy Fluxes and Radiometric Surface Temperatures for Two Arid Vegetation Communities Using the SHAW Model." *Journal of Applied Meteorology* 37(5):449–460.
- Flerchinger GN and KE Saxton. 1989a. "Simultaneous heat and water model of a freezing snow-residue-soil system I. Theory and development." *Transactions of ASAE* 32(2):565–571.
- Flerchinger GN and KE Saxton. 1989b. "Simultaneous heat and water model of a freezing snow-residue-soil system II. Field verification." *Transactions of ASAE* 32(2):573–578.
- Hartman MJ, LF Morasch, and WD Webber. 2002. *Hanford Site Groundwater Monitoring for Fiscal Year 2001*. PNNL-13788, Pacific Northwest National Laboratory, Richland, Washington.

- Holtan HN. 1961. *A concept of infiltration estimates in watershed engineering*. Paper 41-51, U.S. Department of Agriculture, Washington, DC.
- Jacobson EA and MD Freshley. 1990. *An Initial Inverse Calibration of the Groundwater Flow Model for the Hanford Unconfined Aquifer*. PNL-7144, Pacific Northwest National Laboratory, Richland, Washington.
- Kilpatrick FA and VR Schneider. 1983. "Use of flumes in measuring discharge." *Techniques of Water-Resources Investigations*, Vol. 3, Ch. A14. U.S. Geological Survey, Washington, DC.
- Lane LJ, WD Purtymun, and NM Becker. 1985. *New Estimating Procedures for Surface Runoff, Sediment Yield, and Contaminant Transport in Los Alamos County, New Mexico*. LA-10335-MS, Los Alamos National Laboratory, Los Alamos, New Mexico.
- Lenfesty CD and TE Reedy. 1985. *Soil Survey of Yakima County Area, Washington*. U.S. Department of Agriculture Soil Conservation Service, Washington, DC.
- Newcomb RC, JR Strand, and FJ Frank. 1972. *Geology and groundwater characteristics of the Hanford reservation of the U.S. Atomic Energy Commission, Washington*. Professional Paper 717, U.S. Geological Survey, Washington, DC.
- Prych EA. 1994. *Estimating Deep-Percolation Rates at Selected Locations on the USDOE Hanford Site, Washington, Using Two Chloride-Tracer Methods*. Open File Report 94-514, U.S. Geological Survey, Washington, DC.
- Rasmussen JJ. 1971. *Soil Survey of Benton County Area, Washington*. U.S. Department of Agriculture Soil Conservation Service, Washington, DC.
- Skaggs RL and WH Walters. 1981. *Flood risk analysis of Cold Creek near the Hanford Site*. PNL-4219, Pacific Northwest National Laboratory, Richland, Washington.
- Szilagyi J and MB Parlange. 1999. "A geomorphology-based semi-distributed watershed model." *Advances in Water Resources* 23:177-187.
- Vermeul VR, MP Bergeron, CR Cole, CJ Murray, WE Nichols, TD Scheibe, PD Thorne, SR Waichler, and Y Xie. 2003. *Transient Inverse Calibration of the Site-Wide Groundwater Flow Model (ACM-2): FY 2003 Progress Report*. PNNL-14398, Pacific Northwest National Laboratory, Richland, Washington.
- Vermeul VR, CR Cole, MP Bergeron, PD Thorne, and SK Wurstner. 2001. *Transient Inverse Calibration of Site-Wide Groundwater Model to Hanford Operational Impacts from 1943 to 1996—Alternative Conceptual Model Considering Interaction with Uppermost Basalt Confined Aquifer*. PNNL-13623, Pacific Northwest National Laboratory, Richland, Washington.
- Waichler SR and MS Wigmosta. 2004. "Application of Hydrograph Shape and Channel Infiltration Models to an Arid Watershed." *Journal of Hydrologic Engineering* 9(5):433-439.
- Wigmosta MS, B Nijssen, and P Storck. 2002. "The Distributed Hydrology Soil Vegetation Model." *Mathematical Models of Small Watershed Hydrology and Applications*, Singh VP and D Frevert, eds., Ch. 2, pp. 7-42. Water Resources Publications LLC.

Wigmosta MS, LW Vail, and DP Lettenmaier. 1994. "A distributed hydrology- vegetation model for complex terrain." *Water Resources Research* 30(6):1665–1679.

# **Appendix A**

## **New DHSVM Features**

## Appendix A – New DHSVM Features

This appendix briefly describes changes made to DHSVM for the Hanford Natural Recharge project. Recent major code changes and the new input settings that are relevant to the present code are outlined.

### A.1 DHSVM Changes

DHSVM was modified in several important ways to make it more suitable for the arid setting of Hanford. The infiltration capacity of the soil was limited by freezing temperatures and high soil moisture to simulate the ephemeral runoff-generating conditions at Hanford. Overland flow routing was modified to allow faster movement of runoff down the hillslope to simulate ephemeral “flash floods” at Hanford. A “deep” groundwater layer was added to facilitate movement below the root zone and permit for slower lateral groundwater movement (Figure 4.2). This lower groundwater layer can be used to provide base flow to the surface stream network in humid environments. In the arid Hanford application, it is not linked to the drainage network. Flow routing in stream channels was modified to permit infiltration into the channel bed and the simulation of “losing” streams. New variables were added to DHSVM to permit mapping of channel infiltration, recharge from the upper to lower groundwater layer, and deep recharge from the lower groundwater layer.

#### A.1.1 Limiting Infiltration

**New global variables** `Options.FrozenSoil`: flag to potentially limit infiltration into soil. `FrozenSoil[y][x].airTemp`, `*.oldAirTemp`, `*.heatFlux`: frozen soil state and flux variables.

**Source files** `frozensoil.c`, `frozensoil.h`, `MassEnergyBalance.c`

**Comments** Various functions to limit infiltration based on 1) temperature/heat flux out of soil, 2) heat flux and upper layer soil moisture, or 3) snowpack presence. See Cary et al. (1978) for heat flux only method. Set compile flag to choose method via `ifdef` (see `makefile` and `MassEnergyBalance.c`). Input settings for heat flux method are under the heading **FROZEN SOILS INFORMATION SECTION** in the input file.

#### A.1.2 Overland Flow Routing

The existence of overland flow and very sharp hydrographs in the arid setting require a faster overland flow routing than the default DHSVM mode. There are two basic considerations for moving surface water (runoff) in grid-based model like DHSVM: (1) how much ponded water in a cell is to be moved in a time step; (2) how frequently does water move from one cell to the next. Options implemented here for (1) are all of the water in the cell is transferred or some of the water is transferred, according to a power law function. Options implemented here for (2) are that water moves one cell per time step or water moves all the way down the hillslope, across all cells in a flowpath, as a cascade within the time step. In summary:

**1a.** All water moved off the cell; moves one cell per time step. Options.HydraulicRouting = LINEAR. Traditional DHSVM.

**1b.** All water moved off the cell; moves through all cells per time step in order of decreasing elevation. Options.HydraulicRouting = CASCADE\_LINEAR.

**1c.** All water moved off the cell if that cell was already wet at start of the time step before upslope additions; moves through all cells per time step in order of decreasing elevation. Options.HydraulicRouting = CASCADE\_LINEAR\_LIMITED.

**2a.** Some water moved off the cell; moves one cell per time step. Options.HydraulicRouting = POWERLAW.

**2b.** Some water moved off the cell; moves through all cells per time step in order of decreasing elevation. Options.HydraulicRouting = CASCADE\_POWERLAW.

In the original DHSVM, water moved according to method 1a. Subsequently, the capability was added to move water with method 2a (see Szilagyi and Parlange 1999). Comparing the two options, (1a) is the upper limit on water movement rate, while (2a) slows it down. For both options, if the time step or number of cells in a hillslope path is too large, the user may experience too-slow movement of water to the channels and difficulty in reproducing peaks in observed hydrographs.

The latest model version allows movement by (1b) or (2b). In the case of (1b), all of the runoff in the watershed will be moved down to the stream channel and intercepted at the next time step (linear cascade). In the case of (2b), some of the water on each cell will remain according to the power law function and some or all will ultimately infiltrate (power law cascade). For both (1b) and (2b), the movement of water in a cascade downslope to the receiving channel or basin outlet is accomplished by processing the grid cells in descending order of elevation. This results in moving water out of the highest cells first, then down through the lowest cells, according to the flow direction map, all within the same time step. Option (1c), a limited linear cascade, is an empirical compromise between (1b) and (2b), wherein all ponded water moves off the cell if and only if that cell was already wet before upslope contributions flowed into it.

Option 1b will probably rarely be used because it results in little difference between input hydrograph (generation of distributed runoff on the cells) and the output hydrograph (channel interception). These hydrographs would be exactly the same under (1b) if channel interception took place after surface routing in the main program. Option 2b is a true kinematic wave with a delayed rise, peak, and gradual recession. Numerical stability of the wave should be checked in practice. Remember that normally the kinematic wave is solved on the order of seconds or minutes, so some unusual values of the power law coefficients might be needed to slow down flow across the hillslope to realistic rates for a given dx, dt, and hillslope length. Both (1b) and (2b) are a significant departure from the original DHSVM logic. Ultimately, none of these solutions is satisfactory for quick runoff in humid environments, where overland flow is limited and the major runoff pathways are subsurface.

**New global variables** `Options.HydraulicRouting`: flag for type of overland flow routing. `Map.NumCells`: number of cells within basin. `Map.OrderedCellsRowCol`: matrix that is `NumCells x 2` in size, contains the row and col of all basin cells sorted by decreasing elevation.

**Source files** `InitTerrainMaps.c`, `RouteSurface.c`

**Comments** Overland flow routing options are set in Hydraulic Routing field in main input file. See Szilagyi and Parlange (1999) for information about the algorithm and possible parameter values.

### A.1.3 Channel Routing and Infiltration

Channel routing may be done via three methods: 1) **LINEAR** for cascade of linear reservoirs method for routing streamflow; 2) **POWERLAW** for cascade of non-linear (powerlaw storage-discharge relationship) reservoirs method; 3) **FTABLE** for cascade of non-linear reservoirs where user-defined storage-discharge relations are stored in look-up tables. Only the ftable method allows channel infiltration, or loss from the stream to the soil column below it. The new ftable method allows the simulation of losing streams. If this option is set, then the ftable and multiplier files defined under **FTABLE SECTION** in the main input file are read and used to do all channel flow routing, which involves a simultaneous solution of inflow, outflow, and infiltration. Stream segment properties that are relevant to routing and independent of water depth are defined in the multipliers file. Routing properties that depend on water depth are defined in the ftable file. Each stream segment (channel reach) has a unique listing in the multipliers file, which includes a cross reference to the correct flow table to use in the ftable file. For a given depth of water in the stream segment, factors for outflow and infiltration are read or interpolated from the flow table, then multiplied by the corresponding values in the multipliers file to obtain the potential flows. These potential flows are then prorated to the available volume of water in the stream reach, if necessary, to obtain the final outflow and infiltration.

In the multipliers file, **Number of Tables** is the number of stream segments in the stream network and number of rows in this file. **TableNum** is the channel reach number, or segment ID in the stream network file. **Type** is the number of the ftable to use for look-up. **Depth** is set to unity. **SurfArea**, **Vol**, and **Infiltration** are equal to the length of the channel segment (=unit-width area). **DownstreamQ** is the square root of the gradient,  $S_0$ , used for calculation of discharge with Manning's equation.

In the ftable file, **Number of Tables** is the number of discrete channel types you wish to describe for purposes of flow routing and infiltration; each type has its own look-up table. **Area** (m) is actually the width of the stream channel class and should match the variable in the stream class file. **Vol** is actually the water depth (m), **DownstreamQ** is Manning's equation without slope (see below), and **Infiltration** is an empirical factor for infiltration. During simulation, the model linearly interpolates between these depth points (rows in each table) to compute the potential outflow and infiltration for the channel segment. Outflow  $Q$  is defined as Manning's equation:

$$Q = \text{Ftable.DownstreamQ} \times \text{Multiplier.DownstreamQ} \quad (\text{A.1})$$

$$\text{Ftable.DownstreamQ} = \frac{R^{\frac{2}{3}}A}{n} \quad (\text{A.2})$$

$$\text{Multiplier.DownstreamQ} = \sqrt{S_0} \quad (\text{A.3})$$

where  $R$  =hydraulic radius,  $A$  =cross-sectional area,  $S_0$  =slope, and  $n$  = roughness coefficient. In practice, the channel is assumed to have a rectangular cross section. **DownstreamQ** values in the ftable file must be computed as a preprocessing step. **Infiltration** values are set to zero for an impermeable streambed.

**New global variables** `Options.ChannelRouting`: streamflow routing method. `segment.outflow`: outflow to next channel segment. `segment.recharge`: infiltration through channel bed. `SoilMap[y][x].CumChannelLoss`: cumulative infiltration through the channel bed.

**Source files** `channel.c`, `ftable5.cpp`, `ftable.h`, `MainDHSVM.cpp`, `RouteSubSurface.c`

**Comments** Channel flow routing options are set in Channel Routing field in main input file.

#### A.1.4 Recharge and Deep Groundwater

In the new DHSVM, the user may allow some of the water in the shallow system to percolate below the upper perched aquifer and enter a deep groundwater system. The rate at which this shallow recharge happens is governed by Darcy's law and **Groundwater Conductivity** set in the soil table. Once the amount of leakage is computed for the time step, the water is transferred to the lower groundwater layer in the same time step, with no additional rate-dependent vertical percolation. The thickness of the lower aquifer zone is not defined, and the deep groundwater height (saturated thickness) is the height of the water column unadjusted for porosity. Potential outflow of deep groundwater from a cell is computed as the sum of deep lateral outflow, a function of the layer's transmissivity, and leakage through the lower boundary. Deep recharge is given preference over lateral outflow if the available deep groundwater is insufficient to provide for both. If no deep recharge is desired, **Base Layer Conductivity** in the input is set to zero. The deep layer requires its own DEM and flowpath grids to be input; these may be set to the surface/shallow subsurface flowpath map if you can't justify using different grids, as would usually be the case. A stream map file must also be specified for the deep layer and should either be a stream map file where deep groundwater contributes to channel reaches or a dummy file with one row entered for a cell outside the mask. The first option is used in most applications where the motivation to use the deep layer is to provide baseflow for some or all stream segments. The second option was used for Hanford, where all streams are ephemeral and lose water.

**New global variables** `SoilMap[y][x].GwRecharge,*`.`CumGwRecharge`: percolation downward from the upper saturated zone. `Groundwater[y][x].depth,*`.`depth,*`.`Dem`, etc.: parameters for groundwater (shallow) recharge. `Groundwater[y][x].deep-`

Loss, \*cumDeepLoss: parameters for ultimate (deep) recharge. **Source files** *Groundwater.c*, *groundwater.h*, *RouteSubSurface.c*. **Comments** Input settings for recharge from shallow to deep layer are under SOIL tables in main input file: Groundwater Conductivity, Groundwater Conductivity Lat. Input settings for deep groundwater layer are under GROUND-WATER INFORMATION SECTION and SOIL tables in main input file: Gwater DEM File, Gwater Flow Direction File, Gwater To Channel File, Initial Groundwater Depth, Base Layer Conductivity.

### A.1.5 Soil Evaporation Based on Resistance

**Source files** *SoilResistanceEvap.c*, *MassEnergyBalance.c*. **Comments** Choose old or new soil evaporation function by commenting out in *MassEnergyBalance.c*. See de Silans et al. (1989); Peters-Lidard et al. (1997) for information about the algorithm and possible parameter values.

## A.2 References

Cary JW, GS Campbell, and RI Papendick. 1978. "Is the Soil Frozen or Not? An Algorithm Using Weather Records." *Water Resources Research* 14(6):1117–2244.

de Silans AP, L Bruckler, JL Thony, and M Vauclin. 1989. "Numerical modeling of coupled heat and water flows during drying in a stratified bare soil—comparison with field observations." *Journal of Hydrology* 105:109–138.

Peters-Lidard CD, MS Zion, and EF Wood. 1997. "A soil-vegetation-atmosphere transfer scheme for modeling spatially variable water and energy balance processes." *Journal of Geophysical Research* D4:4303–4324.

Szilagyi J and MB Parlange. 1999. "A geomorphology-based semi-distributed watershed model." *Advances in Water Resources* 23:177–187.

## **Appendix B**

### **Statistics for Evaluating Model Skill**

## Appendix B – Statistics for Evaluating Model Skill

Bias and several goodness-of-fit measures were the primary statistics used to evaluate model skill at reproducing climate variables and streamflow. The overall approach and certain definitions are taken from Legates and McCabe (1999), an excellent reference on goodness-of-fit measures.

### B.1 Equations

Bias was defined as the ratio of predicted (simulated) mean to observed mean

$$bias = \frac{\bar{P}}{\bar{O}} \quad (\text{B.1})$$

where

$$\begin{aligned} \bar{P} &= \text{mean of the predictions} \\ \bar{O} &= \text{mean of the observations} \end{aligned}$$

The traditional  $R^2$ , or square of Pearson's product-moment correlation coefficient, describes the portion of total variance in the observed data that can be explained by the model and ranges from 0.0 to 1.0:

$$R^2 = \left\{ \frac{\sum_{i=1}^N (O_i - \bar{O})(P_i - \bar{P})}{\left[ \sum_{i=1}^N (O_i - \bar{O})^2 \right]^{0.5} \left[ \sum_{i=1}^N (P_i - \bar{P})^2 \right]^{0.5}} \right\}^2 \quad (\text{B.2})$$

where

$$\begin{aligned} N &= \text{number of timesteps} \\ O_i &= \text{observed value at timestep } i \\ \bar{O} &= \text{mean of the observations} \\ P_i &= \text{the predicted value at timestep } i \\ \bar{P} &= \text{mean of the predictions.} \end{aligned}$$

There are two disadvantages of  $R^2$  for describing model skill: 1) any linear relationship between the observations and the predictions, not necessarily a 1:1 relationship, results in a high value of  $R^2$ ; and 2) the squaring of terms gives too much weight to large values. In the case of streamflow, a high  $R^2$  value may indicate good fit of peak flows but may mask poor model skill during baseflow periods.

Efficiency  $E$  (Nash and Sutcliffe 1970) is a tougher test than  $R^2$  and casts the mean of the observations as a benchmark for the model:

$$E = 1.0 - \frac{\sum_{i=1}^N (O_i - P_i)^2}{\sum_{i=1}^N (O_i - \bar{O})^2} \quad (\text{B.3})$$

Values of  $E$  tend to be slightly less than R-squared in the case of streamflow.

Three first-degree goodness-of-fit measures from Legates and McCabe (1999) use absolute values of differences instead of squares. The first-degree efficiency is defined as

$$E_1 = 1.0 - \frac{\sum_{i=1}^N |O_i - P_i|}{\sum_{i=1}^N |O_i - \bar{O}|} \quad (\text{B.4})$$

$E_1$  is an improvement over  $E$  when evaluating model skill at low and moderate streamflow levels is important, but the grand mean is still the basis of comparison. A further discrimination can be gained by using a baseline mean involving some kind of seasonal or other categorical variation inherent in the data. Here, the the baseline mean was defined as the mean for each month of the year, where the mean is taken across all years in the simulation. Avoidance of squaring and use of baseline mean instead of the grand mean provides tougher, more revealing tests of model skill.

The baseline-adjusted, first-degree efficiency is

$$E'_1 = 1.0 - \frac{\sum_{i=1}^N |O_i - P_i|}{\sum_{i=1}^N |O_i - \bar{O}'|} \quad (\text{B.5})$$

where

$\bar{O}' =$  baseline mean of the observations, variable in time.

All of the above measures of efficiency have a possible range of  $-\infty$  to 1.0. When efficiency=0, the model is no better or worse than the observed mean as a predictor. The closer the baseline mean is to the individual observations, the lower the efficiency is likely to be.

The baseline-adjusted modified index of agreement is

$$d'_1 = 1.0 - \frac{\sum_{i=1}^N |O_i - P_i|}{\sum_{i=1}^N (|P_i - \bar{O}'| + |O_i - \bar{O}'|)} \quad (\text{B.6})$$

where  $d'_1$  has the advantage of having the same range as the familiar  $R^2$ , 0 to 1.0.

## B.2 References

Legates DR and GJ McCabe. 1999. "Evaluating the use of "goodness-of-fit" measures in hydrologic and hydroclimatic model validation." *Water Resources Research* 35(1):233–241.

Nash JE and JV Sutcliffe. 1970. "River flow forecasting through conceptual models, Part 1—A discussion of principles." *Journal of Hydrology* 10:282–290.

## **Appendix C**

### **Greater Cold Creek Meteorology Data**

## Appendix C – Greater Cold Creek Meteorology Data

The Hanford Meteorology Station operates and/or retrieves data from more than two dozen sites in the Hanford region. Unfortunately, only data from the main station called HMS has a long duration and all of the necessary measurement parameters. In particular, HMS is the only station where precipitation has been measured on an hourly basis for over ten years. Therefore, climate input to DHSVM was developed from hourly data from the Hanford Meteorological Station (HMS) and daily precipitation data from three National Weather Service cooperative stations (NWS): Moxie City 10 E (MOX), Priest Rapids Dam (PRD), and Sunnyside (SUN) (Table 5.1). Hourly data at HMS is available starting January 1, 1955; Moxie City and Sunnyside daily data are available for the entire HMS period; Priest Rapids Dam data begin 12/6/1956.

The HMS hourly dataset was relatively complete. The occurrence of missing variables and the methods used to fill them in are summarized in Table C.1. There was only one extended period of missing data at HMS—wind speed over the last six months of 1974. Sky cover, the percent of the celestial hemisphere covered with clouds, was used in an algorithm to compute longwave radiation. Variables were inspected for erroneous outliers; several instances were found for air temperature and wind speed. These were corrected by flagging them as missing and then processing according to the methods noted in Table C.1. In the case of wind, month/hour means were computed from the entire period of record and used for the large gap in 1974. Missing precipitation records from the NWS stations occurred in whole-month blocks (Table C.2). The DHSVM meteorology input files for MOX, SUN, and PRD contained precipitation based on that station; all other variables were set equal to the HMS meteorology input. Annual precipitation at the four meteorology stations is shown in Figure C.1.

**Table C.1.** Summary of missing climate data, Hanford Meteorology Station

| Parameter         | Start date | End date   | Number of missing steps | Method to fill gap   |
|-------------------|------------|------------|-------------------------|----------------------|
| Air temperature   | 05/05/1973 | 05/06/1973 | 14                      | linear interpolation |
| Wind speed        | 07/01/1974 | 12/31/1974 | 6 months                | month/hour means     |
| Relative humidity | 01/28/1958 | 01/28/1958 | 1                       | linear interpolation |
|                   | 05/05/1973 | 05/05/1973 | 14                      |                      |
|                   | 09/15/1973 | 09/16/1973 | 14                      |                      |
|                   | 02/06/1986 | 02/07/1986 | 1                       |                      |
| Sky cover         | 11/12/1971 | 11/15/1971 | 4-8                     | linear interpolation |
|                   | 12/29/1971 | 12/31/1973 |                         |                      |
|                   | 10/01/1997 | 10/01/1997 |                         |                      |
|                   | 07/21/2000 | 07/21/2000 |                         |                      |
|                   | 11/16/2000 | 11/16/2000 |                         |                      |
|                   | 07/12/2001 | 07/12/2001 |                         |                      |

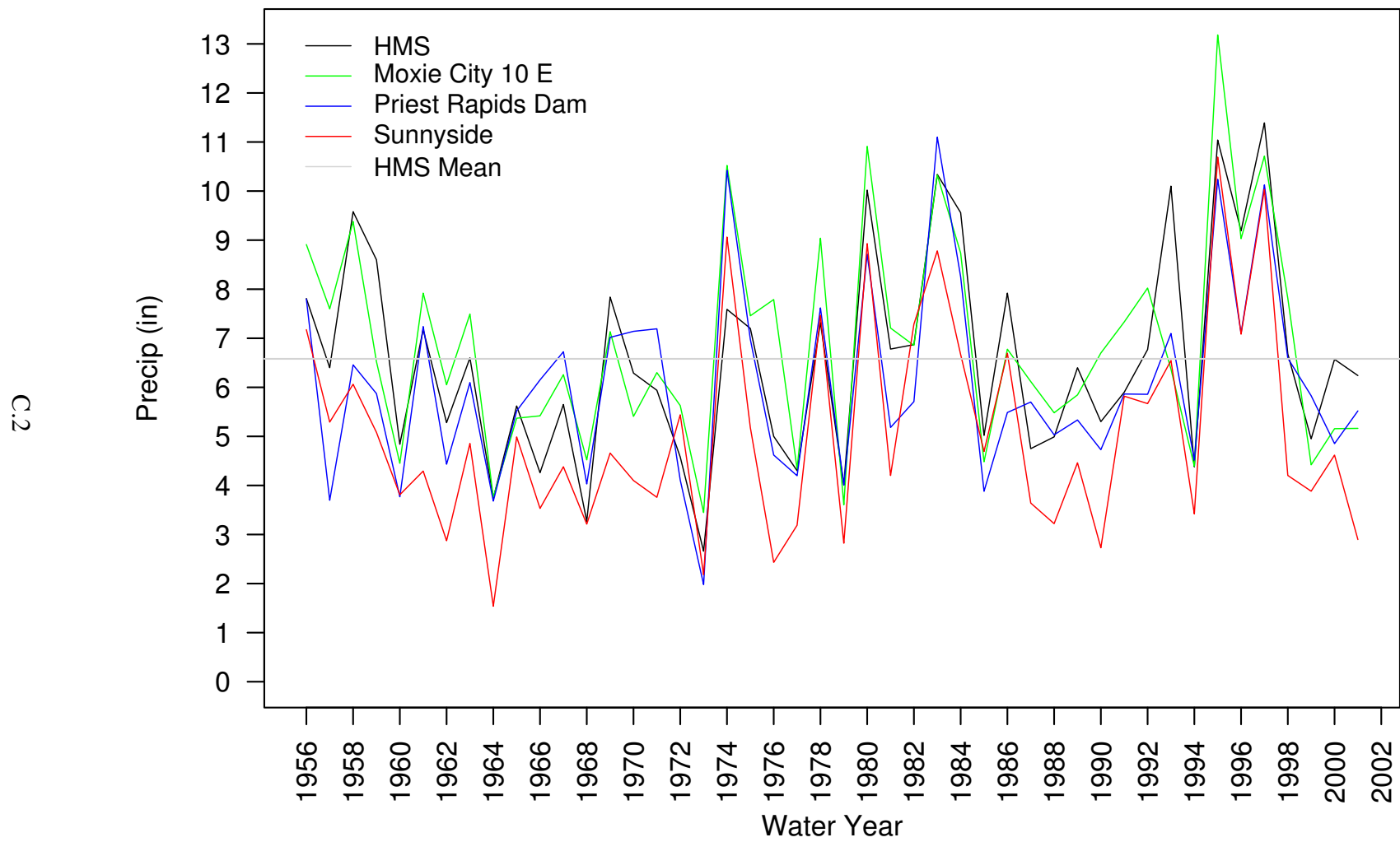


**Figure C.1.** Annual precipitation at four stations near the Hanford Site

**Table C.2.** Summary of missing precipitation data, NWS stations

| Station           | Missing months   |
|-------------------|--|
| Moxie City 10 E   | 3/81, 5/81, 2/96, 3/96, 12/97,<br>4/98, 4/99, 2/00, 6/81-10/83 |
| Priest Rapids Dam | 3/97-11/97, 10/98, 10/00                                       |
| Sunnyside         | 4/91-4/91, 12/96-2/97,<br>11/98-5/99, 9/99                     |

## C.1 Methods for Distributing Precipitation

The methods used for distributing precipitation in Cold and Dry Creeks were modified from Dinicola (1997). He computed factors for multiplying offsite precipitation to arrive at local precipitation in four elevation zones (Table C.3). These factors have a strong linear relationship with elevation (Figure C.2). The first step to adapt his approach for this study was to make his factor a continuous function of elevation, as shown by the simple linear regressions of Dinicola's factors on elevation (Figure C.2). In the equations for each factor, the intercept is unitless and the slope has units of  $\text{m}^{-1}$ . An additional regression using both Lower Cold and Lower Dry factors by Dinicola (1997) as the regressor variable yielded a single equation for HMS (Table C.3). Then for each meteorology station, the constant intercept and slope from Table C.3 were added as two more columns to the meteorology input file. The `LapsePrecip()` function in the model code was modified to include a HANFORD option for lapsing precipitation. When using the HANFORD option, the intercept and slope are used with the local cell elevation to compute the unitless factor  $F$ , and local precipitation  $P_l$  as  $P_l = FP_s$ , where  $P_s$  is precipitation at the meteorology station.

Dinicola (1997) assigned each subwatershed to one of the meteorology stations for providing precipitation input to the HSPF model. That approach was suitable for long-term, semi-distributed simulations, but is less suitable for the current approach that tries to capture variability at short time scales and which explicitly simulates channel routing and infiltration along the stream network of an entire basin. Having different precipitation time-series affecting different parts of the basin is not conducive to tracking runoff and infiltration throughout the watershed. However, given the expected sensitivity of runoff/recharge results to precipitation input, two alternative approaches were used. The first approach followed typical application of DHSVM and used the meteorology inputs from all four stations, computing local precipitation at a grid cell as the inverse distance-weighted average of predicted precipitation from the four stations. This approach has the advantage of using all the geographic and meteorologic information simultaneously and following a simple and consistent rationale across the entire study area. A drawback to this approach is the "smearing" of precipitation values and the resulting increase in the number of days with nonzero precipitation at any given location. The second approach used only one station's meteorology input at a time, resulting in four separate model runs. For calibration using Cold Creek basin, both approaches were tested (the second using just HMS and PRD as the single-station alternatives), but there was no clearly superior approach. For the final simulation we used the first method involving all meteorology stations and inverse distance-weighting.

**Table C.3.** Factors for distributing precipitation, after Dinicola (1997)

| Subwatershed | Elev. zone <sup>(a)</sup> | Precipitation record used | Dinicola Factor | Factor from regression <sup>(b)</sup> |
|--------------|---------------------------|---------------------------|-----------------|---------------------------------------|
| Lower Dry    | 1                         | HMS                       | 1.12            | F = 0.9142 + 1.016e-3 *<br>ELEV       |
|              | 2                         |                           | 1.56            |                                       |
|              | 3                         |                           | 1.83            |                                       |
|              | 4                         |                           | 2.01            |                                       |
| Middle Dry   | 1                         | Sunnyside                 | 0.92            | F = 0.6874 + 9.762e-4 *<br>ELEV       |
|              | 2                         |                           | 1.27            |                                       |
|              | 3                         |                           | 1.54            |                                       |
|              | 4                         |                           | 1.77            |                                       |
| Upper Dry    | 2                         | Moxie City 10 E           | 0.89            | F = 0.5013 + 7.309e-4 *<br>ELEV       |
|              | 3                         |                           | 1.15            |                                       |
|              | 4                         |                           | 1.32            |                                       |
| Lower Cold   | 1                         | HMS                       | 0.95            | F = 0.7034 + 9.412e-4 *<br>ELEV       |
|              | 2                         |                           | 1.25            |                                       |
|              | 3                         |                           | 1.49            |                                       |
| Upper Cold   | 2                         | Priest Rapids Dam         | 1.29            | F = 0.9902 + 5.432e-4 *<br>ELEV       |
|              | 3                         |                           | 1.45            |                                       |
|              | 4                         |                           | 1.61            |                                       |

(a) 1 = 512-1312 ft; 2 = 1313-2297 ft; 3 = 2298-3281 ft; 4 = 3282-4193 ft

(b) F= local factor; ELEV= local elevation (m). For use with DHSVM, the relationships for Lower Dry and Lower Cold were merged into a single regression to use with HMS data:  $F = 0.7532 + 1.098e-3 * ELEV$

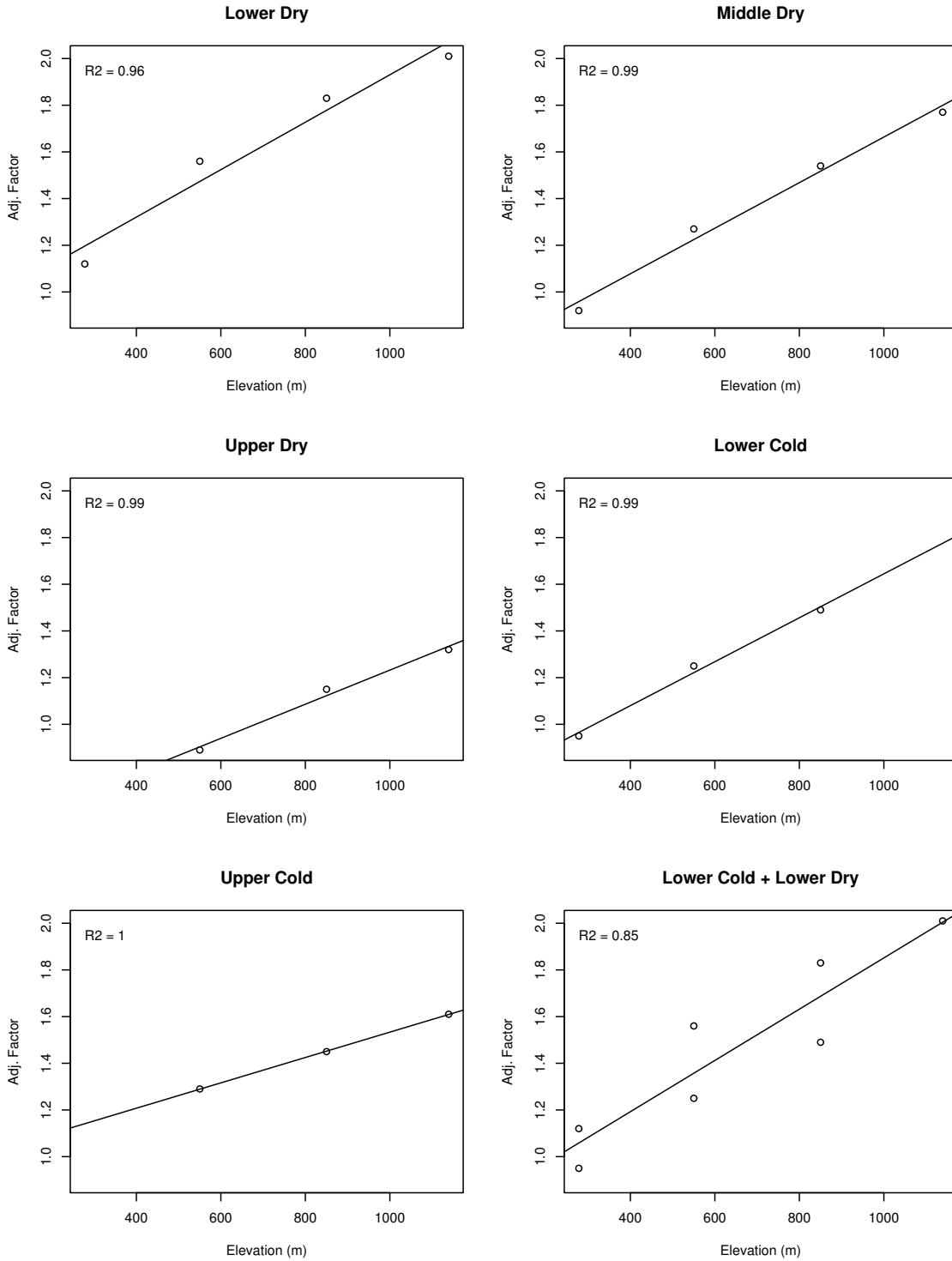
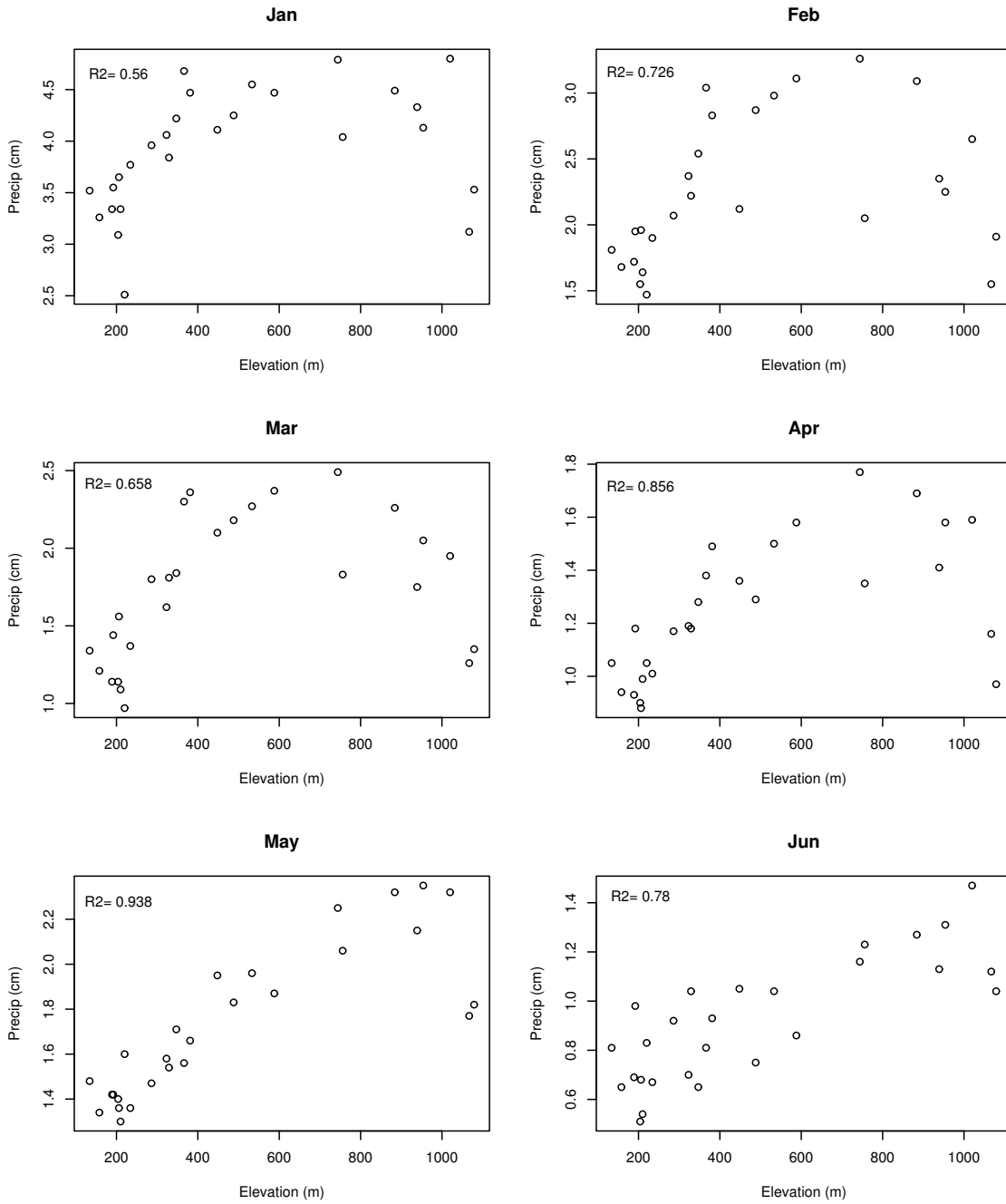
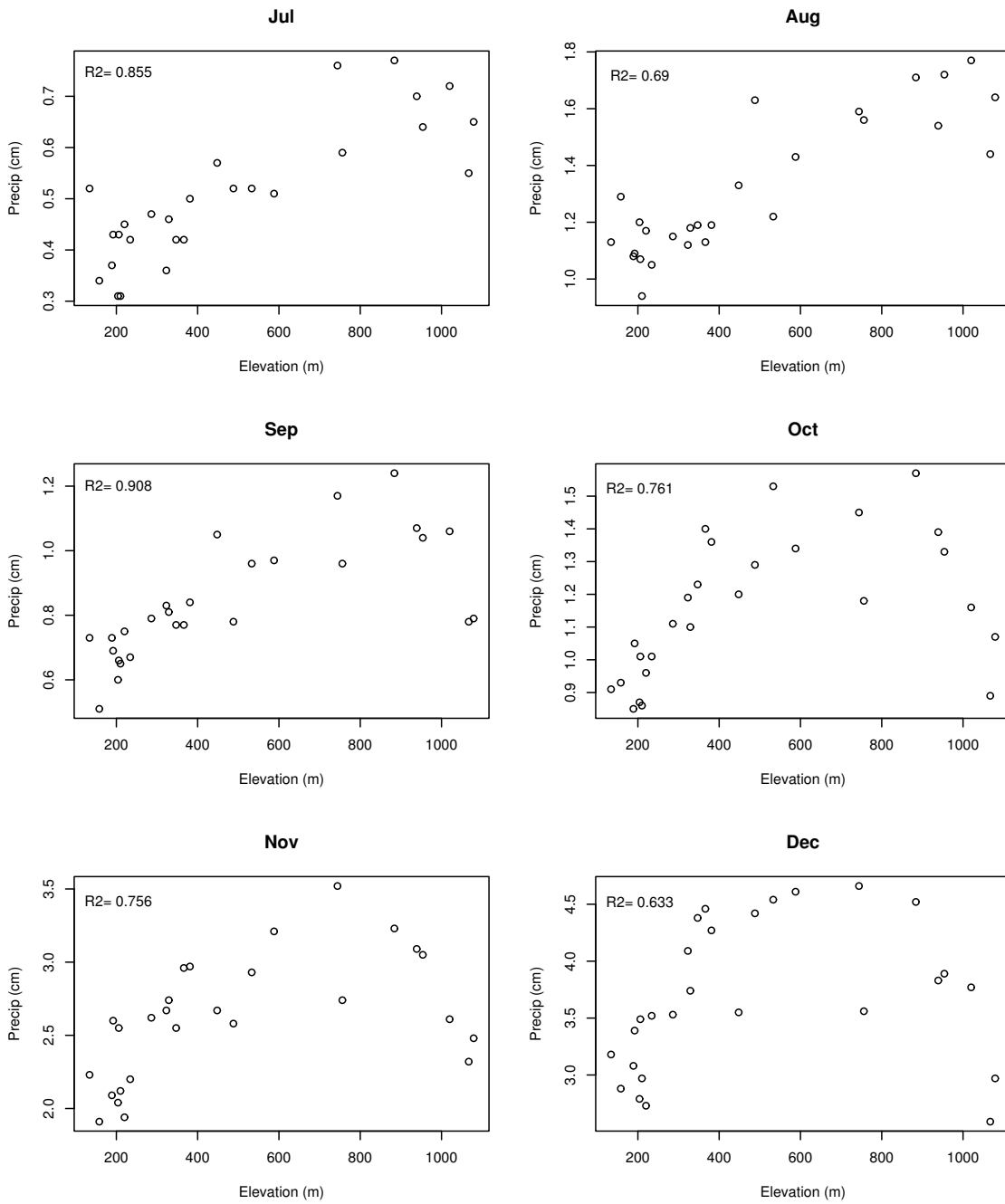


**Figure C.2.** Precipitation adjustment factors for Cold and Dry Creek subbasins from Dinicola (1997)



/projects/cold\_creek/met/ale\_precip\_p1.ps, script= hanford/scripts/precip\_lapse.R

**Figure C.3.** January to June mean monthly precipitation (1969-80) versus elevation at all Thorp and Hinds (1977) ALE study sites



/projects/cold\_creek/met/ale\_precip\_p2.ps, script= hanford/scripts/precip\_lapse.R

**Figure C.4.** July to December mean monthly precipitation (1969-80) versus elevation at all Thorp and Hinds (1977) ALE sites.

## C.2 Background Information on Rattlesnake Mountain Precipitation

A third approach for distributing precipitation was considered for the face of Rattlesnake Mountain but was rejected in favor of the simple and consistent approaches documented above. The third approach is described below for the sake of completeness and background for future studies. Thorp and Hinds (1977) did a study of microclimates and vegetation types in the Arid Lands Ecology reserve (ALE) and compiled monthly total precipitation at 27 stations in the area. After their report was issued, the study continued until 1980. Stone et al. (1983) reported the final precipitation results including mean monthly values at the 27 stations from 1969-80. The data in Table A.V-2 of Stone et al. (1983) was used to explore relationships between local mean monthly precipitation, HMS mean monthly precipitation, and elevation difference between the local station and HMS. First, the relationship of mean monthly precipitation to elevation was explored. Thorp and Hinds (1977) noted that gauges near the crest of Rattlesnake Mountain had lower totals than stations downslope, and they attributed this to measurement problems caused by the high winds that are common along the ridge crest. However, the wind flow over the mountain may cause a real reduction of precipitation near the top compared to downslope areas. The resulting nonlinear relationship is evident in Figures C.3 and C.4. Considerable scatter around stations at similar elevation also indicates the presence of significant variability due to map location rather than elevation. If the ridgetop stations are removed from the analysis, a linear relationship is more tenable (Figures C.5 and C.6).

The most general regression model and one that is useful for deriving a method for predicting precipitation at the short time steps of DHSVM includes precipitation at HMS and elevation as regressor variables:

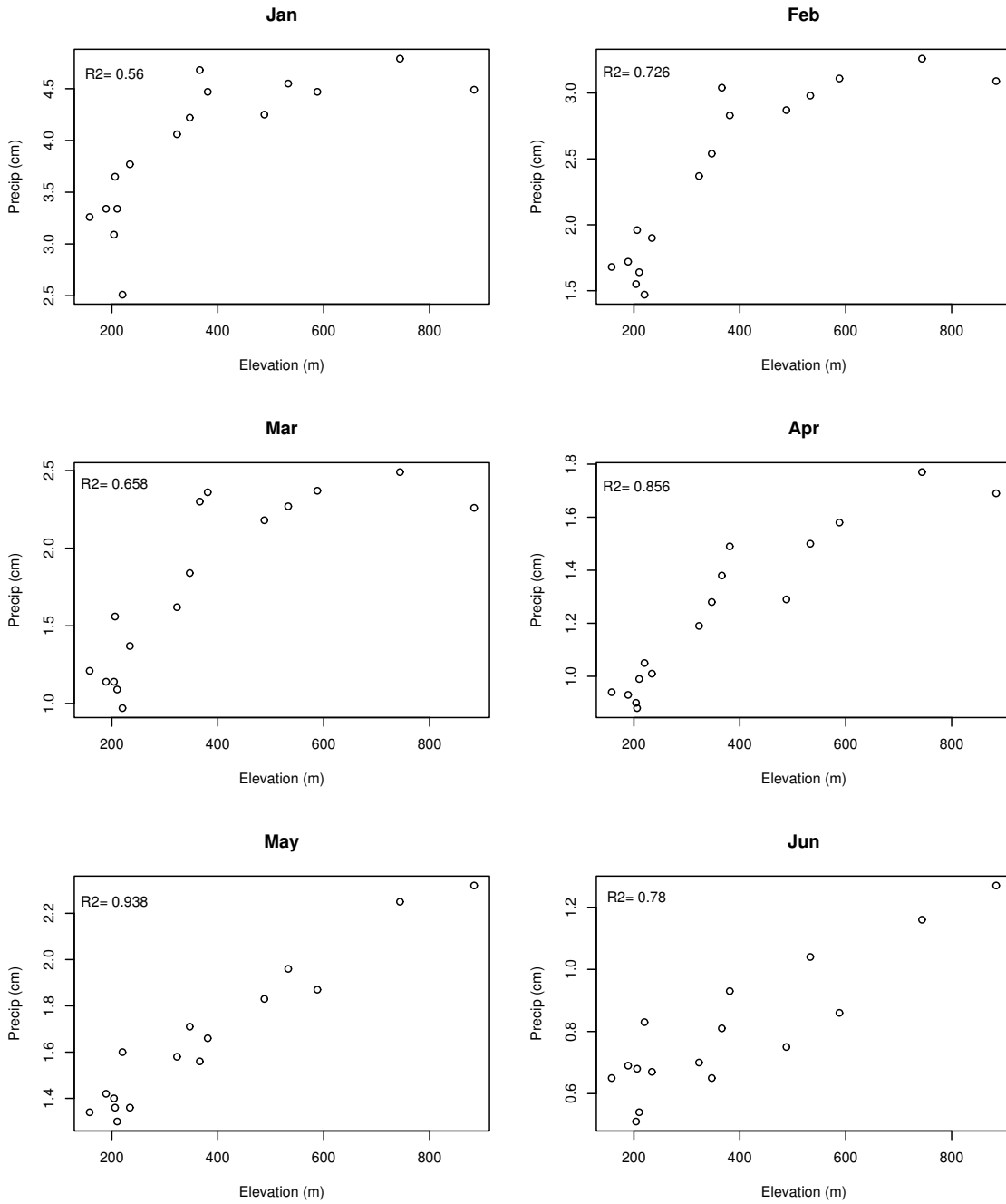
$$A = a_0H + a_1E + a_2HE + a_3HE^2 \quad (\text{C.1})$$

where

- $A$  = local mean monthly precipitation (cm)
- $H$  = HMS mean monthly precipitation (cm)
- $E$  = elevation difference between local station and HMS (m)
- $a_i$  = regression coefficients

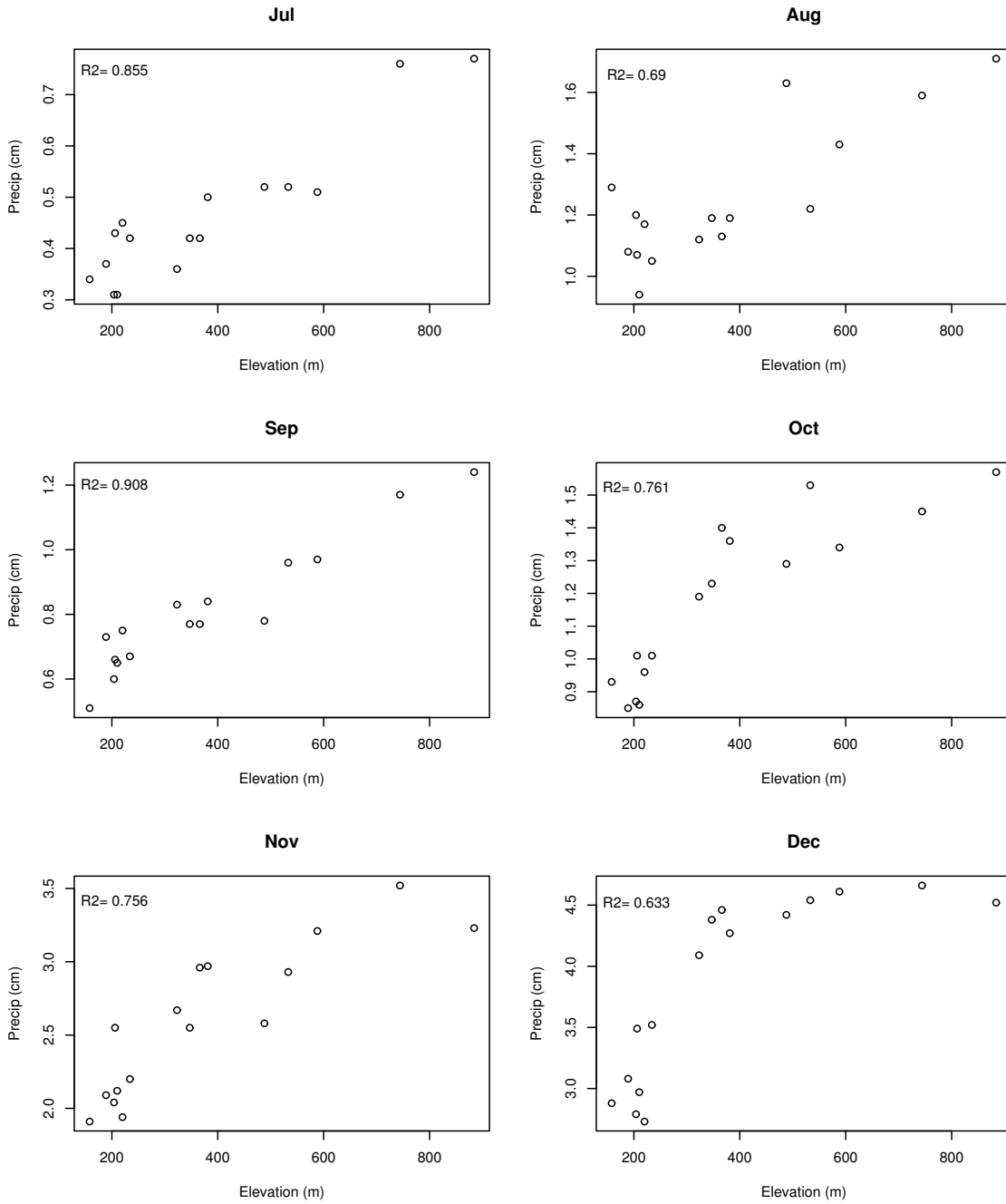
Although Thorp and Hinds (1977) noted that stations on Rattlesnake Mountain commonly have precipitation when HMS does not, for process-based modeling at short time steps it would not be appropriate to have precipitation occurring all the time. Also, to scale correctly at different timescales, all terms in the regression need to include HMS precipitation. Therefore, only models that met this constraint were selected for further consideration and of these, the four best models are summarized in Table C.4 and shown in Figure C.7. The possible justification for the  $a_0$  model term is that precipitation may be greater near Rattlesnake Mountain, independent of elevation. The  $a_1$  and  $a_2$  interaction terms account for elevation difference between HMS and the ALE sites, and the squaring of elevation difference  $E$  with term  $a_2$  is used to explain the decrease in precipitation near the summit (Figures C.3 and C.4). Of these, model 7 was considered to be the best choice, because of acceptable  $R^2$  value (0.88) and because it predicts ALE precipitation will be the same as HMS if the elevations are the same, a desirable result for grid cells near Highway 240:

$$A = H + a_1HE + a_2HE^2 \quad (\text{C.2})$$



/projects/cold\_creek/met/ale\_precip2\_p1.ps, script= hanford/scripts/precip\_lapse.R

**Figure C.5.** January to June mean monthly precipitation (1969-80) versus elevation at non-ridgetop Thorp and Hinds (1977) ALE study sites.



/projects/cold\_creek/met/ale\_precip2\_p2.ps, script= hanford/scripts/precip\_lapse.R

**Figure C.6.** July to December mean monthly precipitation (1969-80) versus elevation at non-ridgetop Thorp and Hinds (1977) ALE sites.

where  $A$  = ALE precipitation,  $H$  = HMS precipitation and  $E$  = elevation difference between ALE and HMS. Rearranging Equation C.2 to make a single factor to HMS yields

$$A = H(1 + a_1E + a_2E^2) \quad (\text{C.3})$$

For application of Equation C.3 it would be desirable to enforce a minimum value of 1.0 for the factor  $F = 1 + a_1E + a_2E^2$ .

**Table C.4.** Regression models for predicting mean monthly precipitation at ALE sites ( $A$ ) as a function of HMS precipitation ( $H$ ) and elevation difference from HMS ( $E$ ). All models and coefficients were significant ( $p < 0.00001$ ).

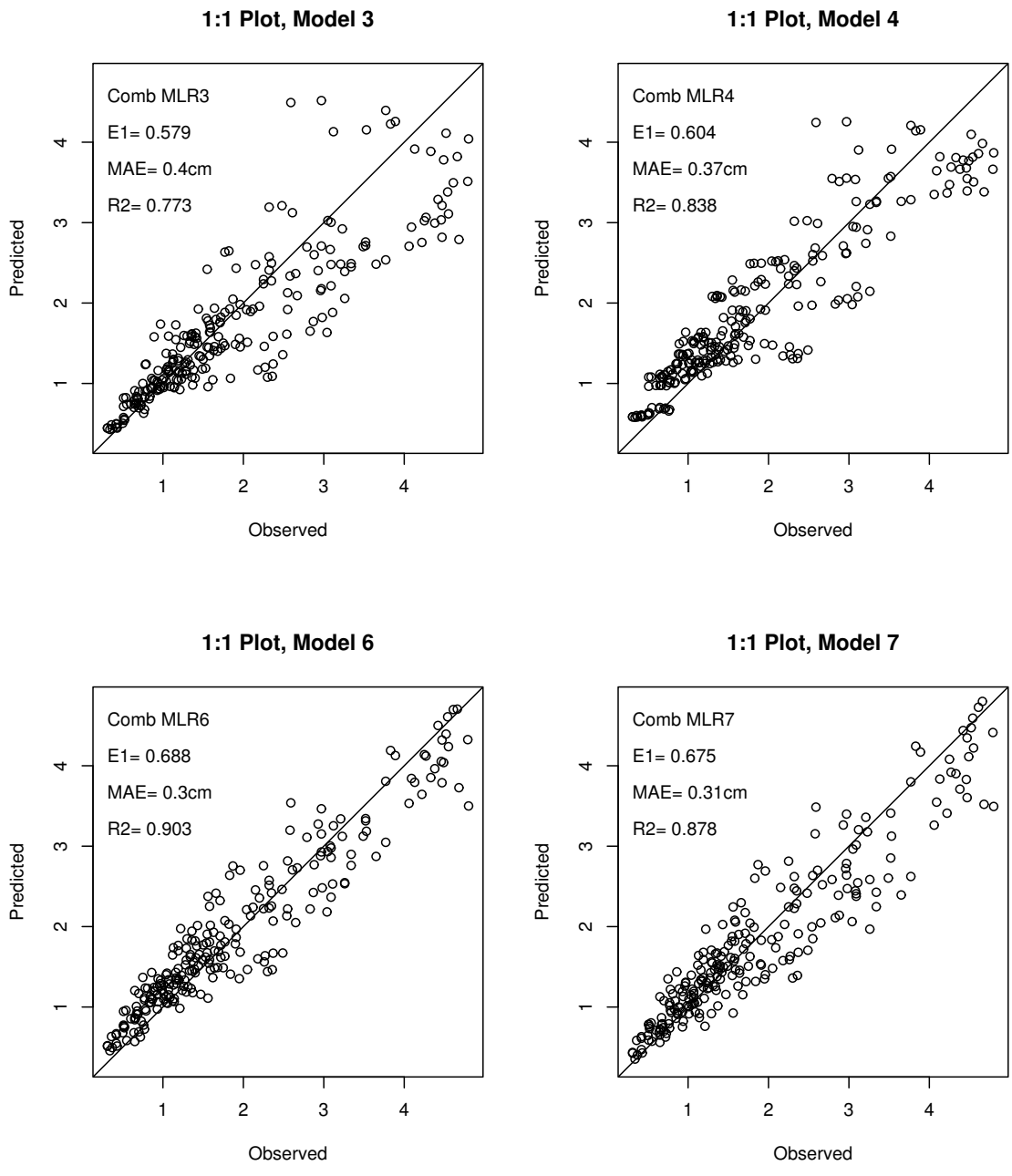
| # | Model                        | $R^2$ | $a_0$ | $a_1$                                 | $a_2$                                  |
|---|------------------------------|-------|-------|---------------------------------------|--|
| 3 | $A = H + a_1HE$              | 0.77  |       | $7.623 \times 10^{-4} \text{ m}^{-1}$ |  |
| 4 | $A = a_0H + a_1HE$           | 0.84  | 1.304 | $7.623 \times 10^{-4} \text{ m}^{-1}$ |  |
| 6 | $A = a_0H + a_1HE + a_2HE^2$ | 0.90  | 1.180 | $2.495 \times 10^{-3} \text{ m}^{-1}$ | $-2.784 \times 10^{-6} \text{ m}^{-2}$ |
| 7 | $A = H + a_1HE + a_2HE^2$    | 0.88  |       | $3.265 \times 10^{-3} \text{ m}^{-1}$ | $-3.469 \times 10^{-6} \text{ m}^{-2}$ |

### C.3 References

Dinicola RS. 1997. *Estimates of Recharge from Runoff at the Hanford Site, Washington*. Water-Resources Investigations Report 97-4038, U.S. Geological Survey, Washington, DC.

Stone WA, JM Thorp, OP Gifford, and DJ Hoitink. 1983. *Climatological Summary for the Hanford Area*. PNL-4622, Pacific Northwest Laboratory, Richland, Washington.

Thorp JM and WT Hinds. 1977. *Microclimates of the Arid Lands Ecology Reserve 1968-1975*. BNWL-SA-6231, Pacific Northwest Laboratory, Richland, Washington.



/projects/cold\_creek/met/ale\_mlr2\_precip.ps, script= hanford/scripts/precip\_lapse.R

**Figure C.7.** Regression models for local mean monthly precipitation (1969-80) as a function of HMS precipitation and elevation difference. Model 7 was considered to be best equation in terms of structure and fit.

## **Appendix D**

### **Regional Streamflow Frequency Analysis**

## Appendix D – Regional Streamflow Frequency Analysis

Another perspective on runoff and streamflow at Hanford can be gained by analysis of flow data from other stream gauges in the region with longer periods of record. The USGS calculated instantaneous peak annual flows from crest height measurements collected at five stations in the Yakima-Hanford region during the 1950s–70s (Figure D.1). The flow rates ranged from  $0.0028$  to  $15.6 \text{ m}^3\text{s}^{-1}$  ( $0.1$ – $550 \text{ ft}^3\text{s}^{-1}$ ), with flow occurring in approximately half the years (Figure D.2). Most of the peak flows, as well as the highest flow rates, occurred during the winter months (Figure D.3). An analysis of local meteorological records indicates that most of these events were likely the result of situations involving rain-on-snow over frozen soils. However, some peak flows also seem to be the result of summer thunderstorms (e.g., August events). For the analysis described below, peak annual flows measured at UC in the early 1990s (Section 2) were also included.

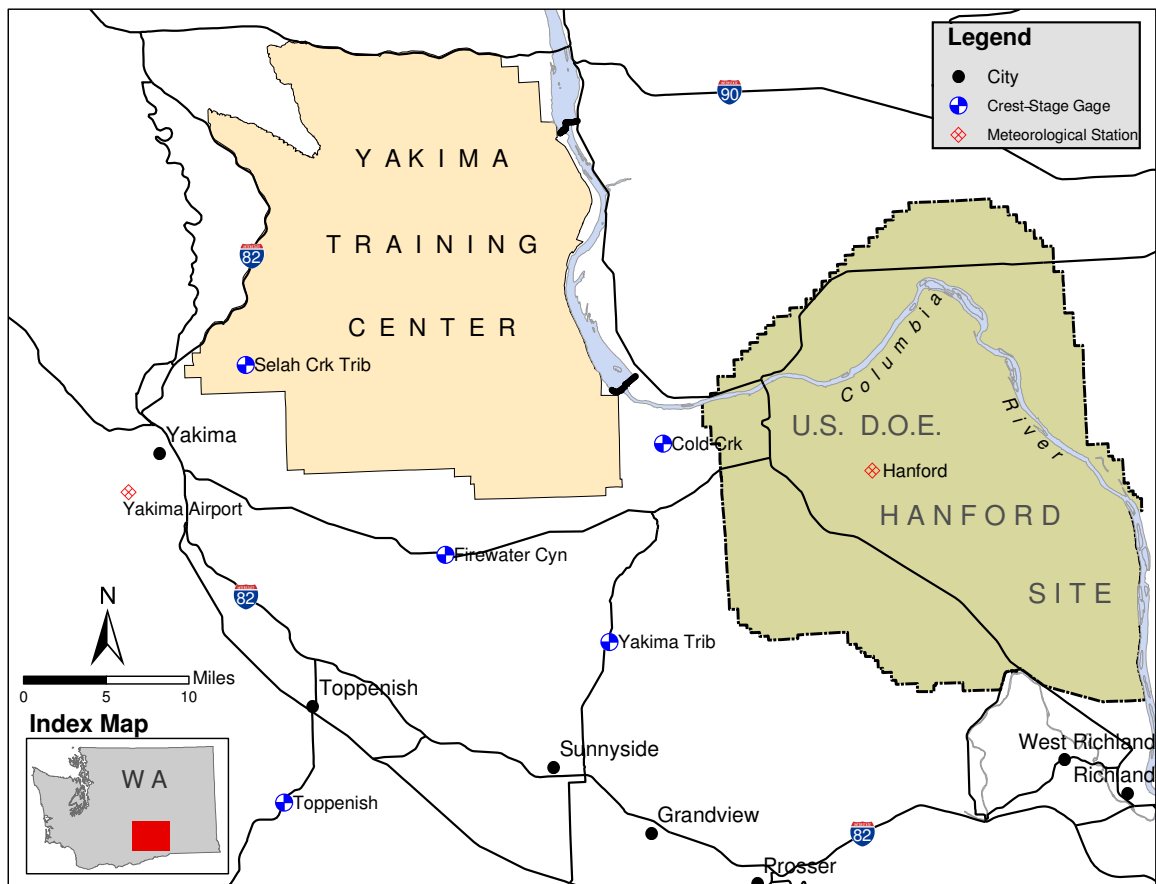


**Figure D.1.** Crest height gauges near Hanford. Selah Creek Tributary, Cold Creek Tributary, Firewater Canyon, Yakima Tributary, and Toppenish were active during the 1950s–70s. Upper Cold Creek Tributary was active during 1991–1995.

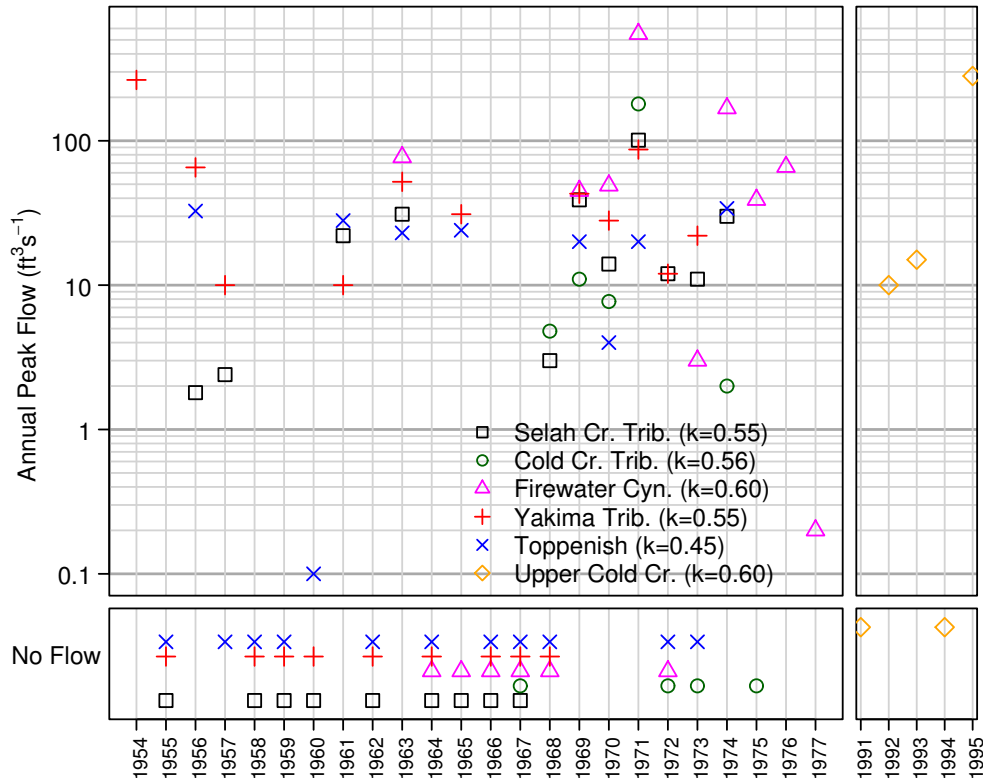


**Figure D.2.** Annual peak flows at regional USGS crest height gauges. Lower plots show years in which there was no flow.  $k$  = fraction of years with flow.

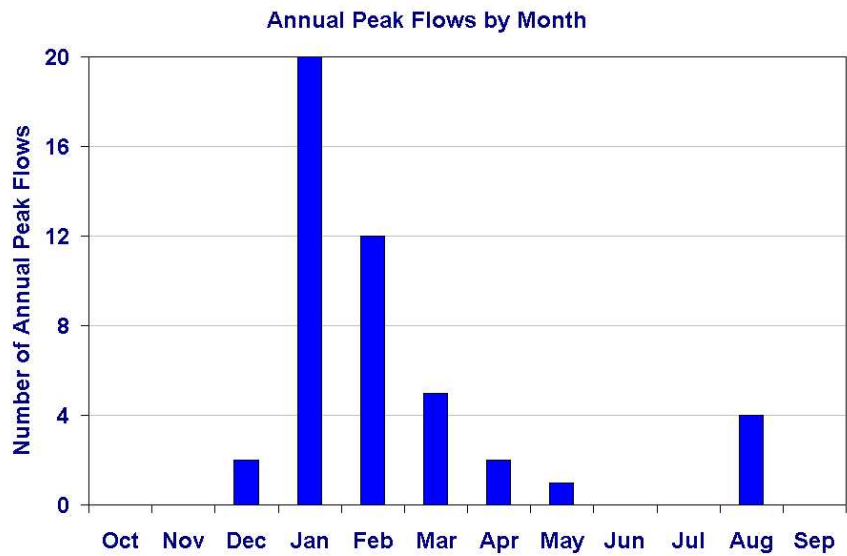


**Figure D.3.** Monthly distribution of instantaneous peak annual flows based on 84 station-years of record at regional USGS crest height gauges (see Figure D.1)

## D.1 Methods

A flow frequency analysis was done on the peak flow data, assuming a lognormal distribution (Figure D.4). Peak flow rates were normalized to basin size by converting units of  $\text{ft}^3\text{s}^{-1}$  to  $\text{mm h}^{-1}$ . The analysis methods were adapted from those by Haan (1977) and account for the fact that in some years no flow was observed at all. Analysis of the data suggests that peak flows in the region are around  $0.8 \text{ mm h}^{-1}$  at a return interval of 5 years (cumulative probability = 0.8), and around  $2 \text{ mm h}^{-1}$  at a return interval of 10 years (cumulative probability = 0.9) (Figure D.4). The flow rates measured at UC are mostly at the low end of the range, though the value from January 1995 is closer to other data. This analysis suggests that a longer period of record in Cold Creek would result in the measurement of more events like those that occurred during January 1995 and that flow events up to 5 times larger than those observed may happen on average every 10 years or so.

## D.2 Results

Using the flow frequency model for peak annual flows at UC and the relationship between flow volume and peak rate in Figure 3.2, an average annual recharge from Cold Creek streamflow can be derived. The lognormal model was used to generate 2000 “years” of peak annual flows, including zero-valued flows in 40% of the years. The mean annual recharge, based on the 2000 realizations of peak annual flows, was then computed as  $55,200 \text{ m}^3\text{y}^{-1}$  using mean peak flow and the regression equation in Figure 3.2 of the main report. This estimate of recharge from flow at UC is conservatively low because it excludes subsurface flow, is based on a short data set, and allows a maximum of just one flow event per year. The perennial flow of Rattlesnake Spring just upstream of LD is much larger than this, at  $0.420 \text{ Mm}^3\text{y}^{-1}$ . The combined recharge volumes yield a lower-bound estimate of recharge from all of GCC,  $0.471 \text{ Mm}^3\text{y}^{-1}$ .

## D.3 References

Haan CT. 1977. *Statistical Methods in Hydrology*. Iowa State University Press, Ames, Iowa.

### Lognormal Model of Annual Peakflows

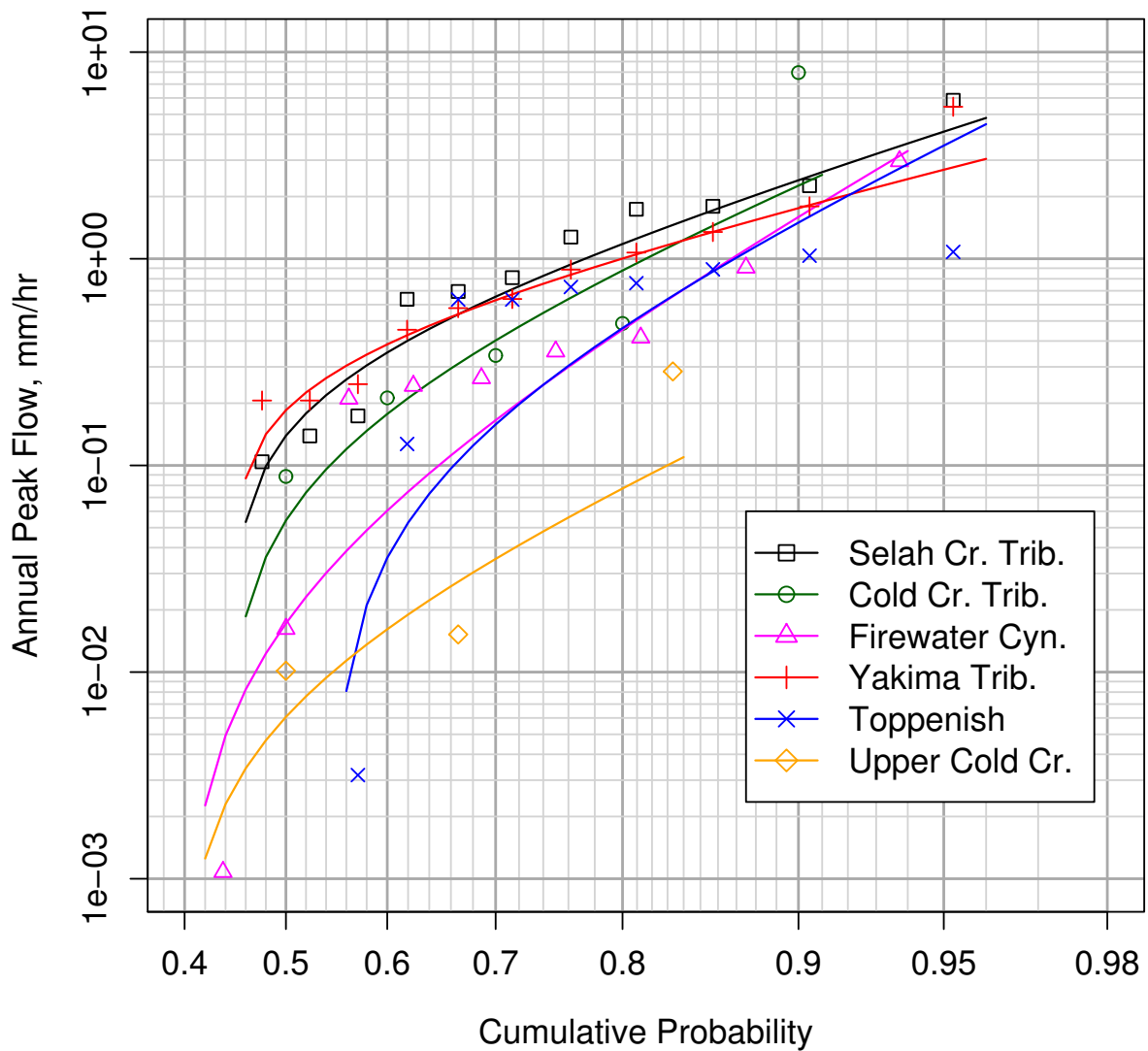


**Figure D.4.** Cumulative probability of annual peak flow data (points) and lognormal distribution model (lines) from regional USGS crest height gauge data. Probability of zero flow in any year was  $> 0.40$  at all locations. The Weibull method was used for plotting position (Haan 1977).

## Distribution

No. of  
Copies

No. of  
Copies

### OFFSITE

- K. Niles\*\*  
Oregon Department of Energy  
625 Marion St. N.E.  
Salem, OR 97310
- S. Bede\*\*  
U.S. Ecology  
P.O. Box 638  
Richland, WA 99352
- 2 R. Buck, Jr.\*\*  
Wanapum Indian Band  
P.O. Box 878  
Ephrata, WA 98823
- 5 D. N. Goswami\*\*  
Washington State Dept. Ecology  
1315 West 4th  
Kennewick, WA 99336-6018
- 2 Yakima Indian Nation\*\*  
P.O. Box 151  
Toppenish, WA 98948  
ATTN: R. Jim  
W. Riggsbee
- 2 S. Harris\*\*  
Confederated Tribes of the Umatilla  
P.O. Box 638  
Pendleton, OR 97801
- 2 Nez Perce Indian Tribe\*\*  
P.O. Box 365  
Lapwai, ID 83540-0365  
ATTN: D. L. Powauke

- 2 B. W. Drost\*\*  
U.S. Geological Survey  
1201 Pacific Avenue, Suite 600  
Tacoma, WA 98402
- Richard Link\*\*  
U.S. Bureau of Reclamation  
PN-3600  
1150 N. Curtis Rd., Suite 100  
Boise, ID 83706-1234
- Kayti Didricksen\*\*  
U.S. Bureau of Reclamation  
P.O. Box 620  
Grand Coulee, WA 99133

### ONSITE

- 3 DOE Office of River Protection  
R. M. Yasek\*  
R. W. Lober\*  
Steve Wiegman\*
- 13 DOE Richland Operations Office  
B. L. Charboneau\*  
B. L. Foley\*  
R. D. Hildebrand (5) A6-38\*\*\*  
R. D. Hildebrand (2) A6-38\*\*  
J. G. Morse\*  
K. M. Thompson\*  
Doug Chapin\*  
Kevin Leary\*
- Bechtel Hanford Inc.  
K. R. Fecht\*

|    |  |          |                               |          |
|----|--|----------|-------------------------------|----------|
| 7  | <u>CH2M HILL Hanford Group, Inc.</u>         |          | E. J. Freeman*                |          |
|    | M. P. Connelly*                              |          | V. Freedman*                  |          |
|    | F. J. Anderson*                              |          | M. D. Freshley*               |          |
|    | A. J. Knepp*                                 |          | J. Fruchter*                  |          |
|    | F. M. Mann*                                  |          | G. W. Gee*                    |          |
|    | W. J. McMahon*                               |          | D. G. Horton*                 |          |
|    | D. A. Myers*                                 |          | C. T. Kincaid*                |          |
|    | C. D. Wittreich*                             |          | G. V. Last*                   |          |
|    |  |          | S. Luttrell*                  |          |
|    |  |          | W. J. Martin*                 |          |
| 2  | <u>Fluor Federal Services</u>                |          | C. J. Murray*                 |          |
|    | R. Khaleel*                                  |          | T. Naymik*                    |          |
|    | R. J. Puigh*                                 |          | W. E. Nichols*                |          |
| 8  | <u>Fluor Hanford, Inc.</u>                   |          | S. P. Reidel*                 |          |
|    | J. V. Borghese*                              |          | M. Richmond*                  |          |
|    | M. Byrnes*                                   |          | M. L. Rockhold*               |          |
|    | B. H. Ford*                                  |          | F. Spane*                     |          |
|    | T. W. Fogwell*                               |          | M. B. Triplett*               |          |
|    | V. J. Rohay*                                 |          | P. D. Thorne*                 |          |
|    | L. C. Swanson*                               |          | S. Waichler (5)               | K9-36*** |
|    | M. E. Todd-Robertson*                        |          | S. Waichler (2)               | K9-36**  |
|    | M. I. Wood*                                  |          | A. L. Ward*                   |          |
|    |  |          | M. Wigmosta                   | K9-36*** |
|    |  |          | M. D. Williams*               |          |
|    |  |          | S. K. Wurstner*               |          |
| 43 | <u>Pacific Northwest National Laboratory</u> |          | S. B. Yabusaki*               |          |
|    | M. P. Bergeron (3)                           | K9-36*** | Hanford Technical Library (2) | H2-53*** |
|    | M. P. Bergeron (2)                           | K9-36**  |                               |          |
|    | B. N. Bjornstad*                             |          |                               |          |
|    | R. W. Bryce*                                 |          |                               |          |
|    | C. R. Cole*                                  |          |                               |          |
|    | A. Coleman                                   | K9-36*** |                               |          |
|    | M. J. Fayer*                                 |          |                               |          |

## Distribution method:

\* Email notification of availability at  
ERICA

\*\* CD

\*\*\* Hardcopy